ISTANBUL TECHNICAL UNIVERSITY ★ INSTITUTE OF SCIENCE AND TECHNOLOGY

WAVE POWER POTENTIAL ASSESSMENT OF AEGEAN SEA

M.Sc. THESIS

Navid JADIDOLESLAM

Department of Civil Engineering

Hydraulic and Water Resources Engineering Programme

MAY 2014

ISTANBUL TECHNICAL UNIVERSITY ★ INSTITUTE OF SCIENCE AND TECHNOLOGY

WAVE POWER POTENTIAL ASSESSMENT OF AEGEAN SEA

M.Sc. THESIS

Navid JADIDOLESLAM
(501121517)

Department of Civil Engineering

Hydraulic and Water Resources Engineering Programme

Thesis Advisor: Assoc. Prof. Mehmet ÖZGER

MAY 2014

İSTANBUL TEKNİK ÜNİVERSİTESİ ★ FEN BİLİMLERİ ENSTİTÜSÜ

EGE DENİZİNİN DALGA GÜCÜ POTANSİYELİNİN BELİRLENMESİ

YÜKSEK LİSANS TEZİ

Navid JADIDOLESLAM
(501121517)

İnşaat Mühendisliği Anabilim Dalı

Hidrolik ve Su Kaynakları Programı

Tez Danışmanı: Assoc. Prof. Mehmet ÖZGER

MAYIS 2014

Navid JADIDOLESLAM, a M.Sc. student of ITU Institute of Science and Technology 501121517 successfully defended the thesis entitled **"WAVE POWER POTENTIAL ASSESSMENT OF AEGEAN SEA"**, which he prepared after fulfilling the requirements specified in the associated legislations, before the jury whose signatures are below.

Thesis Advisor :	**Assoc. Prof. Mehmet ÖZGER** Istanbul Technical University	.....
Jury Members :	**Asst. Prof Ali UYUMAZ** Istanbul Technical University	.....
	Asst. Prof Ali Osman PEKTAŞ Bahçeşehir University	.....

Date of Submission : **3 May 2014**
Date of Defense : **29 May 2014**

To whom I love,

FOREWORD

This thesis is supported by TÜBİTAK and prepared in Hydraulic and Water Resources Engineering Laboratory of Istanbul Technical University. Great effort has been spent on modeling with MIKE 21 SW software and specially for data analysis. The thesis is written by using LaTeX word processing program.

Most of all, I wish to thank my supervisor, Assoc. Prof. Mehmet ÖZGER, for giving me the chance to perform this work and to have guided and helped me through the whole MSc. process. His supervision and advises have made it a great and positive experience. I owe my thanks to Prof. Dr. Necati AĞIRALİOĞLU for his precious helps and guidance.

Furthermore, I would like to express my gratitude to all the other colleagues at the Hydraulic and Water Resources Engineering Laboratory that have helped me and made this study such a pleasant journey.

Finally, I would like to give my special thanks to my parents and my friends. Their motivation and continuous support have made this happen and more than enjoyable. I am very grateful for everything you have done for me.

May 2014 Navid JADIDOLESLAM

TABLE OF CONTENTS

Page

ABBREVIATIONS

ANFIS : Adaptive-Network-Based Fuzzy Inference System
BCM : Billion Cubic Meters
DDP : Directional Decoupled Parametric
DHI : Danish Hydraulic Institute
ECMWF : European Center for Medium-Range Weather Forecasts
GEODAS : GEOphysical DAta System
GFS : Global Forecast System
GSHHS : Global Self-consistent, Hierarchical, High-resolution Shoreline
HCMR : Hellenic Center for Marine Research
IPCC : Intergovernmental Panel on Climate Change
NCEP : National Center for Environmental Prediction
NDBC : National Data Buoy Center
NGDC : National Geophysical Data Center
NOAA : National Oceanic and Atmospheric Administration
REMO : Regional Atmosphere Model
SWAN : Simulating Waves Near-shore
TPE : Tonne Petroleum Equivalent
TÜBİTAK : The Scientific And Technological Research Council of Turkey
WAMC4 : WAve Model Cycle 4
WEC : World Energy Council
WRI : World Resource Institute
WW3 : WAVE WATCH 3

LIST OF TABLES

Page

LIST OF FIGURES

Page

WAVE POWER POTENTIAL ASSESSMENT OF AEGEAN SEA

SUMMARY

In this study the wave power in Aegean Sea was simulated over the period from 1999 to 2013 using a third-generation spectral wave model MIKE 21 SW.

The model is built in MIKE Zero mesh generator and the mesh consists of 5927 nodes and 10081 elements. Bathymetry data obtained from NOAA and Significant Wave Height and Mean Wave Period of the 5 stations: Dalaman, Bozcaada obtained from NATO-TU WAVES and Athos, E1M3A and Saronikos originally taken from HCMR database.

Wind data with $0.125^\circ \times 0.125^\circ$ resolution for every $6h$ interval was obtained from ECMWF (Era-Interim) database. The wave model calibrated by 5 buoy stations measurements and the generated wave characteristics such as significant wave height and mean wave period gave a high accuracy of the model.

Wave power atlas was generated based on an averaged 15 years wave data obtained from model. Near Turkish coast, mean wave power found 2 kW/m depending on the way of the waves, waves traveling after islands have less power in Turkish coasts.

Wave power in the middle Aegean have higher wave power potentials compared to coastal regions where the calculated mean wave power in this area is more than 4 kW/m. Maximum mean wave power observed from simulations are located in 2 locations between Ikaria and Mykonos islands and between Kasos and Crete islands reaching 5.2 kW/m.

Results of the seasonal analysis in this study demonstrate that the maximum wave power values in winter occurs in northern part of the Aegean Sea with more than 8 kW/m. Maximum mean wave power occurrence location from winter to spring changes from north to middle southern part of the study region, between Crete and Kasos islands.

The western and middle part of study area found to have least and most wave power potential respectively.

For the Turkish coast it was seen that the shading effect had decreased the wave energy for this regions. Though there were some locations which had a higher wave power potential compared with other parts of east coast of Aegean Sea.

In a glance to the 15-year mean significant wave height map it was seen that high wave potential is available in Northern part of Aegean Sea specially in Bozcaada, Gökçeada and Baba Burnu. In this part mean wave power is between 1.0 - 2.8 kW/m.

For middle-Aegean Sea, Karaburun and Çesme have a 2.0 kW/m of wave power potential.

EGE DENİZİNİN DALGA GÜCÜ POTANSİYELİNİN BELİRLENMESİ

ÖZET

Türkiye enerji kullanımında %74 oranında dışa bağımlıdır. Bu oranın 2020 yılına kadar % 80 civarında olacağı enerji ile ilgilenen yöneticiler ve otoriteler tarafından tahmin edilmektedir.

Enerji tüketiminde dışa bağımlılığın, Türkiye'nin jeopolitik konumu dikkate alındığında her an yaptırım aracı veyahut ambargo malzemesi olarak kullanılabilme olasılığı yüksektir.

Büyük hidroelektrik santraller çevre acısından temiz olmasına karşın, canlı hayat alanlarını kısıtlamakta ve bazen eko sistem üzerinde zararlı etkiler ortaya koyabilmektedir. Türkiye, eldeki verilere göre her yıl enerji tüketiminde artışla karşılaşıyor ve bu rakamlar gittikçe artıyor.

Dalga enerjisinin temiz ve güç kaynağının yenilenebilir olması dünya üzerinde ilgiyi bu yöne doğru taşımaktadır. Özellikle, Amerika, Kanada, İngiltere, Kuzey Avrupa Ülkeleri, İspanya ve Portekiz çok ciddi yatırımlar ve teşvikler vererek dalga enerjisinden faydalanma hususunda önemli araştırmalar yapmaktadırlar. Örneğin, şu an İspanya'nın Bask bölgesinde bulunan Mutriku yerleşim yerinde dalga enerjisi dönüşüm santrali ile enerji ihtiyacı bütünüyle karşılamaktadır.

Hükümetler arası İklim Değişikliği Panelinin verilerine göre küresel enerji ihtiyacının % 30'nun deniz dalgalarının hareket enerjisinden karşılanması mümkündür.

Dünya da önde giden ülkelerden geriye kalmamak için enerji üretiminde yeni yöntemler kullanmak ve uygulamak gerekir ki bu kapsamda bilimsel araştırma her uygulamadan daha çok önem taşır.

Birinci adımda Ege Denizi için çalışma sınırları belirlenerek ve harita üzerinde sınır şartları seçilmiştir. Kıyı çizgisi verileri değişik kaynaklardan bulabilmektedir. Bu kaynaklardan en hassas ve en çok kullanılanı seçilmiştir.

MIKE 21 SW'de kurulan benzeştirmede kullanılan bir diğer veri ise rüzgâr verisidir. Ege Denizini kapsayan alan için 1999-2013 yılları arasında 6 saatlik zaman aralıklarına sahip rüzgâr hızları "x" ve "y" bileşenleri olarak ECMWF'den elde edilmiştir.

Ağ üretimi projenin diğer adımlarından daha fazla önem taşır. Düzenli ve uygun bir ağ üretimi yapabilmek ileri adımlarda yaşanacak problemlerinde önüne geçecektir. Ağ üretiminin hem batimetre interpolasyonunda hem de hesaplamalarda etkisi büyük olduğundan uygun bir ağ yüksek başarılı bir modele sebep olacaktır.

Bu tez'de kullanılan batimetri verilerinin çözünürlükleri 0.004° (400 m)'dir. Veriler, XYZ dosya formatında Ağ üretici modülüne yüklenerek dikkatle incelenmiş ve düzenlenmiştir. Bu kapsamda kıyı çizgisinin arkasında kalan bazı noktalar elenmiştir.

MIKE 21 SW'de kurulan benzeştirmede kullanılan bir diğer veri ise rüzgâr verisidir. Ege Denizini kapsayan alan için 1999-2013 yılları arasında 6 saatlik zaman aralıklarına sahip rüzgâr hızları "x" ve "y" bileşenleri olarak ECMWF'den elde edilmiştir.

Elde edilen rüzgâr verisi 0.125 derece çözünürlükte olup, 6 saatlik zaman dilimlerini kapsamaktadır. Rüzgâr verileri mevcut olan en yüksek çözünürlükte olup ECMWF'in ERA-Interim yeniden analizleri ile üretilmiştir.

Bu çalışmada, 1999-2013 dönemi için üçüncü nesil olan spektral dalga modeli MIKE 21 SW'i kullanarak Ege Denizinin dalga gücü incelenmiştir. Bu modellemede ilgili bölgede mevcut çoklu yüzen istasyon verileri kullanılmıştır.

Bu istasyonlar Dalaman, Bozcaada, Athos, E1M3A, Lesvos, Mykonos, Santorini, Saronikos ve Skyros'dan ibaretler.

Dalaman ve Bozcaada istasyonlarının ölçülmüş verileri NATO-TU WAVES Projesinden alınmıştır ve diğer istasyonlar yunanistanın tarafından yönetilen kurum HCMR tarafından temin edilmiştir.

Kalibrasyon için kullanılan 9 istasyon için bulunmuş olan istastistik değerlerndirmelerin neticesinde modelin güvenilebilirliği denetilmiştir ve modelin yüksek dayanabilirliği ortaya konulmuştur.

Bu çalışmada belirgin dalga yüksekliği için modelin verdiği değerler ve ölçülmüş değerlerin korelasyon katsayıları yüksek derecede cevaplar vermiştir.

Bu model MIKE Zero Ağ üretimine dayanmaktadır. Bu ağın 5927 düğümü ve 10081 elemanı vardır. Batimetre verileri NOAA'dan sağlanmıştır. Her 6 saat ara'ile $0.125^\circ \times 0.125^\circ$ çözünürlükle rüzgar verileri ECMWF (Era-Interim) veri tabanından sağlanmıştır.

Dalga modeli 9 yüzen istasyondaki ölçümlerle kalibre edilmiştir. Belirgin dalga yüksekliği ve ortalama dalga periyodu gibi dalga karakteristikleri modelde yüksek bir hassaslıkla hesaplanmıştır.

Kalibrasyonun hedefi, model parametrelerinin değerlerini optimize etmektir. Bu parametrelerin karşılaştırması için kullanılacak olan istatiksel ölçü indeksleri aşağıda verilmiştir. Bu ölçü kriterleri kullanılarak elde edilen değerler simülasyon sonuçları ve ölçüm değerleri arasında yüksek bir korelasyon vardır.

Bu çalışmada, dalga modeli oluşturulması için DHI MIKE yazılımının MIKE 21 SW modülü kullanılmıştır. MIKE 21 SW, rüzgâr dalgalarının kıyıdan uzak ve kıyı yakınlarındaki büyüme, azalma ve transformasyonunu hesaplayan Danimarka Hidrolik Enstitüsü (DHI) tarafından geliştirilmiş ve dünya genelinde güvenilerek uygulanan bir yazılımdır. MIKE 21 SW aşağıdaki fiziksel hesaplamaları kapsamaktadır.

Model sonuçları 6 saatlik hassasiyette sonuçlar vermektedir. Dolayısıyla 1999 yılında başlayan ve 2013 yılına kadar devam eden süreçte 6 saatlik zaman çözünürlüğünde belirgin dalga yüksekliği ve dalga periyodu dalga özellikleri model çıktısı olarak elde edilmiştir.

Bu sonuçları kullanarak aylık ve mevsimsel hesaplamalar yapılmıştır. Her ay ve mevsimin 15 yıllık ortalama belirgin dalga yükseklileri ve ortalama dalga güçleri hesaplanmıştır.

Bu araştırmada benzeştirmeler 1999-2013 yıllarını kapsayan 15 yıllık bir süre için yapılmıştır. Her bir yıl için kalibre edilmiş parametreler ile model ayrı ayrı çalıştırılmıştır.

Bir yıllık zaman dilimi için modelin 16GB ram ve 2.2GHz işlemci hızına sahip bilgisayarda çalışma süresi 30 saat sürmüştür. Yapılan 15 yıllık benzeşim için toplam hesaplama süresi yaklaşık 30 günde bitmiştir.

Yıllık sürelerle yapılmış olduğundan her yıl için farklı ortalama belirgin dalga yükseklikleri ve ortalama dalga gücü elde edilmiştir. Aylık değerlerin ayırılması için zaman adımları belirlenmiş ve her yılın 12 ayı için dalga özellikleri teker teker çıkartılmıştır.

Ortalama 15 yıllık verilere dayanarak modelden dalga gücü atlası üretilmiştir. Türkiye kıyılarına yakın, dalgaların geliş yoluna bağlı olarak ortalama dalga gücü 2 kW/m bulunmuştur. Türkiye'nin adalara bakan kıyılarında, adalardan sonra kıyıya yaklaşan dalgaların daha gücü vardır.

Ege Denizinin orta kısımlarında, kıyı bölgesine göre daha yüksek dalga gücü potansiyeli mevcuttur. Bu kısımdaki dalga gücü 4 kW/m'den daha büyüktür. Model çalışmalarında hesaplanan en büyük ortalama dalga gücü iki yerde ortaya çıkmıştır.

Bunlardan bir tanesi İkara ve Mykonos adaları arasında, diğeri ise Kasos ve Crete adaları arasında meydana gelmiştir. Bu iki noktada maksimum ortalama dalga gücü 5.2 kW/m'ye ulaşmıştır.

Zaman incelemeleri aylar ve mevsimler göz önüne alınarak yapılırken mekân incelemelerinde bu parametrelerin çalışma alanı içinde nasıl değiştiğine bakılmıştır. Belirgin dalga yüksekliği ve dalga gücü zaman ve mekânla değişim göstermektedir. Bu değişimler çok belirgin olarak karşımıza çıkmaktadır.

Dolayısıyla pratikte yapılacak bir çalışmada zaman ve mekân değişim dağılımına bakılması önem arz etmektedir. Kış aylarında hem dalga yüksekliği hem de dalga gücü diğer aylara göre çok yüksek değerler vermektedir. En az güç potansiyeli ise yaz aylarında görülmüştür.

Belirgin dalga yüksekliği ve dalga gücünün 15 yıllık aylık ortalamalarına bakıldığında en yüksek değerlerin Şubat ayında çıktığı belirlenmiştir. Şubat ayında yer yer 9 kW/m kadar çıkan bir dalga gücü potansiyeli görülebilmektedir. Buna karşın en düşük değerlerin ise Temmuz ve Ağustos aylarında görüldüğü tespit edilmiştir.

Ege Denizinde bulunan adalar dalga oluşumunu engellediği için belirgin dalga yüksekliği ve dalga gücü potansiyeli daha çok adaların bulunmadığı boş kısımlarda oluşmaktadır.

Bu çalışmada mevsimlik analiz sonuçları 8 kW/m'den daha yüksek olarak Ege Denizinin kuzey kısmında, kışın meydana geldiğini göstermiştir.

En büyük ortalama dalga gücü oluşma yeri, kıştan ilkbahara geçerken, çalışma alanının kuzeyinden orta güney kısmına, yönü Crete ve Kasos adaları arasına kaymaktadır. Modelleme ile çalışma alanının batısı ve ortasında sıra ile en düşük ve en yüksek dalga gücü potansiyeli bulunmuştur.

1. INTRODUCTION

Water plays a crucial role in human life whereas 70 % of the Earth is covered with water that most of them are connected to each other forming oceans and seas. Waves are one of the most important elements of oceans and seas that carry mass and energy by them, sometimes traveling from a continent to another. Waves are different in magnitude depending on the source of their formation cause.

Natural resources are so important for every country's economy. Best utilization of these resources can make a country nearly independent from outside of country. According to the WRI more than 80 % of the world countries have coastal line, while Turkey is surrounded by seas. This could be called as a chance for this country to get used from wave energy.

The green house gas effect of fossil fuels encouraged scientists and researchers to make a replacement for this kind of energy resources, so that green energy resources became more important than before in last century. Wave energy is one of the green energies available without the most of disadvantages of the fossil fuels had.

On the other hand behavior of waves in a basin is principal for future planning constructions in the region but measurement of the wave characteristics for a long period of time demand more budget to install measurement buoys in the interested area, so that simulation of the waves characteristics is like an economical answer to an expensive question.

There is a great wave energy potential throughout world which should be seen as a green energy resource that can be harvested in near future. Global wave power atlas [1]with a high accuracy of model which shows that world has a great wave energy in different districts and oceans which could be taken into account and used either by an individual national or multinational projects, so that more research and development is demanded for a higher precision of energy derivation from waves.

Table 1.1: Turkey's energy supply in 2009, 2010 and 2011.

	2009 (1000 TPE)	2010 (1000 TPE)	2011 (1000 TPE)
Coal	32,913	33,531	35,841
Natural Gas	32,775	34,907	36,909
Petroleum	30,565	29,221	30,499
Hydraulic	3,092	4,454	4,501
Wood	3,530	3,392	2,446
Geotherm etc.	1,250	1,391	14,63
Animal waste etc.	1,136	1,166	1,091
Geothermal	375	575	597
Solar	429	432	630
Wind	129	251	406
Biofuel	9	12	18
Total	106,138	109,266	114,480

Last century could be called as a population explosion in the world as the statistics show that world population has became 7 billion in 2011 from 2 billion in year 1927, this fact is similar in Turkey where it has reached 75 million from 13 million between 1927-2012 years. Population increase made Turkey to import 43 billion cubic meters of gas in year 2011, this statistic made Turkey 7th in the world top gas importers. More than 74% of the Turkey's energy is imported , according to the energy executives and authority's estimations this percentage would grow to reach 80% by year 2020.

As it can be seen from Table 1.1 the statistical numbers of the Turkish Energy Ministry show that Turkey's energy demand in 2011 was 114,480 Tones petroleum equivalent.

Hydroelectric centrals can be a good green energy resource but they change the wildlife ecosystem and have other side effects. In the last decade there is a great enthusiasm for building wave energy converters and wave farms as a clean and renewable energy. Specially in United States, Canada, Britain, and northern European countries there are vast investments in this sector.

In 2005 the global electricity consumption was around 15 TW. With a total energy consumption of 131400 TWh/year According to the data of IPCC 30% of the global energy demand could be supplied by the energy of oceans and seas. According to the WEC, the global wave energy resource is estimated to be 1-10 TW.

For an efficient harvest of a energy resource, detailed research and analysis plays an crucial role in a future decision making process. This study shows wave

characteristics' distribution and magnitude throughout Aegean Sea while having detailed analysis on the obtained data from a 15 years period simulations done by a third generation spectral wave software which is produced by DHI. A deep study of the Aegean Sea can lead to a better decisions in later steps for investors in energy sector, so that this study's aim was to make a complete reference of the Aegean Sea wave properties either in near shore and offshore locations.

1.1 Purpose of Thesis

The main purpose of the thesis which is funded by TÜBİTAK and it took 12 months of hard work, was to investigate the Aegean Sea's 15-year mean wave power, locations of the maximum and minimum values, statistical analysis of the data obtained from simulations and comparing results of the model with the measured data and calibration of the model. This work is the result of deep study of the waves characteristics in this basin with detailed analysis and technical comments. Also the model constructed in this study could be used in future for other purposes like estimation of the waves in Aegean Sea for a short period of time by having an estimation of winds in this area.

- Main purpose
  - Making a complete database of the wave's characteristics for Aegean Sea
  - Spatial and temporal analysis for significant wave height and wave power
  - Deep study of the waves in Turkish coasts
- Literature review
  - Making an abstract of the researches in regional aspect on wave power
  - Spectral wave modeling theoretical description
- Modeling
  - Building a unstructured mesh for interested area
  - Application of MIKE 21 SW to Aegean Sea
  - Simulation of waves with 15 years time span with ECMWF wind data

- Calibration
  - Digitization and organization of the measured data to be ready for calibration
  - Synchronization of the measured and simulated data
  - Comparison of the observed data with the simulated data with statistical values
- Waves analysis
  - Making 15-year, yearly, monthly and seasonal mean wave power atlases
  - Investigation of the wave power potential in east coasts of Aegean Sea
  - Wave rose and frequency analyses for important points in the study region.
  - Comparison of the waves in different distances from eastern coast of Aegean Sea

1.2 Literature Review

By the rise of importance of wave energy and its beneficial aspects in world wide, every country has encouraged its researchers and scientists to invest their time on this subject. Therefore numerous researches have been conducted in recent years on wave power.

Hatada, Y. & Yamaguchi, M. (1998) applied 9 years ECMWF wind data with period from 1986 to 1994 to evaluate shallow water waves in Pacific coast of Japan. Wave estimation was done by a shallow water wave prediction model [2] which traces the change of directional spectrum along a refracted ray of each component focusing on a hindcast point is applied for long-year wave hindcasting in order to save computer processing time. In this study 6 buoy stations were used to verify model. Reasonable correlation coefficients were found by comparison of the measured and calculated data. Also in this study the result of simulation in the location of offshore station were more close to measured data in that point. On the other hand for waves higher than $2m$ a good agreement has reached between calculated and simulated wave heights [3].

Golshani et al. (2005) simulated wave characteristics in Caspian Sea using MIKE 21 SW. in this study 12 years of wind data every $6h$ were applied to the third generation

model. The calibration of model resulted values 2, 0.8, 0.002 for white-capping, wave breaking, bottom friction parameters respectively. For extreme conditions analysis done by EVA software developed by DHI Water and Environment statistic distribution of the wind and wave data was most fitting to Truncated Gumble that gave less less standard deviation and smoother spatial pattern of extreme values. Some points adjacent to southern coast of Caspian sea were predicted by unrealistic values. These results were due to land interpolations were removed from results [4].

Jose & Stone (2006) investigated entire Gulf of Mexico's wind generated wave and swell waves using MIKE 21 SW while the resolution of mesh used for coastal parts of this study is 2 *km* a coarser grid of 30 *km* used for boundary. For Southern part of basin a bathymetric data with a 2.3 *km* resolution and for other parts 34.4 *km* resolution were used. Wind data was obtained from NCEP of NOAA. This is study is conducted with a period 36 *hrs* whereas the comparisons between wave and wind data were done in both coastal and offshore parts of the domain. offshore station results demonstrated a close values to the measured however coastal station located in shallow water did not give a good calculated values for wind data measured, the effect of higher difference in wind data reflected in simulated wave values. The results of the study shows that during fair weather condition predicted wave parameters show a good correlation with measured data while this is not the same in the extreme weather conditions that estimated values are lower than measured. The diversity of the data could be related to the scale and accuracy of the input wind data [5].

Moeini & Etemad-Shahidi (2007) modeled Lake Erie's wave characteristic located in North America. In this study simulations was done by MIKE 21 SW and SWAN then the comparisons and evaluations were taken part in this investigations. Wind data sets were obtained from National Data Buoy Center and 1 field data was obtained Marine Environmental Data Service which is hourly data sets. Comparisons between simulated data of SWAN model and results from Janssen wind input formulation [6] and cumulative steepness method were done and reached to good agreements. Results of the comparisons from SWAN and MIKE 21 SW demonstrate that SWAN model gives better results for H_s while MIKE 21 SW performs better in prediction of T_p. Also this study shows that using Komen's formulation led to more accurate estimations of

H_s while having less accurate T_p results from model. The cumulative steepness method for white-capping dissipation in SWAN model has a 2 times of Komen's method [7] computational time so that it is not suggested to be used [8].

Kazeminezhad et al. (2007) evaluated neuro-fuzzy and numerical wave prediction models in Lake Ontario located in North America, where as used MIKE 21 spectral wave program and ANFIS for simulations. By application of the directional decoupled parametric formulation and fully spectral wave formulation which is based on the wave action conservation [9]. In DDP formulation, parameterization is made in the domain of frequency and first and zeroth moments of wave action is considered as dependent variable [10]. Domain consists of 1322 unstructured triangle elements and calibration took place with a 611 number of hourly wind and wave measurements. The buoy station is located in deep water, so that the only parameter calibrated is white-capping factor (c^*_{ds}). The results show that MIKE 21 SW is performing more accurate in estimation of both H_s and T_p [11] .

Cherneva et al. (2008) validated WAMC4 wave model for the Black Sea basin, wind data were obtained from regional atmosphere model(REMO) [12] [13] The spatial resolution for these simulations was chosen to be about 50×50 km and the simulated wind fields have been stored at every hour [14]. Validation is done with 4 different point measurements in the Black Sea and gratifying statistical results were obtained from model while showing that WAMC4 underestimates the significant wave height H_s in the case of rapid change of wind direction combined with low wind velocities. This model generally gave good agreements between output and measured data but model gives more accurate output as wind speed increases to a severe state [15] .

Rusu (2009) calculated the wave power potential in Black Sea by both WAM and SWAN models for 1971 to 1994 by using wind data resolution of 0.25° and investigations done in Northern Black Sea. Analysis of the measured wave and wind data and comparison with model output values is taken part also in this study the wave characteristics were modeled by totally 4 different approach: 1. Komen's parameterization [7], 2. Janssen's model for atmospheric input [16] coupled with same pulse-based model of Hasselmann [17], 3. Komen's model coupled with the cumulative steepness method (CSM) [18] for whitecapping, and 4. Yan's model for

atmospheric input [19] coupled with the saturation-based model of Alves and Banner for whitecapping [20]. Monthly mean wave direction for 8 directions and significant wave height H_s scatter table generated. The model is tested with 3 different stations, 2 buoy and 1 wave gauge. Reasonable correlation coefficients are derived from collations of methods; Alves and Banner's method for white-capping gave the best results for significant wave heights H_s through all other models [21] .

G. Iglesias & R. Carballo (2009) modeled wave energy potential of the Death Coast in North Spain using WAM for offshore and SWAN for nearshore simulations. In this study 3 hourly hindcast wind from 1958 to 2001 is used. Wave data is computed by WAM cycle 4 forced with wind data of REMO for offshore locations and on the other hand coastal wave model is built on the SWAN model based on the wave action conservation [22]. The computational grid of this model is $0.15' \times 0.15'$. The evaluation of the results were done by 16 SIMAR-44 site and 2 buoy measurements. It is concluded that mean wave power potential of the the study region is more than 40 kW/m, also it was found that significant wave heights are between 2 m and 5 m and wave periods of 11-14 s [23].

Arinaga & Cheung (2011) acquired global atlas of wave energy model by using WAVEWATCH 3 with 10 years (2000-2009) of NCEP's Final Global Tropospheric Analysis (FNL) wind data which was obtained from Global Forecast System (GFS) [24]. This study has implemented WW3 with $1.25^\circ \times 1^\circ$ resolution of wind data and ice concentrations from National Ice Center. The separation of wind waves and swell is done in WW3. This study has validated it's results with altimetry data of 6 different regions for a period of four and a half months from January 15 to May 24 2002, also 19 buoy measurement data is used to evaluate the model. Regression between altimetry data and model output has given a good correlation coefficient for significant wave height H_s and a RMSE of 0.36-0.48 m at 6 regions of the world. Mean wave period and peak wave period values simulated by the model do not have a agreeable closeness to measured values. Monthly median wave power of wind waves above 30°N has a range 17-130 kW/m . The results also prove that the southern coasts of Australia and New Zealand are most appropriate for wave energy development, though

further investigation is needed wave energy infrastructures implementations for coastal regions [1] .

Liberti et al. (2013) studied wave energy resources in Mediterranean Sea with a more concentration on the west part of this sea. In this study which is conducted by 10 years (2001-2010) of wind data with a $0.125^\circ \times 0.125^\circ$ resolution obtained from ECMWF, more accurate model is built in contrast with the previous researches done for the region [25] [26] [27]. Simulations are done with 3rd-generation wave model WAM wave model cycle 4.5.3, domain's discretization is done with a regular grid with 667×251 nodes in spherical coordinates. The domain consists of Mediterranean, Agean Seas while reaching to Italian coasts in the western part. Wind data resolution employed in this study is 0.25°. The effects of currents and variations in sea surface elevation is neglected from calculations. The domain is considered as a closed basin. Wave characteristics are derived from model for every 3 hours and model values are calibrated with satellite and buoy measurements and statistical evaluations show a good results for calibrations. For further study of the wave behavior in the domain, 20 sites are selected in different parts of the domain for a deeper investigation. The most energetic parts of the Italian coastline is found to be in western coast of Sardinia and along the north-western and southern coast of Sicily [28].

Ayat (2013) created wave power atlas of Mediterranean and Aegean seas by using MIKE 21 SW, taking wind wave growth and nonlinear wave-wave interaction, dissipation due to white capping, bottom friction and depth-induced wave breaking refraction and shoaling. Triangular unstructured mesh is implemented in this study having 4098 nodes and 7035 elements. Wind data source is ECMWF with $0.1^\circ \times 0.1^\circ$ spatial and 6 hours of temporal resolution for 15 years (1994-2009). The calibration of model parameters parameters gamma (γ), bottom friction (k_N) and wave breaking (C_{dis}) is done by using NATO-TU Waves Project while reaching to results as 0.8, 0.04 and 1.5 respectively. Wave roses and scatter diagrams for H_s and T_p is produced for 7 different points in the study region; 5 points located in middle parts of Aegean Sea and 2 points in Mediterranean Sea's south coast. Good agreements between measured and simulated data is achieved in this study [29].

Aydoğan et al. (2013) investigated wave power of Black Sea by using 3rd-generation wave model MIKE 21 SW with a 13 years(1996-2009) ECMWF. Computational mesh while being smoother in coastal areas and coarser in offshore parts of the model, mesh consists of 4755 nodes and 8213 elements with a triangular shape. The wind data implemented in the model has a $0.1^\circ \times 0.1^\circ$ of spatial resolution and a 6 hour temporal resolution. The calibration of three different wave parameters gamma (γ), bottom friction (k_N) and wave breaking (Δ_{dis}) takes part by trial and error corrections reaching to best results 0.8, 0.4, 0.5 respectively. Also 14 points were selected for in-depth analysis while 12 of them being in nearshore and 2 points offshore. Nearshore points were selected with a regularity for an arranged distribution. Further scatter tables were produced for these points showing distribution frequency of significant wave heights with wave periods. The largest average wave power is found to be in South Western part of Black Sea with a 7 kW/m value. On the other hand results of the model show that by approaching to the eastern part of the basin wave power decreases and reaches to the least energetic part with mean wave power of 3 kW/m [30].

Zodiatisa (2014) used a 3rd-generation wave model for simulation of the eastern part of Mediterranean Sea's wave characteristics. In this study data used 3 hourly wind data obtained from SKIRON regional atmospheric system with $0.05^\circ \times 0.05^\circ$ spatial resolution. WAM model applied with $0.01^\circ \times 0.01^\circ$ spatial and 45 minutes of temporal resolution of wave model. The validation of this study is done by 3 month measured buoy in south east of the basin in shallow water(27 m depth). The long period simulations is done for 10 years (2001-2010), analysis are done in different coastal parts of countries in this region and summarizing of each country's coastal maximum points of wave power [31].

2. DATA

Resolution of the data is one of the most important factors in simulation's results. Data resolution being high quality makes the results more accurate. Taking this fact into consideration, in this study it is tried to gain the best quality data from international resources.

One of the most time consuming parts of this thesis was data assimilation and organization, in most parts of this thesis computer programming is used for data arrangements. This codes will be shown and detailed information will be given in Section 2.5. Fifteen years long data assimilation which has been successfully done in this study could be separated as a different project.

2.1 Geometry of Domain

Every simulation needs boundary conditions to be specified in good details so as to simulator program can recognize the boundary points specifications. While this boundary conditions could be temporal and spatial depending on the properties of the model.

First of all the geometry of the domain where the simulation is done was derived from the data resources available. There were many sources for coastline extraction of model area. The list of available resources of coastline data is arranged as shown in Table 2.1.

NOAA was recognized as the best resource for the coastline data for its resolution and the details of the data. First of all the data was in SHAPE file format which is not

Table 2.1: List of coastline data resources.

Coastline Source	Details
GSHHS (NOAA)	WGS84 datum
Digitization from Map/Chart	N/A
Sea Zone	Coarse data & not free
Ordnance Survey Master Map	Datum :British National Grid

Table 2.2: A sample boundary conditions definition file content.

Longitude	Latitude	Start & End	Land or Water
24.481304	38.993252	1	10
24.481597	38.992959	1	10
24.482477	38.992959	1	10
24.483651	38.994132	1	10
24.483357	38.994719	1	10
24.481597	38.994426	1	10
24.481304	38.994132	1	10
24.481304	38.993252	0	10

compatible with MIKE Zero, so it needed to be converted to XYZ file format with GEODAS (Version 5.0.19) program which is a product of NGDC and it is license free.

Next step of the data corrections was to make the file fixes with Excel 2013. The polygons were defined as "0" and "1" where "1" defines the polygon's vertices and "0" for the points shows the end point of the polygon and the node in mesh generation process.

Where "10" means that the point is Land also we can define the point as Water with "2" in 4th column of the data where the columns are separated by TAB. MIKE Zero module which is for mesh generation accepts only XYZ file format. A simple polygon in XYZ format could be coded as shown in Table 2.2.

The importance of the geometry edition can be understood in mesh generation. The next steps would be more visible where the mesh would be configured to have much smoother mesh in coastal parts and coarser in offshore parts of the modeling area. So that having a regular geometry which nodes and vertices are distributed in the way that the geometry of whole domain does not change, on the other hand it could be helpful for the nest stages of this thesis.

Considering the fact that there is a large number of islands in Aegean Sea and most of them are small and negligible ones from engineering aspect, so that the islands which had less area than the effecting area in this domain were eliminated from the geometry for more efficient computation of the model and making the calculations simpler and faster.

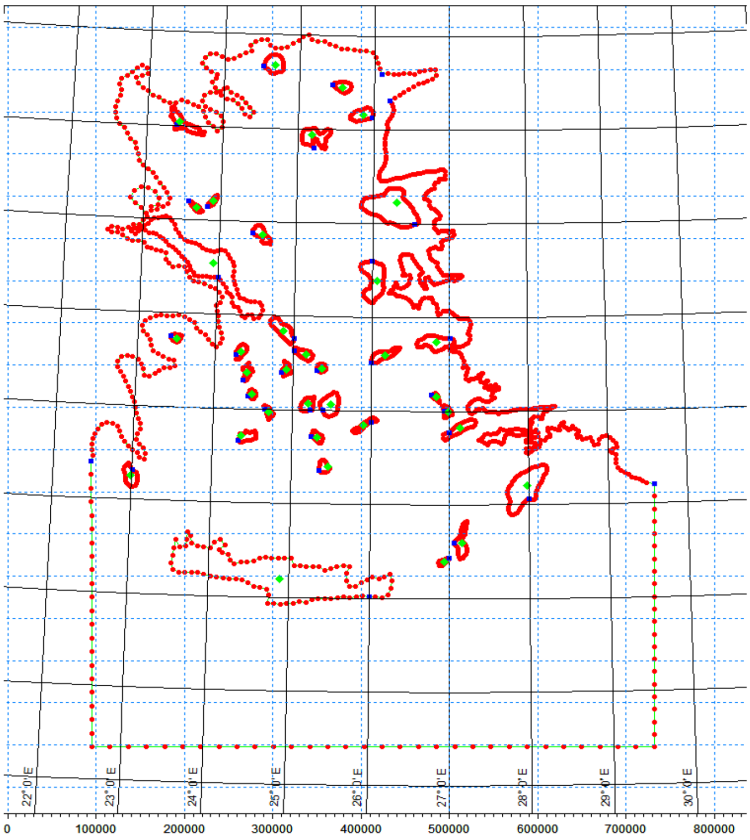

Figure 2.1: Geometry of the Aegean Sea and nodes and vertices used in mesh generation process.

As shown in the Figure 2.1 the domain is located between $33°N - 41°N$ and $22°E - 30°E$, our domain is in UTM-35 zone also nodes in Turkish coastal lines have been taken very close to each other for a smoother mesh generation.

2.2 Boundary Conditions

The boundary condition for the domain in different parts was defined quickly by studying the boundary conditions types in DHI MIKE Mesh Generator Manual. By selecting a number for every boundary it could be very simple for the future steps of the calculations for the program to recognize the boundary type and the process would be without any problems.

For this study there is 2 different type of boundaries:

- Closed Boundary
- Open Boundary

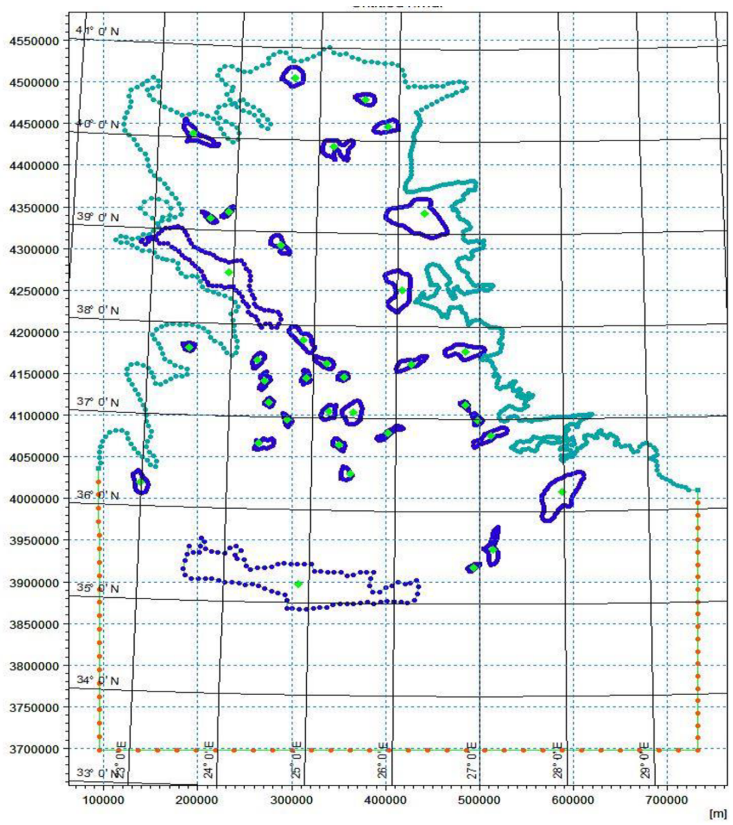

Figure 2.2: Boundary conditions of the domain.

Each boundary type is defined in mesh generation process and it's specified in nodes' attributes, where as "1" means land boundary and values for points and arcs' attributes that are equal or more than "2" are open boundary conditions.

Boundary conditions which their attribute is specified more than "2" can be later changed in the MIKE 21 SW module. In this case we didn't have any data on our boundaries to submit to MIKE 21 so that southern boundary of the domain is defined as an open boundary that can pass wave to out of the domain.

As it is shown in Figure 2.2 there are 3 attribute values for arcs available in our domain for which islands are given as "0" as default and defined as land boundaries, Also the coastline of our domain is given as "1" that it means it is land boundary, and the open boundary is given as "2".

2.3 Mesh Generation

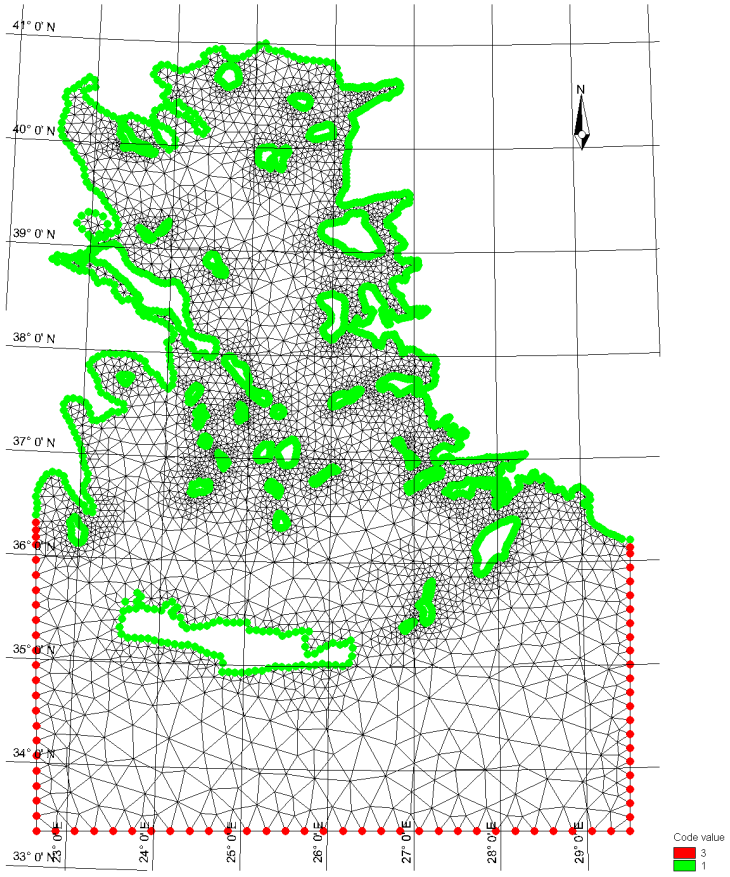

Figure 2.3: General view of unstructured mesh used for the Aegean Sea.

Mesh nodes and elements play an important role in computation time and stability of the model. So that this part of the study was conducted with high accuracy to build a high quality mesh to avoid negative consequences in the next levels of the study.

Bathymetry data is loaded in Mesh file, and then interpolated by this mesh, also the computations of the wave parameters in the domain will be done with this unstructured mesh. It was tried to produce the best mesh for the study domain.

The meshes generated by the MIKE Zero was not logical in aspect of computation time for numbers of nodes in mesh, sometimes more than 20000 nodes were recommended by the mesh generator, but modifications have taken place to decrease the number of mesh nodes.

Mesh which is used for this thesis consists of 5927 nodes and 10081 elements, the mesh is taken smoother in coastal parts and coarser in offshore to minimize the computation time.

2.4 Bathymetry Data

Bathymetry data of the Aegean Sea was obtained from EMODNet website. This data was determined by ships and other observation instruments and gathered together at this portal, also interpolated with a high resolution. EMODNet portal is user-friendly that the data could be downloaded as many different data file types, like as XYZ, NETCDF, CSV, GEOTIFF, ESRI ASCI, SD file formats.

The main advantage of this website is to obtain the data free of charge and downloading data with more flexible file formats. XYZ file format was chosen for this study because of MIKE Zero compatibility to this file type. The scattered data was applied to mesh by mesh generator module of DHI MIKE.

The resolution of the bathymetric data in this study is 0.004°. While the domain and the boundaries are defined to MIKE Zero Mesh Generator and interpolation is done, the values out of boundary conditions are excluded.

Also the points which were in the domain was interpolated by the neighboring values and set the value for those points. The data were interpolated by the mesh which was at first generated for the domain and it is obvious that no more data points involved in the calculation for taking more computation time.

Figure 2.4 shows the details of this unstructured mesh which contains mesh nodes and elements, bathymetry and boundary points' attribute values in Çeşme region of Aegean Sea. It can be obviously seen from this figure that the mesh is smoother in the nearshore parts of the domain and coarser in offshore.

Figure 2.5 shows general view of bathymetry while it could be seen in detail when it is zoomed in MIKE ZERO data viewer.

2.5 ECMWF Data

After finishing the data submission to mesh file and building a mesh file, it was time to take step into next stage of the study which was to work with MIKE 21 Spectral Wave module and to define the parameters available in this module.

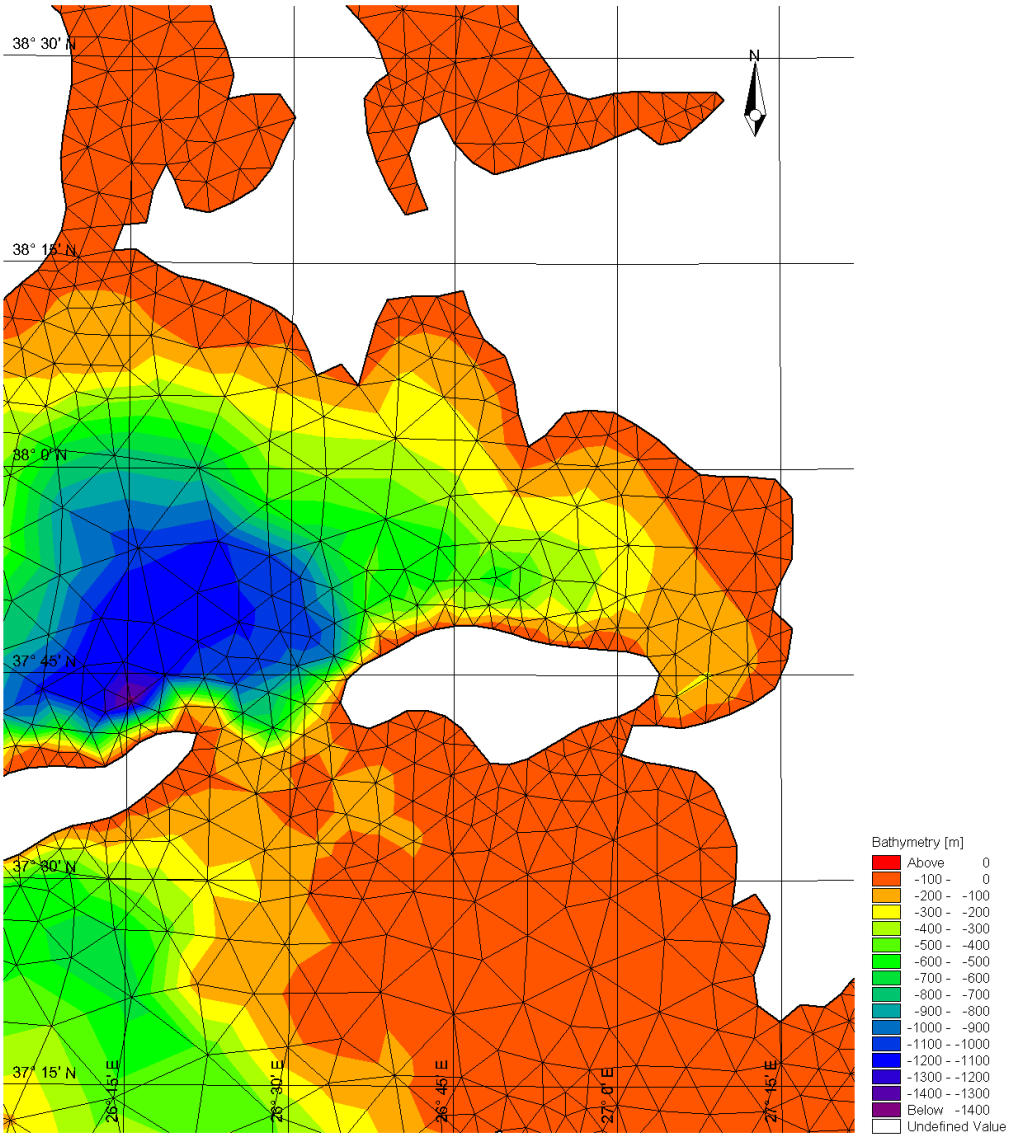

Figure 2.4: Detailed view of the bathymetry in eastern coasts of Aegean Sea.

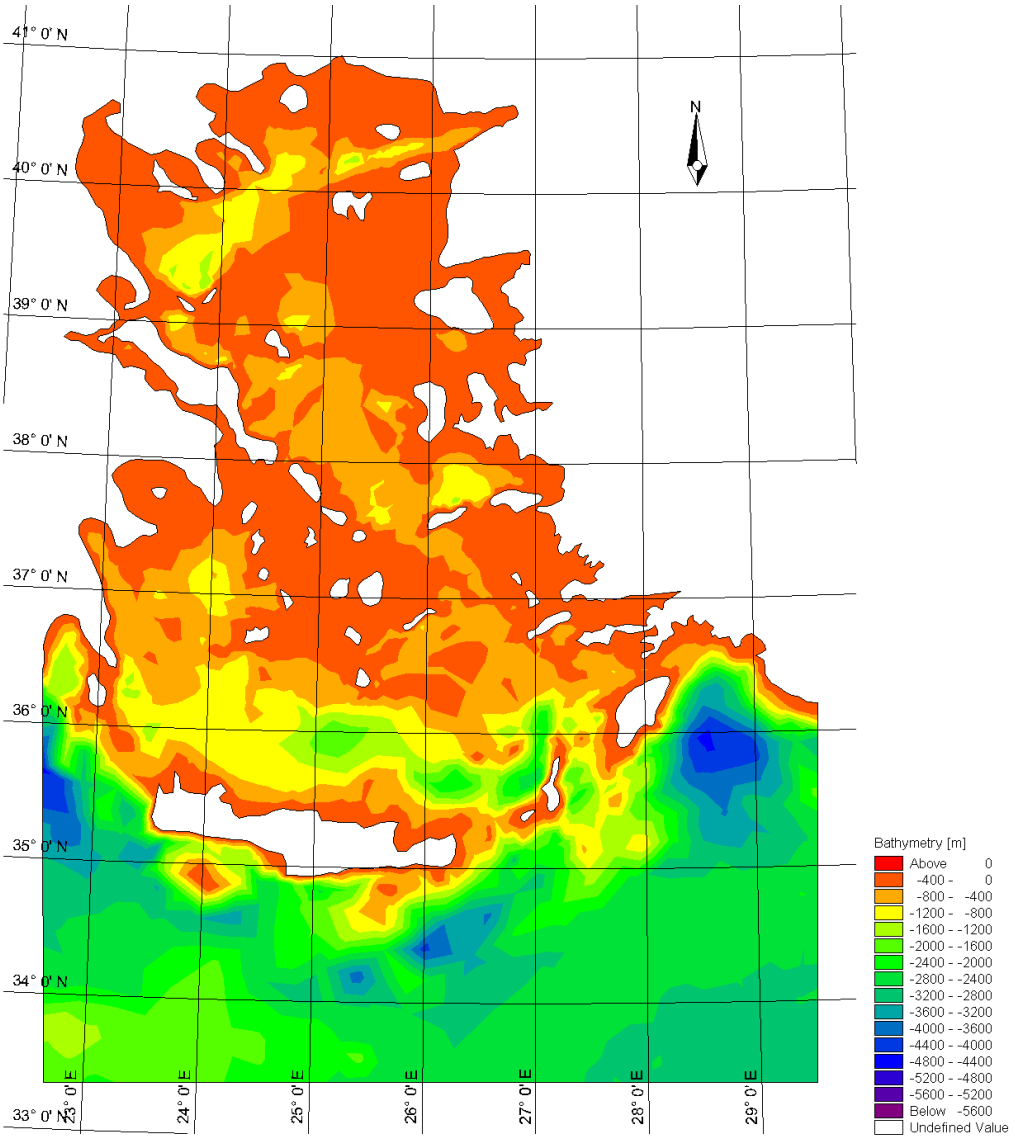

Figure 2.5: Bathymetry map of the domain.

The most important data which is compulsory for the module is wind forcing data to be loaded to program in correct form that could be accepted by MIKE 21. A great effort has been made in this phase to get the data and process to be used efficiently.

2.5.1 ERA-Interim wind data

ERA-Interim data which is the latest global atmospheric reanalysis produced by European Center for Medium-Range Weather Forecasts (ECMWF). The data coverage of this database is from January 1st 1989 until present. This data is measured by satellite every 6 hours in 24 hours, and The best resolution of the data is $0.125^\circ \times 0.125^\circ$. ERA-Interim is a large data set which provides other meteorological parameters. In this data set the wind speeds are given for 10 m height from surface in 2 directions.

2.5.2 Preparation of wind data

DFS2 file format is a Grid Series for loading data sets being changed by time. This chapter of the project consisted of these steps:

1. Downloading data files from ECMWF website
2. Changing the format of the GRIB files to CSV format
3. Writing a code for data organization
4. Creating DFS2 file format
5. Loading data in MIKE 21

Data set obtained from ECMWF is called ERA-Interim, that is the most updated and reliable data sets attainable in this field. The values are in U and V surface wind velocity components are presented as matrices that sorted by every time step. The best resolution for the grid is 0.125° and it was selected for our project.

Data was downloaded for 2 purposes and 2 time periods:

1. Data for calibration

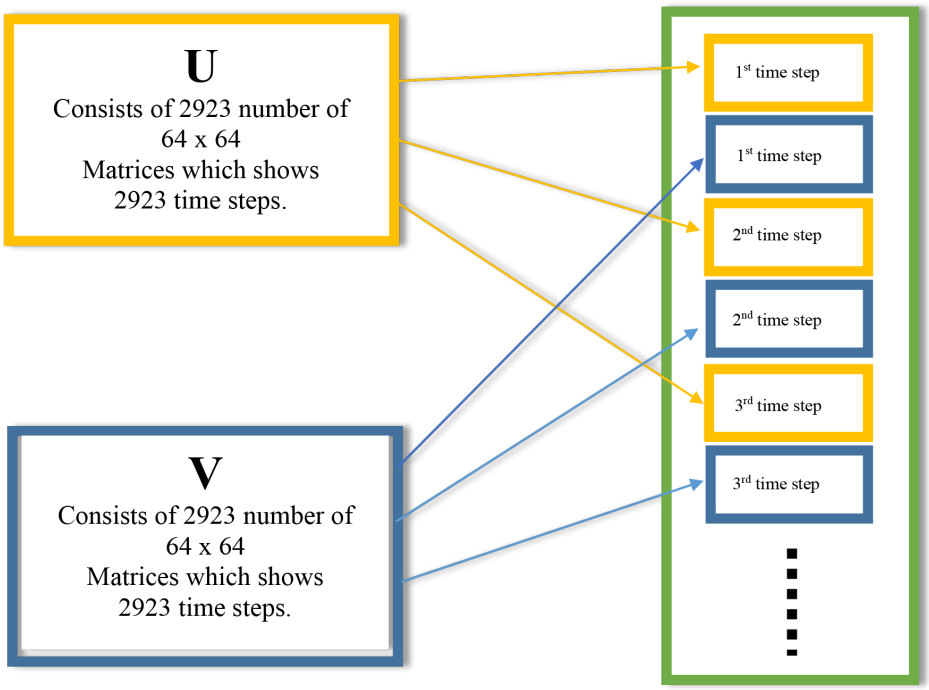

Figure 2.6: Sort of wind speed matrices in 2 directions.

- 1994-1996 (Bozcaada & Dalaman stations)
- 2011 (Athos, E1M3A, Lesvos, Mykonos,Santorini, Saronikos, Skyros stations)

2. Long-time simulation period

- 1999-2013

The data for calibration was downloaded for the area being discussed and reformatted the file from GRIB to Excel format by an open source JAVA program named Panoply.

It is essential to first mention properties of the ASCI file in first lines then referring to the values of data for every step. For this aim, Visual Basic is used to custom coding for processing the data more fast and efficiently.

The U and V wind speed components should be sorted in the form shown in Figure 2.6.

The visual basic code which is used from macro part of the Excel is shown in Figure 2.7. This code is for selection of each matrice related to wind speed in each x and y

```
Sub select_cell()

Dim i As Integer
Dim j As Integer
Dim k As Integer
Dim l As Integer
Dim m As Integer
Dim u As String
Dim v As String
Dim x As String

u = "u"
v = "v"
x = "x"
i = 0
j = 0
   Do Until i = 2925
    k = 0
    m = 0
      Sheets(u).Select
    l = (65 * i) + 1
m = ((i + 1) * 65) + 1
    Range(Cells(l, 1), Cells(m,
65)).Select
    Selection.Copy
    Sheets(x).Select
    k = (66 * j) + 1
    Cells(k, 1).Select
    ActiveSheet.Paste
    Sheets(v).Select
    Range(Cells(l, 1), Cells(m,
65)).Select
    Selection.Copy
    k = k + 66
    Sheets(x).Select
    Cells(k, 1).Select
    ActiveSheet.Paste
    i = i + 1
    j = j + 2

    Loop

End Sub
```

Figure 2.7: Visual basic code for cell selection in excel and data organization.

direction. Also taking the matrices one from wind speed in x direction and one in y direction respectively for each time step.

For numbering the title of every matrice to set the data into form of the ASCI format the code shown in Figure 2.8 is used.

The last step of DFS2 file preparation is to add the data properties text to ASCI file. A sample ASCI format which is used to define the properties of data and is used in this study is shown in Table 2.3. In this table properties of the DFS2 file is defined.

The last step of the DFS2 file creation is to import the data files which are prepared in TXT file format to be loaded into a Grid Series file in MIKE Zero.

2.6 Measured Data

Measured data is an essential part of the project which is needed to find out the accuracy of the model and to be sure of the results with a high percentage. In this study 9 stations were used to validate model, the locations of each station is shown in Figure 3.1.

```
Sub enumeration_process()


Dim i As Long
Dim n As Long
Dim m As Long

i = 0
   Do Until i = 2923
    n = (130 * i) + 1
    m = ((2 * i + 1) * 66) + 1
    tstep = i
    Cells(n, 1) = "tstep"
    Cells(m, 1) = "tstep"
    Cells(n, 2) = tstep
    Cells(m, 2) = tstep
    Cells(n, 3) = "item"
    Cells(m, 3) = "item"
    Cells(n, 4) = 1
    Cells(m, 4) = 2
    Cells(n, 5) = "layer"
    Cells(m, 5) = "layer"
    Cells(n, 6) = 0
    Cells(m, 6) = 0

    i = i + 1

    Loop

End Sub
```

Figure 2.8: Visual basic code for building z in excel and data organization.

Table 2.3: Format for MIKE DFS2 files.

1 "Title" "File Title"
2 "Dim" 2
3 "Geo" "LONG/LAT" 22 33 0
4 "Time" "EqudistantTimeAxis" "1994-01-01" "00:00:00" 1460 21600
5 "NoGridPoints" 65 65
6 "Spacing" 0.125 0.125
7 "NoStaticItems" 0
8 "NoDynamicItems" 2
9 "Item" "U" "Wind Velocity" "m/s"
10 "Item" "V" "Wind Velocity" "m/s"
11 NoCustomBlocks 0
12 "Delete" -1E-030
13 "DataType" 0

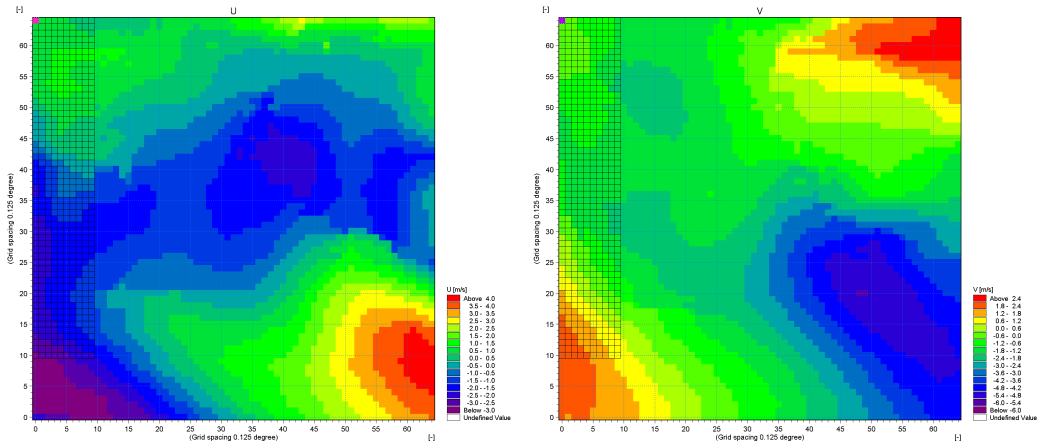

Figure 2.9: DFS2 wind data view in MIKE Zero data viewer.

There were 2 different wave parameters needed in this study to be obtained for calibration: 1. Significant Wave Height 2. Mean Wave Period

2.6.1 Buoy data of NATO-TU waves project

This data was measured nearly 10 years ago by a project done by a team members of NATO-TU Waves Project. This project was alive from 1994 to 2000 and was supported by NATO Science for Stability program. The buoys were available in Black Sea, Marmara Sea, Mediterranean Sea and Aegean Sea.

The data which were available from November 1994 to October 1996, free to access on the website of the NATO-TU waves, but the data were plotted on the image format and uploaded on the portal. Also the data were printed as GIF file formats with every 10 days data plot, so that the image processing of the data was a time consuming job.

A sample of the data plot of NATO-TU waves is shown in Figure 2.10, where the red dots and lines are the values of the parameter being discussed and the x-axis demonstrates the day of the month. After digitizing every month‘s values then the data were gathered together and a constant value was added to make the days more organized and sorted.

The data attainment was done fast while the data needed to be organized in one file for each parameter, so that 10 days interval data files were attached to each other and has been made a single file of Excel. For further analyses the data was gathered and organized in monthly and yearly periods.

The data was digitized point by point and finding the center of every scatter point to be accurately processed and exported to EXCEL file. A general view of the digitization process is shown in Figure 2.11. The was done by GetDataDigitizer (version 2.26 licensed).

There was 204 plots awaiting to be image processed by hand and it was done completely that the data is ready to be compared with the result of the MIKE 21 test results.

2.6.2 POSEIDON wave buoys data

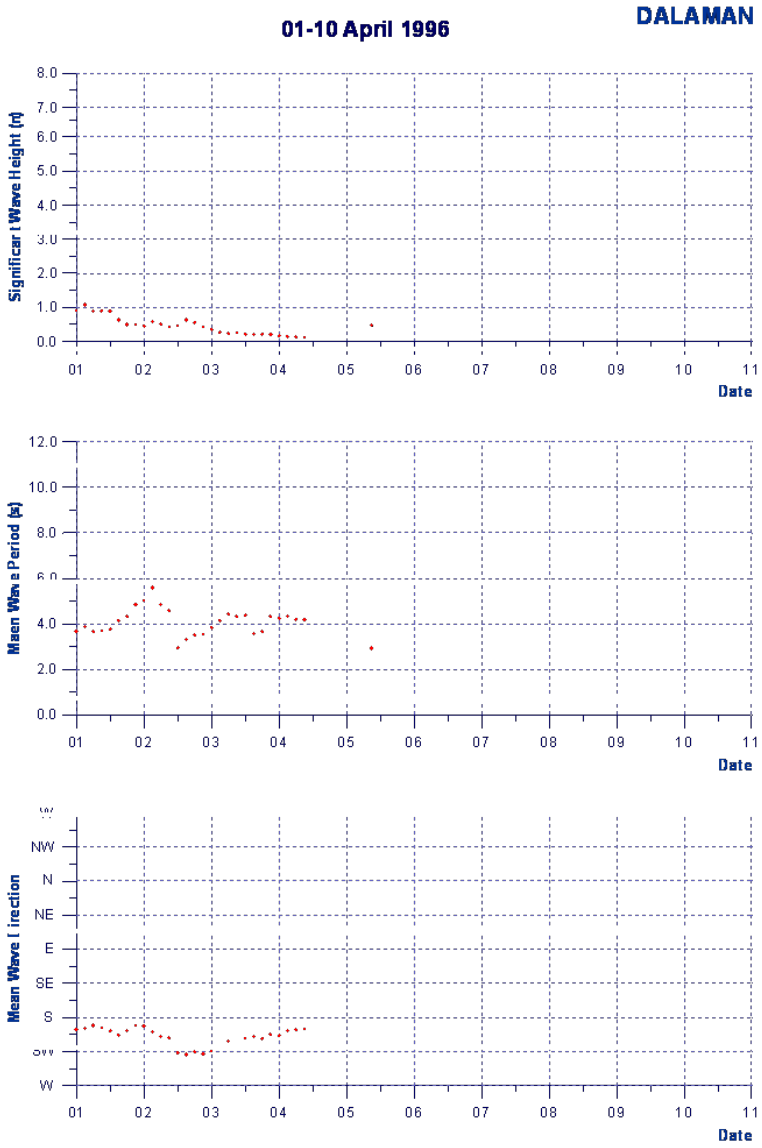

Figure 2.10: Sample image of measured data plotted in GIF file format by NATO-TU Waves.

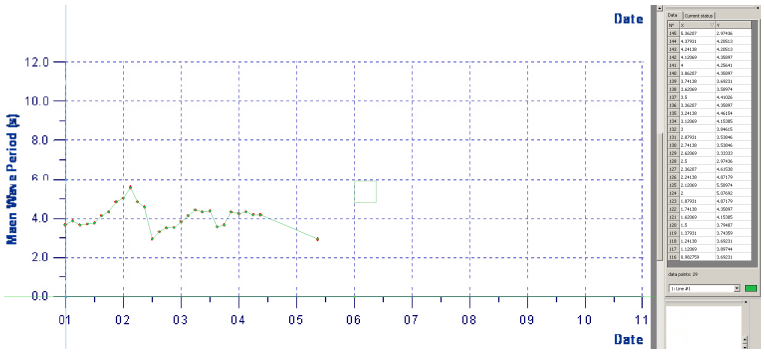

Figure 2.11: General view of the digitization steps of the NATO-TU Waves plotted data with Get Data Graph Digitizer.

POSEIDON system which is managed and developed by HCMR is a planning tool for marine protection. This network consists of buoys in Greek coastal and offshore parts which is measuring different wave and marine parameters. The measurements of the data in POSEIDON wave buoy is done with 3 hours interval.

The data source files of this station was obtained in NetCDF file format and converted to excel files to be used easily. The data source for this buoy was obtained from MyOcean website with a monthly period. There are 7 different stations located in study domain.

For every Station, monthly data downloaded and then merged with together with a program named NCO 4.4.4 which is distributed under GNU Free Documentation License, Version 1.3. This program made the whole process more easier to deal with the large number of files of these stations. NCRCAT is an operator of NCO which merges independent data files with common record dimensions into one file.

Table 2.4 shows specifications of different buoys used for calibration in this thesis. The buoy station types used in this study was wave scan Datawell directional wave rider for Dalaman and Bozcaada and multi-parametric deep water Seawatch-Wavescan type for POSEIDON wave buoy.

Table 2.4: Specifications of wave buoys used in calibration.

	Longitude	Latitude	Depth	Type
Athos	24.724	39.973	220 m	Wave-Scan
Bozcaada	26.0492	39.703	62 m	Wave-Scan
Dalaman	28.755	36.691	100 m	Wave-Scan
E1M3A	24.919	35.786	1670 m	Wave-Scan
Lesvos	25.807	39.156	130 m	Sea-watch
Mykonos	25.462	37.523	110 m	Sea-watch
Santorini	25.501	36.262	280 m	Sea-watch
Saronikos	23.569	37.610	211 m	Sea-watch
Skyros	24.464	39.113	120 m	Sea-watch

3. MODEL VALIDATION

Every model has to be validated with one or series of measured data, to define the model's reliability. The evaluation of the measured and simulated data could have a great effect on every model's success degree in estimation of the parameters.

There are many parameters needed for spectral wave model to start the computation, the most important part of this project is to estimate the accuracy of the model, this is not possible without trial and error correction of the parameters to find the best fitting parameters with the results of stations data, this process is called calibration.

3.1 MIKE 21 SW

MIKE 21 SW a new generation spectral wind-wave model is a part of the MIKE program which is developed by Danish Hydraulic Institute (DHI). This program has a high reputation across the wave hydrodynamics researchers and water resources institutes. This model which is based on unstructured meshes simulates growth, decay and transformation of wind generated waves and swell in offshore and coastal regions.

There are two main formulation for spectral wave module of MIKE 21:

- Directional decoupled parametric formulation
- Fully spectral formulation

These two formulation are different in the approach to the solution, whereas directional decoupled parametric formulation uses parameterization of the wave action conservation equation, in which the parameterization is done in the frequency domain by introducing the zeroth and first moment of the wave action spectrum as dependent variable [10].

On the other hand fully spectral formulation uses wave action conservation equation which is described in [7] and [32] where the directional-frequency wave action spectrum is the dependent variable.

3.1.1 MIKE 21 SW features

The main features of MIKE 21 SW are as follows:

- Fully spectral or directionally decoupled parametric formulations
- Source functions based on the state-of-art 3rd generation formulations
- Instationary and Quasi-stationary formulation
- Optimal degree of flexibility interpolation of bathymetry with unstructured mesh
- Effects of ice coverage(N/A in this study)
- Extensive range of output parameters

3.2 Definitions

1. Significant Wave Height, $H_{m0}(m)$;

$$H_{m0} = 4\sqrt{m_0} \tag{3.1}$$

2. Maximum wave height,$H_{max}(m)$;

   The maximum wave height H_{max} is estimated as

$$H_{max} = min(H^1_{max}, H^2_{min}) \tag{3.2}$$

   H^1_{max} is determined assuming Rayleigh distributed waves

$$H^1_{max} = H_{m0}\sqrt{\frac{1}{2}Ln(N)} \tag{3.3}$$

   where N is the number of waves estimated as $N = duration/T_{01}$. The duration is set to 3 hours (10800s). H^2_{max} is determined assuming monochromatic waves

$$H^2_{max} = d\frac{0.141063\alpha + 0.0095721\alpha^2 + 0.0077829\alpha^3}{1 + 0.0788340\alpha + 0.0317567\alpha^2 + 0.0093407\alpha^3} \tag{3.4}$$

where $\alpha = \frac{L}{d} = \frac{2\pi}{kd}$, where k is the wave number corresponding to the peak wave period and d is the water depth.

3. Peak period, $T_p(s)$;

$$T_p = \frac{1}{f_p} \tag{3.5}$$

The peak frequency f_p is calculated from one-dimensional frequency spectrum using a parabolic fit around the discrete peak. The scheme for computing the peak frequency can be formulated :

- Search through 1D frequency spectrum and obtain the index, i_p corresponding to maximum spectral density.
- Using $f_0 = f(i_p - 1)$, $f_1 = f(i_p)$, $f_2 = f(i_p + 1)$ and similarly for E_0, E_1, E_2, the peak frequency is given by

$$f_p = f(i_p - 1) - \frac{b}{2c} \tag{3.6}$$

where

$$b = \frac{(f_2 - f_0)^2(E_1 - E_0) - (f_1 - f_0)^2(E_2 - E_0)}{(f_1 - f_0)(f_2 - f_0)^2 - (f_1 - f_0)^2(f_2 - f_0)} \tag{3.7}$$

$$c = \frac{(f_1 - f_0)^2(E_2 - E_0) - (f_2 - f_0)^2(E_1 - E_0)}{(f_1 - f_0)(f_2 - f_0)^2 - (f_1 - f_0)^2(f_2 - f_0)} \tag{3.8}$$

4. Mean Period, $T_{01}(s)$;

$$T_{01} = \frac{m_0}{m_1} \tag{3.9}$$

5. Zero crossing period, $T_{02}(s)$;

$$T_{02} = \sqrt{\frac{m_0}{m_2}} \tag{3.10}$$

6. Energy averaged mean period, $T_{-10}(s)$;

$$T_{-10} = \frac{1}{\bar{f}} = \frac{m_{-1}}{m_0} \tag{3.11}$$

7. Mean wave direction, $\bar{\theta}(degree)$;

$$\bar{\theta} = 270 - tan^{-1}(\frac{b}{a}) \tag{3.12}$$

where a and b is defined as:

$$a = \frac{1}{m_0}\int_0^{2\pi}\int_0^{\infty}\cos\left(\frac{3}{2}\pi-\theta\right)E(f,\theta)\mathrm{d}f\mathrm{d}\theta \tag{3.13}$$

$$b = \frac{1}{m_0}\int_0^{2\pi}\int_0^{\infty}\sin\left(\frac{3}{2}\pi-\theta\right)E(f,\theta)\mathrm{d}f\mathrm{d}\theta \tag{3.14}$$

8. Directional standard deviation, $\sigma(degree)$:

$$\sigma = \left[2\left(1-(a^2+b^2)^{\frac{1}{2}}\right)\right]^{\frac{1}{2}}\cdot\frac{180}{\pi} \tag{3.15}$$

9. Particle velocities

The calculation of the horizontal and vertical particle velocity components u and w is based on Stokes first order theory for progressive waves, see e.g. [33]:

$$u(z,\phi) = \frac{1}{2}\omega H\frac{\cosh k(z+d)}{\sinh kh}\cos\phi \tag{3.16}$$

$$W(z,\phi) = \frac{1}{2}\omega H\frac{\cosh k(z+d)}{\sinh kh}\sin\phi \tag{3.17}$$

where ω is the cyclic angular frequency, h is wave height, k the wave number, d water depth, z vertical coordinate and ϕ the phase of the wave. Using the directionally decoupled parametric formulation the root mean square of the maximum value of two components can be calculated as

$$u_{max}(z) = \sqrt{\int_0^{2\pi}\left(2\omega\frac{\cosh k(z+d)}{\sinh kh}\right)^2 E(\theta)\mathrm{d}\theta} \tag{3.18}$$

$$W_{max}(z) = \sqrt{\int_0^{2\pi}\left(2\omega\frac{\sinh k(z+d)}{\sinh kh}\right)^2 E(\theta)\mathrm{d}\theta} \tag{3.19}$$

where $E(\theta)$ is wave energy at wave direction θ.

While using the fully spectral formulation the root mean square of the maximum value of the two components can be calculated as:

$$u_{max}(z) = \sqrt{\int_0^{2\pi}\int_0^{\infty}\left(2\omega\frac{\cosh k(z+d)}{\sinh kh}\right)^2 E(f,\theta)\mathrm{d}f\mathrm{d}\theta} \tag{3.20}$$

$$w_{max}(z) = \sqrt{\int_0^{2\pi}\int_0^{\infty}\left(2\omega\frac{\sinh k(z+d)}{\sinh kh}\right)^2 E(f,\theta)\mathrm{d}f\mathrm{d}\theta} \tag{3.21}$$

where $E(f,\theta)$ is the wave energy at wave direction θ.

The following values are included in the output:

- Maximum horizontal particle wave velocity at the sea bottom, $U_{max}(z=-d)$
- Maximum horizontal particle wave velocity at the free surface, $U_{max}(z=0)$
- Maximum vertical particle wave velocity at the free surface, $W_{max}(z=0)$
- Maximum horizontal particle wave velocity at a level, z_0, $U_{max}(z=z_0)$
- Maximum vertical particle wave velocity at a level, z_0, $W_{max}(z=z_0)$

and z_0 is defined as:

$$z_0 = d + \Delta d \tag{3.22}$$

where Δd is user-defined distance above the bed.

10. Wave power;

The energy transport for a harmonic wave is $P_{energy} = \rho g c_g E$ in magnitude, where E is the energy density and c_g is the group velocity, ρ is the density of water and g is the acceleration of gravity. In random seas the following to definitions of the wave power can be used

- Omni-directional wave power(energy sink) P_{energy}

$$P_{energy} = \rho g \int_0^{2\pi}\int_0^{\infty} c_g(f,\theta)E(f,\theta)\mathrm{d}f\mathrm{d}\theta \tag{3.23}$$

- Directional wave power(energy transport)

$$\vec{P}_{energy} = (P_{energy,x}, P_{energy,y}) \tag{3.24}$$

$$\vec{P}_{energy} = \rho g \int_0^{2\pi}\int_0^{\infty} \vec{c_g}(f,\theta)E(f,\theta)\mathrm{d}f\mathrm{d}\theta \tag{3.25}$$

$$P_{energy,x} = \rho g \int_0^{2\pi}\int_0^{\infty} c_g(f,\theta)\cos(\theta)E(f,\theta)\mathrm{d}f\mathrm{d}\theta \tag{3.26}$$

$$P_{energy,x} = \rho g \int_0^{2\pi} \int_0^{\infty} c_g(f,\theta)\sin(\theta)E(f,\theta)\mathrm{d}f\mathrm{d}\theta \qquad \textbf{(3.27)}$$

3.3 Model Parameters

MIKE 21 SW demands different parameters to run the model which is built and described in the Chapter 2 of this thesis. In this Section different model parameters will be discussed and described thoroughly.

The calculation method of MIKE 21 SW module is an important thing to know in the computation process. The computation time and calculations duration is mostly dependent on this approaches.

3.3.1 Source functions

The energy source term, S, represents the superposition of source functions describing various physical phenomena

$$S = S_{in} + S_{nl} + S_{ds} + S_{bot} + S_{surf} \qquad \textbf{(3.28)}$$

Here S_{in} represents the generation of energy by wind, S_{nl} is the wave energy transfer due non-linear wave-wave interaction, S_{ds} is the dissipation of wave energy due to white-capping, S_{bot} is the dissipation due to bottom friction and S_{surf} is the dissipation of wave energy due to depth-induced breaking.

3.3.2 Basic equations

Waves dynamics are dependent on the wave action density. The wave action density is a function of two wave phase parameters. The two wave phase parameters can be the wave number vector $\vec{k}$ with magnitude, k, and direction, θ. On the other hand wave phase parameters can also be the wave direction, θ, and either relative angular frequency,

$$\sigma = 2\pi f_r \qquad \textbf{(3.29)}$$

or the absolute angular frequency,

$$\omega = 2\pi f_a \qquad \textbf{(3.30)}$$

in the present model the wave direction, θ, and the relative angular frequency, σ, was used. The action density $N(\sigma,\theta)$, is dependent on the energy density $E(\sigma,\theta)$ by Equation 3.31.

$$N = \frac{E}{\sigma} \tag{3.31}$$

Linear dispersion relation is given for the wave propagation over slowly varying depths and currents

$$\sigma = \sqrt{gk\tanh(kd)} = \omega - \vec{k}\cdot\vec{U} \tag{3.32}$$

in which g is acceleration of gravity, d is the water depth and $\vec{U}$ is the current velocity vector. While magnitude of group velocity, c_g, of the wave energy is relative to the current is given by

$$c_g = \frac{\partial\sigma}{\partial k} = \frac{1}{2}\left(1+\frac{2kd}{\sinh(2kd)}\right)\frac{\sigma}{k} \tag{3.33}$$

The phase velocity, c, of the wave relative to the current is given by

$$c = \frac{\sigma}{k} \tag{3.34}$$

The frequency spectrum is limited to the range between a minimum and maximum frequency, (σ_{min},σ_{max}). The frequency spectrum is split up into a deterministic prognostic part for frequencies lower than a cut-off frequency and an analytical diagnostic part for frequencies higher than the cut-off frequency. A dynamic cut-off frequency depending on the local wind speed and the mean frequency is used as in the WAM Cycle 4 model. The deterministic part of the spectrum is determined solving the transport equation for wave action density using numerical methods. Above the cut-off frequency limit of the prognostic region, a parametric tail is applied

$$E(\sigma,\theta) = E(\sigma_{max},\theta)\left(\frac{\sigma}{\sigma_{max}}\right)^{-m} \tag{3.35}$$

where m is a constant. In MIKE 21 SW 2012, $m = 5$ is applied. The maximum prognostic frequency is determined as

$$\sigma_{cut-off} = min\left[\sigma_{max}, max(2.5\bar{\sigma}, 4\sigma_{PM})\right] \tag{3.36}$$

where σ_{max} is the maximum discrete frequency used in the deterministic wave model, $\bar{\sigma}$ is the mean relative frequency and $\sigma_{PM} = g/(28u_{10})$ is the Pierson-Moskowitz peak frequency for fully developed waves (10 U is the wind speed at 10 m above the mean sea level) The diagnostic tail is used in the calculation of the non-linear transfer and in the calculation of the integral parameters used in the source functions. Below the minimum frequency the spectral densities is assumed to be zero.

As standard the mean frequency, used in 3.36, is calculated based on the whole spectrum. For swell dominated wave conditions this can result in a too low cut-off frequency and thereby an underestimation of the local generated wind waves. The predictions can be improved by calculation the mean frequency based on only the wind-sea part of the spectrum.

3.3.3 Wave action conservation equations

The governing equation for calculation is wave action balance equation in Cartesian coordinates [9].

In horizontal Cartesian coordinates, the conservation equation for wave action can be written as

$$\frac{\partial N}{\partial t} + \nabla \cdot (\vec{v} N) = \frac{S}{\sigma} \tag{3.37}$$

where $N(\vec{x}, \sigma, \theta, t)$ is the action density, t is the time, $\vec{x} = (x, y)$ is the Cartesian coordinates, $\vec{v} = (c_x, c_y, c_\sigma, c_\theta)$ is the propagation velocity of a wave group in the four dimensional phase space $\vec{x}$, σ and θ, and S is the source term for energy balance equation. ∇ is the four-dimensional differential operator in the $\vec{x}$, σ and $\theta - space$. The four characteristics propagation speeds are given by

$$(c_x, c_y) = \frac{\mathrm{d}\vec{x}}{\mathrm{d}t} = \vec{c}_g + \vec{U} \tag{3.38}$$

$$c_\sigma = \frac{\mathrm{d}\sigma}{\mathrm{d}t} = \frac{\partial \sigma}{\partial d}\left[\frac{\partial d}{\partial t} + \vec{U} \cdot \nabla_{\vec{x}} d\right] - c_g \vec{k} \cdot \frac{\partial \vec{U}}{\partial s} \tag{3.39}$$

$$c_\theta = \frac{\mathrm{d}\theta}{\mathrm{d}t} = -\frac{1}{k}\left[\frac{\partial \sigma}{\partial d}\frac{\partial d}{\partial m} + \vec{k} \cdot \frac{\partial \vec{U}}{\partial m}\right] \tag{3.40}$$

Here, s is the space co-ordinate in wave direction θ, and m is a coordinate perpendicular to s. $\nabla_{\vec{x}}$ is the two dimensional differential operator in the $\vec{x}$-space.

3.3.4 Spectral discretizaion

3.3.4.1 Frequency discretization

The dependent variable in the spectral mode is the directional-frequency wave action spectrum in each node point. In this step the discrete frequencies and directions used to resolve the wave action spectrum in the computations are specified.

Two types of discretization are available; logarithmic and equidistant distribution. It is recommended by MIKE 21 to always use the logarithmic distribution of frequencies, which is given by

$$f_n = f_0 c^n \quad , n = 1, 2, 3, ... \tag{3.41}$$

where f_n is the frequency, f_0 minimum frequency and c the frequency factor (= 1.1 as default). The frequency range should cover wave frequencies expected to occur in the computational domain. For typical offshore applications wave periods from 4 s to 25 s (i.e. frequencies from 0.25 Hz to 0.04 Hz) are found.

3.3.4.2 Directional discretization

Two types of discretisation are available; 360 degree rose and directional sector. The 360 degrees compass rose is typically chosen for varying wind/wave/swell directions. However, if the expected wind/wave/swell directions fall within a predefined range of directions, the choice of a directional sector type of discretisation is recommended by MIKE 21 as it reduce the computational time.

3.3.4.3 Separation of wind-sea and swell

The separation of wind-wave and swell is neglected in this thesis and both of them are calculated within the wave power.

3.3.5 Solution technique

The discretization in spatial and spectral space is performed using cell-centered finite volume method. In the geographical domain, a mesh is used which is divided the

domain by triangles, and nodes and elements are used in the mesh. Every element is interpolated on its own length. The integration in time is based on a fractional step approach.

Firstly, a propagation step is performed calculating an approximate solution at the new time level by solving the basic conservation equations without the source functions. Secondly, a source function step is performed calculating the new solution from the estimated solution taking into account only the effect of the source functions.

3.3.5.1 Algorithms for discretization in geographical and spectral domain

The simulation time and accuracy can be controlled by specifying the order of the numerical schemes which are used in the numerical calculations. The schemes for discretization in the geographical domain and the spectral domain can be specified.

The order of discretization in spatial space is divided into two type in MIKE 21 SW:

- First order scheme
- Higher order scheme

A first-order technique could be faster but less accurate, while selecting higher order technique in this thesis made it take much more time of calculation. In here detailed numerical solution techniques which is implemented in this study would be discussed and related formulations will be mentioned.

In frequency space, a logarithmic discretization is used

$$\sigma_1 = \sigma_{min} \quad \sigma_1 = f_\sigma \sigma_{l-1} \quad \Delta\sigma_1 = \sigma_{l+1} - \sigma_{l-1} \quad l = 2, N_\sigma \tag{3.42}$$

where f_σ is a given factor,σ_{min} is the minimum discrete angular frequency and N_σ is the number of discrete frequencies. In the directional space, an equidistant discretization is used

$$\theta_m = (m-1)\Delta\theta \quad \Delta\theta_m = \frac{2\pi}{N_\theta} \quad m = 1, N_\theta \tag{3.43}$$

where N_θ is the number of discrete directions. The action density is represented as a piece wise constant over discrete intervals, $\Delta\sigma_1$ and $\Delta\theta_m$, in the frequency and directional space.

Integration of the Equation (3.37) over area A_i of the i-th element, the frequency increment $\Delta\sigma_1$ and directional increment $\Delta\theta_m$ give

$$\begin{aligned}\frac{\partial}{\partial t}\int_{\Delta\theta_m}\int_{\Delta\sigma_1}\int_{A_i} N\mathrm{d}\Omega\mathrm{d}\sigma\mathrm{d}\theta - \int_{\Delta\theta_m}\int_{\Delta\sigma_1}\int_{A_i}\frac{S}{\sigma}\mathrm{d}\Omega\mathrm{d}\sigma\mathrm{d}\theta \\ = \int_{\Delta\theta_m}\int_{\Delta\sigma_1}\int_{A_i}\nabla\cdot(\bar{F})\mathrm{d}\Omega\mathrm{d}\sigma\mathrm{d}\theta\end{aligned} \tag{3.44}$$

where Ω is an integration variable defined on A_i and $\bar{F} = (F_x, F_y, F_\sigma, F_\theta) = \bar{v}N$ in the convective flux. The volume integrals on the left-hand side of Equation (3.44) are approximated by one point quadrature rule. Using divergence theorem, the volume integral on the right-hand side of Equation (3.44) can be replaced by integral over the boundary of the volume in the $\bar{x}$, σ,θ-space and these integrals are evaluated using a mid-point quadrature rule. So that Equation (3.44) can be written

$$\begin{aligned}\frac{\partial N_{i,l,m}}{\partial t} = &-\frac{1}{A_i}\left[\sum_{p=1}^{NE}(F_n)_{p,l,m}\Delta l_p\right] \\ &-\frac{1}{\Delta\sigma_1}\left[(F_\sigma)_{i,l+\frac{1}{2},m} - (F_\sigma)_{i,l-\frac{1}{2},m}\right] \\ &-\frac{1}{\Delta\theta_m}\left[(F_\theta)_{i,l,m+\frac{1}{2}} - (F_\theta)_{i,l,m-\frac{1}{2}}\right] + \frac{S_{i,l,m}}{\sigma_l}\end{aligned} \tag{3.45}$$

where NE is the total number of edges in the cell(NE=3 for triangles). $(F_n)_{p,l,m} = (F_x n_x + F_y n_y)_{p,l,m}$ is the normal flux through the edge p in the geographical space with length $\Delta l_p \cdot \vec{n} = (n_x, n_y)$ is the outward pointing unit normal vector of the boundary in the geographical space. $(F_\sigma)_{i,l+\frac{1}{2},m}$ and $(F_\theta)_{i,l,m+\frac{1}{2}}$ are the flux through the face in the frequency and directional space, respectively.

3.3.5.2 Propagation step

The propagation is carried out by an explicit Euler scheme. To overcome the severe stability restriction using an explicit scheme, a multi-sequence integration scheme is employed following the idea by [34]. Here, the maximum time step is increased by locally employing a sequence of integration steps, where the number of levels (steps) may vary from element to element.

Convective flux in geographical space The convective flux in geographical space is derived using either a first-order up-winding scheme or a higher-order scheme. The convective flux at the edge between element i and j is given by is given by

The order of numerical scheme can be changed from the module and this will lead to computation duration change. In this study the higher order technique is used.

3.3.6 Wind forcing

Wind Data format used in this study is 2-dimensional velocities which is loaded by DFS2 file format to MIKE 21 SW. In this file the wind speed in every time step consists of U_{10} and V_{10}.

A "coupled" formulation means the momentum transfer from the wind to the waves or drag depends not only on the wind but also on the waves according to the formulation in [9]. Thus, the "coupled" formulation is a sea-state dependent roughness similar to the community WAM Cycle 4 wave model. The default value of the background roughness Charnock parameter is 0.01.

3.3.7 Energy transfer

The quadruplet-wave interaction controls

- the shape-stabilization of the high-frequency part of the spectrum
- the downshift of energy to lower frequencies
- frequency-dependent redistribution of directional distribution functions

The quadruplet-wave interaction in the spectral wave module is described by the accepted approximate Discrete Interaction Approximate (DIA), [9]. The DIA has been found quite successful in describing the essential features of a developing wave spectrum.

3.3.8 Wave breaking

Depth-induced breaking (or surf breaking) occurs when waves propagate into very shallow areas, and the wave height can no longer be supported by the water depth. The γ used in this study is applied by specified gamma.

3.3.9 Bottom friction

A constant friction factor f_w in which the friction coefficient is calculated as

$$C_f = f_w u_b \tag{3.46}$$

where u_b is the root mean square wave orbital velocity at the bottom given by

$$u_b = \left[2 \int_{f_1}^{f_{max}} \int_{\theta} \frac{\bar{\sigma}^2}{\sinh^2(kh)} E(f,\theta) \mathrm{d}\theta \mathrm{d}f \right]^{\frac{1}{2}} \tag{3.47}$$

The default value for f_w is $0.015 \times \sqrt{2} = 0.021$.

A constant geometric roughness size k_N, as suggested by [35] in which the friction coefficient is calculated by Equation (3.46) and the friction factor is calculated using the expression of [36]

$$f_w = \exp^{-5.977+5.213(\frac{a_b}{k_N})^{-0.194}} \frac{a_b}{k_N} \geq 2.0163890.24 \frac{a_b}{k_N} < 2.016389 \tag{3.48}$$

Here a_b is the orbital displacement at the bottom given by

$$a_b = \left[2 \int_{f_1}^{f_{max}} \int_{\theta} \frac{1}{\sinh^2(kh)} E(f,\theta) \mathrm{d}\theta \mathrm{d}f \right]^{\frac{1}{2}} \tag{3.49}$$

The default value for k_n is 0.04 m. This value was suggested by Weber, 1991 as being compatible with the flow conditions for a range of swell and wind sea spectra.

3.3.10 White-capping

The mathematical development of a whitecap model can be traced to [17]. Assuming that the mechanism for whitecap dissipation is pressure induced decay, he obtained a dissipation source function that is linear in both the spectral density and the frequency

$$S_{ds} \approx -\omega E \tag{3.50}$$

With the introduction of the Janssen's description for the wind input, it was realized [6] that the dissipation source function needs to be adjusted in order to obtain a proper

balance between wind input and dissipation at high frequencies. Thus, the formulation introduced by [9] was modified as

$$S_{ds}(f,\theta) = -C_{ds}\left(\frac{\widehat{\alpha}}{\widehat{\alpha}_{PM}}\right)^{m}\left\{(1-\delta)\frac{k}{\bar{k}}+\delta\left(\frac{k}{\bar{k}}\right)^{2}\right\}\bar{\sigma}E(f,\theta) \tag{3.51}$$

C_{ds}, δ and m are constants. In WAM cycle 4 the values for C_{ds}, δ and m are respectively, 4.1×10^{-5}, 0.5 and 4. In the present implementation the tunable constants are $C^{*}_{ds} = C_{ds}/(\alpha_{PM})^{4}$ and δ while $m = 4$. The default values for while m = 4. The default values for C^{*}_{ds} and δ are respectively, 4.5 and 0.5.

Also $\widehat{\alpha}$ is the overall steepness of wave field and $\widehat{\alpha}_{PM}$ is the value of $\widehat{\alpha}$ for the Pierson-Moskowitz spectrum. The overall steepness is defined as

$$\widehat{\alpha} = \bar{k}\sqrt{E_{tot}} \tag{3.52}$$

where E_{tot} is the total energy of energy spectrum The formulation of the source term due to whitecapping is as standard applied over the entire spectrum and the integral wave parameters used in the formulation is calculated based on the whole energy spectrum

$$\bar{\sigma} = 2\pi\bar{f} = 2\pi\left(\frac{\int_0^{2\pi}\int_0^{\infty}E(f,\theta)f^{p}\sigma\mathrm{d}f\mathrm{d}\theta}{\int_0^{2\pi}\int_0^{\infty}E(f,\theta)\mathrm{d}f\mathrm{d}\theta}\right)^{p_\sigma} \tag{3.53}$$

$$\sqrt{\bar{k}} = \left(\frac{\int_0^{2\pi}\int_0^{\infty}E(f,\theta)(\sqrt{k})^{p_k}\mathrm{d}f\mathrm{d}\theta}{\int_0^{2\pi}\int_0^{\infty}E(f,\theta)\mathrm{d}f\mathrm{d}\theta}\right)^{p_k} \tag{3.54}$$

where $p_\sigma = p_k = -1$ is applied. The integrals are calculated by a split into a resolved part (prognostic region) and unresolved part (deterministic region).

To improve the the whitecapping for wave conditions with a combination of wind-sea and swell proposed a revised formulation of whitecapping. Here Equation (3.51) is still applied but the mean relative angular frequency and the mean wave number are calculated using Equations (3.53 & 3.54), respectively, with $p_\sigma = p_k = 1$ and the default values for C^{*}_{ds} and δ are changed to 2.1 and 0.6, respectively.

3.3.11 Parameters used in model

Table 3.1: Model parameters specified after calibration.

Time			
No. Time Steps		Different Time Steps used for different stations	
Time step interval		600 sec	
Spectral Wave Model			
Basic Equations	Spectral Formulation	Full Spectral Formulation	
	Time Formulation	Instationary Formulation	
Spectral Discretization	Frequency Discretization	Discretization Type	Logarithmic
		No. of Frequencies	25
		Minimum Frequency	0.055
		Frequency Factor	1.1
	Directional Discretization	Discretization type	360 degree rose
		Number of directions	16
	Separation of Wind-Sea & Swell	Type of separation	No separation
Solution Technique	Instationary formulation	Geographical Space Discretization	Higher Order
		Max No. Of levels in transport calculation	32
		Number of steps in source calculation	1
		Minimum time step	0.01
		Maximum time step	600
Wind Forcing	Type	U and V components DFS2	
Energy Transfer	Type	Include quadruplet-wave interaction	
Wave Breaking	Specified Gamma γ	Constant	0.8
	Alpha α	Constant	1
Bottom Friction	Nikuradse roughness k_N	Constant	0.04
Whitecapping	Dissipation coefficient C_{dis}	Constant	2
	Dissipation coefficient δ	Constant	0.8
Initial Condition	Zero Spectra		

Table 3.1 shows the MIKE 21 SW parameters and the values given in this study for the simulation after the calibration process. Table 3.1 shows the MIKE 21 SW parameters and the values given in this study for the simulation after the calibration process.

3.4 Model Output Formats

MIKE 21 SW is capable of producing wave characteristics output files in different formats which makes this program very flexible for the further analysis and evaluation of the model. The output formats of MIKE 21 SW could be in 3 different formats:

- Point series
  - Selected field data in geographical defined points
  - The geographical co-ordinates are either given from the dialog or from an ASCII file
- Line series
  - Selected field data in geographical defined lines
  - The geographical co-ordinates are either given from by dialog or from an ASCII file
- Area series
  - Selected field data for the defined area in domain
  - The coordinates of the area is entered from dialog

3.5 Calibration Results

A vital part of a model to be proven and accepted is the calibration and the comparison of the measured and simulated values. Every model needs to be investigated if it is matching the observed data or not. For this purpose in this thesis, The comparisons is done by the figures and printing the values of the measured and simulated values derived from model in a figure, in the second part of the calibration investigation the statistical measures are done for Significant Wave Height (H_s) and Mean Wave Period

(T_{01}). Detailed information of the data is given in every comparison figure for each station.

The simulated data for each station is gained from model by entering the same coordinates of the stations and obtaining DFS0 file format consisting of the 2 wave characteristics parameters (SWH & MWP), then the raw data taken from model was exported to Excel to be compared with the observed data.

An important point to be mentioned in here, is that the simulations were done with 10 minutes interval, so that the temporal resolution of the output data was high enough to cover each observed data.

Locations of the wave buoys are shown in Figure 3.1. The distribution of the buoys for calibration is very good for testing the results of the model with observed data. The buoys which are used in this thesis for calibration are the all available buoys in Aegean Sea.

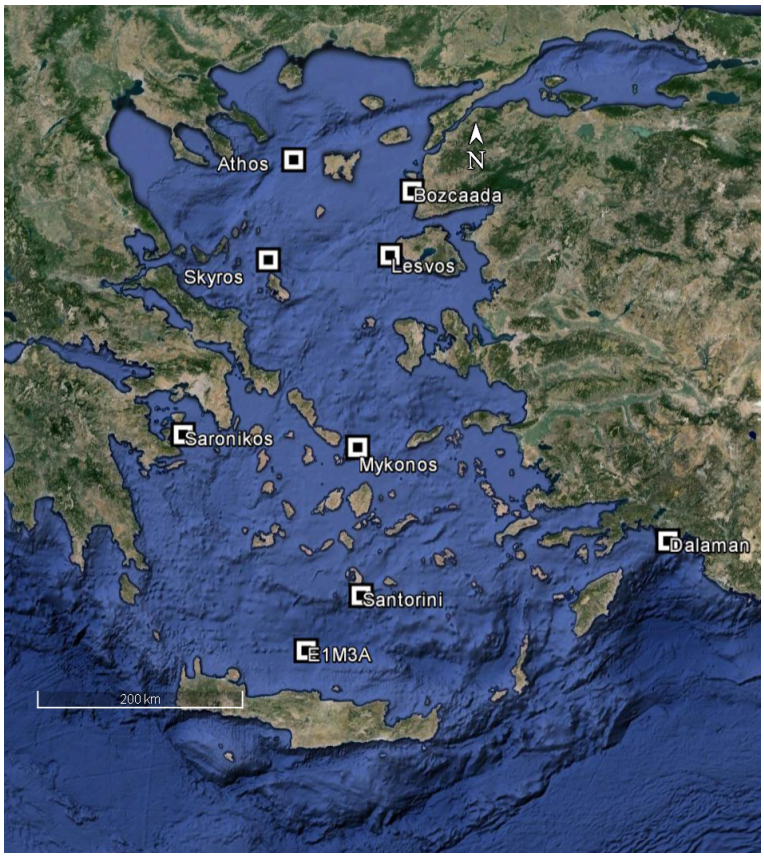

Figure 3.1: Locations of the buoys in Aegean Sea used as measured data.

The comparison of simulated and observed data is shown in Figure 3.2, blue dots show observation data values and red line shows the simulation result for 2011 year for Athos station. Simulated significant wave heights have matched measured values in most of the cases.

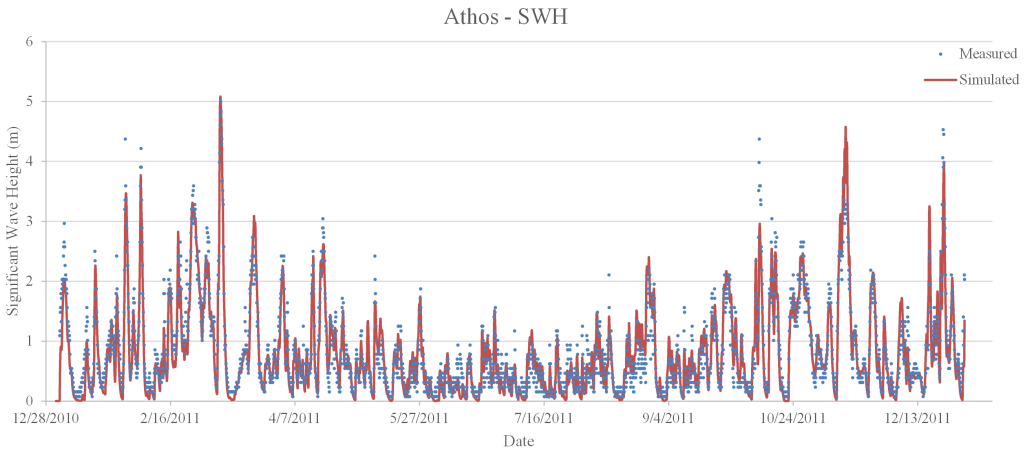

Figure 3.2: Comparison of the simulated and measured significant wave height for Athos station.

As it can be seen from Figure 3.3 that the fluctuations of simulated mean wave period is nearly matching the observed data.

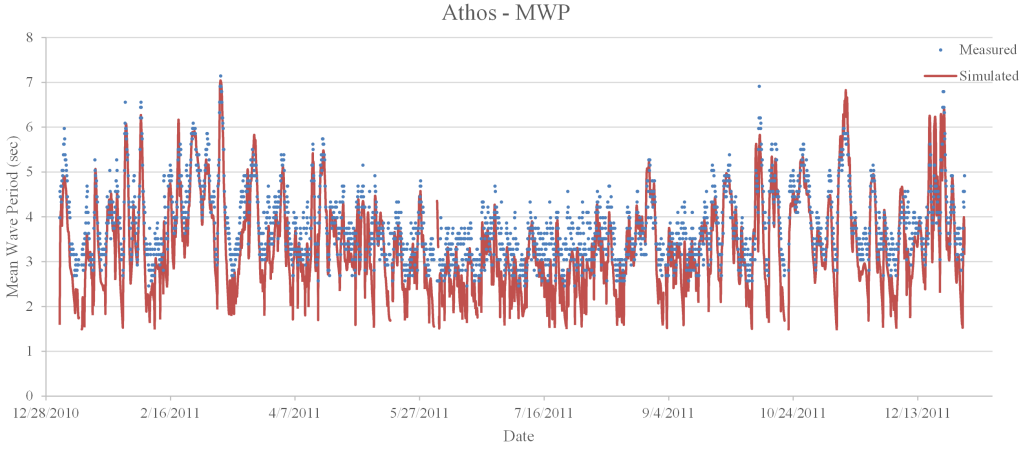

Figure 3.3: Comparison of the simulated and measured mean wave period for Athos station.

Though the data available for Bozcaada was not enough to decide on the model with that small number of data but comparison is done for both SWH and MWP for this station. The values obtained for the correlation coefficient and other statistical

parameters show a better closeness for SWH than MWP for this station, though both of the modeled data for this station has less relation with the observed data in contrast to Dalaman and E1M3A stations. It is possible to investigate the difference of the stations agreement with the model by taking their characteristics like depth and location into account. An important point which should be noted in here is that in some other researches done on wave modeling, the calibration results did not show a good agreement for the station nearshore.

Figure 3.4 and Figure 3.5 show the comparison of the measured and simulated data of Bozcaada station for SWH and MWP respectively.

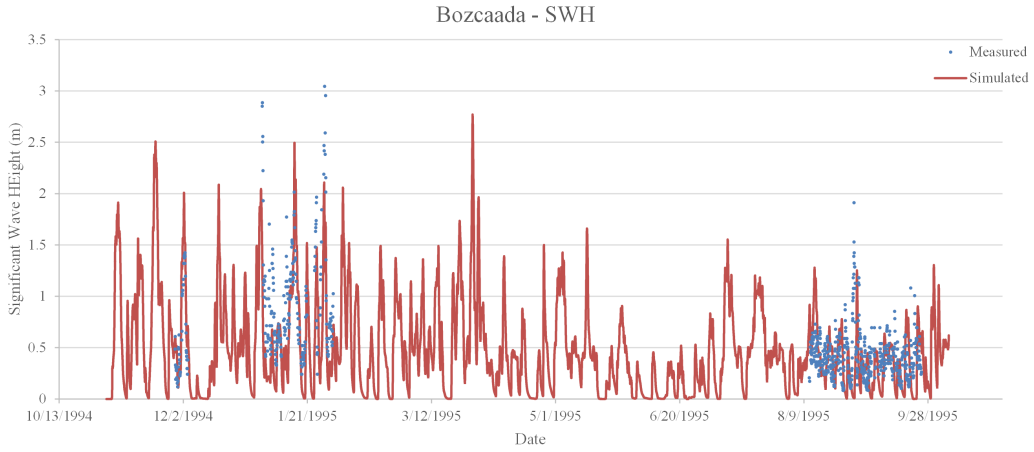

Figure 3.4: Comparison of the simulated and measured significant wave height for Bozcaada station.

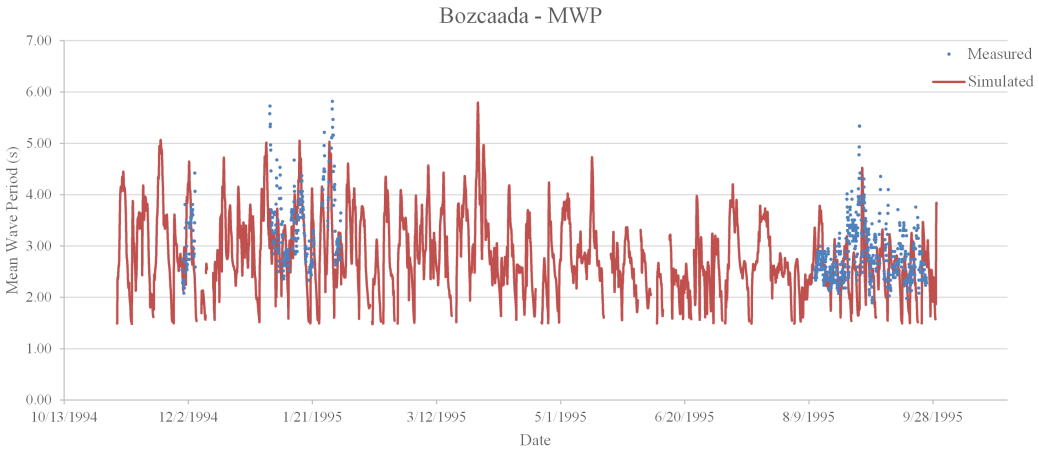

Figure 3.5: Comparison of the simulated and measured mean wave period for Bozcaada station.

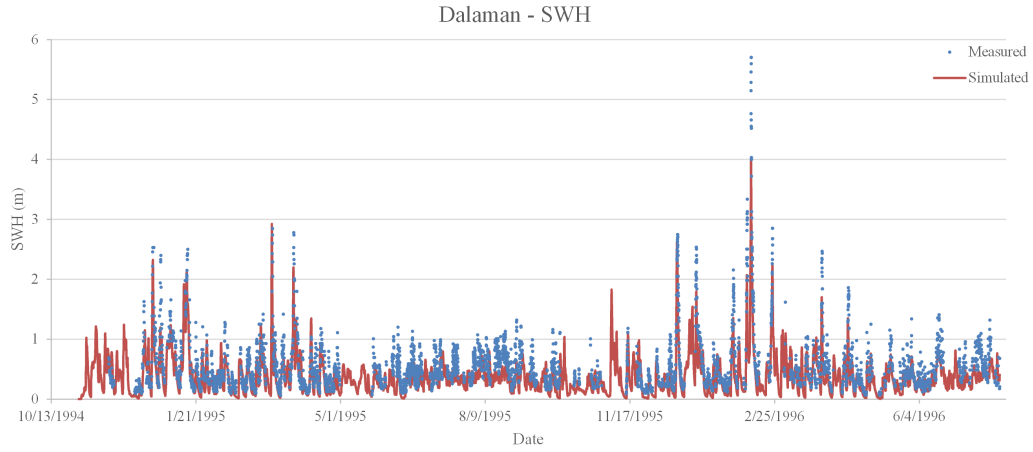

Figure 3.6: Comparison of the simulated and measured significant wave height for Dalaman station.

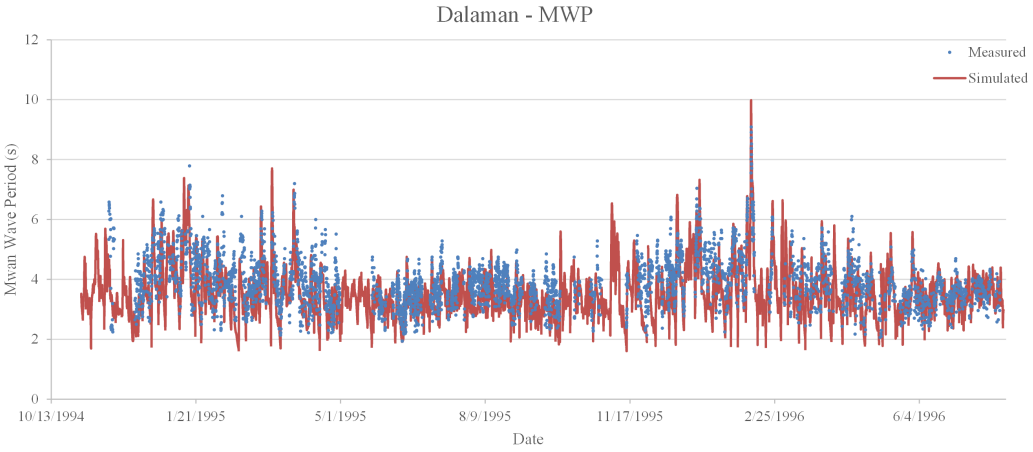

Figure 3.7: Comparison of the simulated and measured mean wave period for Dalaman station.

Figure 3.6 demonstrates the simulated and measured in Dalaman station. The data was available for nearly 20 months, significant wave height data for this station shows that there is higher magnitudes in winter season in contrast to summer. On the other hand the peak points of the observation data is covered by simulation values but in only one point in this duration the model could not estimate the extremely high wave height.

Mean wave period estimations of the model are in a good agreement with the observed data in Dalaman station as shown in Figure 3.6.

The data provided from MyOcean portal and originated from POSEIDON system, is available for year 2011, so the data was not fully covering the year but the regularity of the data was acceptable.

Figure 3.8 shows the data comparison of the observed and simulated data for E1M3A, the simulated significant wave heights cover the extreme values of observed data i.e. the peak points of the measured data matching with the simulation results.

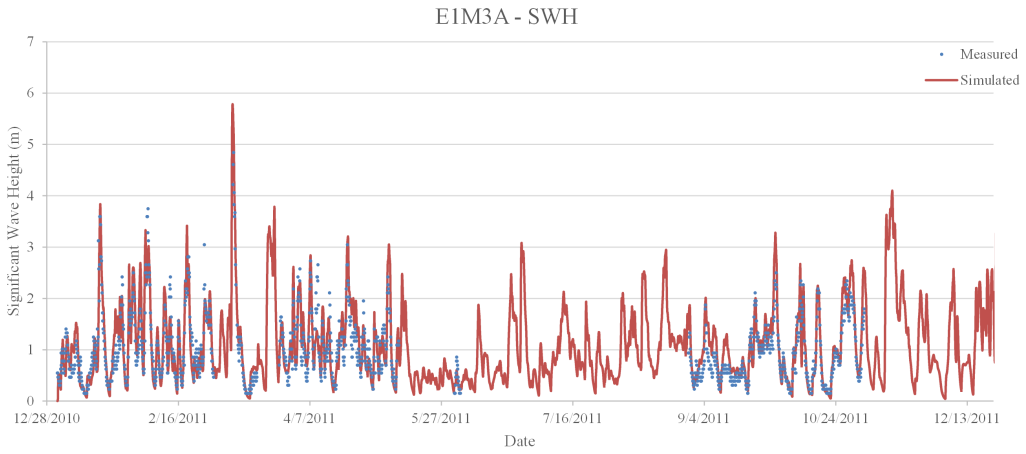

Figure 3.8: Comparison of the simulated and measured significant wave height for E1M3A station.

The second wave characteristic parameter investigated in this study is mean wave period, while the closeness of model results and observations are not as well as the significant wave height was, but the simulations and observation values are in a good agreement with each other for this station. Figure 3.9 exhibits the results of the calibration for the E1M3A for MWP.

Simulation data for significant wave height for Lesvos station show a high correlation with observed data. As shown in Figure 3.10 simulation in Lesvos has given a high accuracy of the simulation. The data obtained from MIKE 21 SW for this point is in a good agreement with observed data. The maximum significant wave height reaches 3.2 m which data from simulation has a higher value for this point.

The observation data for this station is unavailable for May 5th to June 20th 2011 but total agreement between measured and simulated data is in a good condition. The

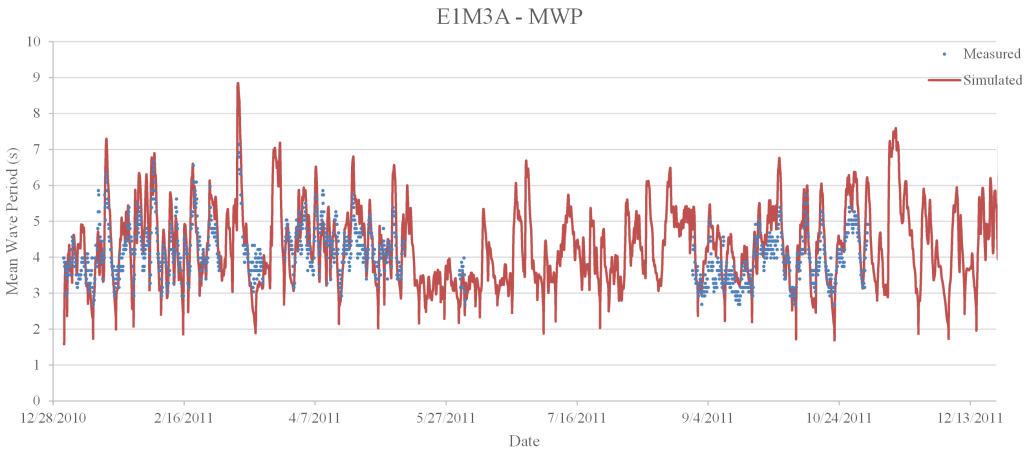

Figure 3.9: Comparison of the simulated and measured mean wave period for E1M3A station.

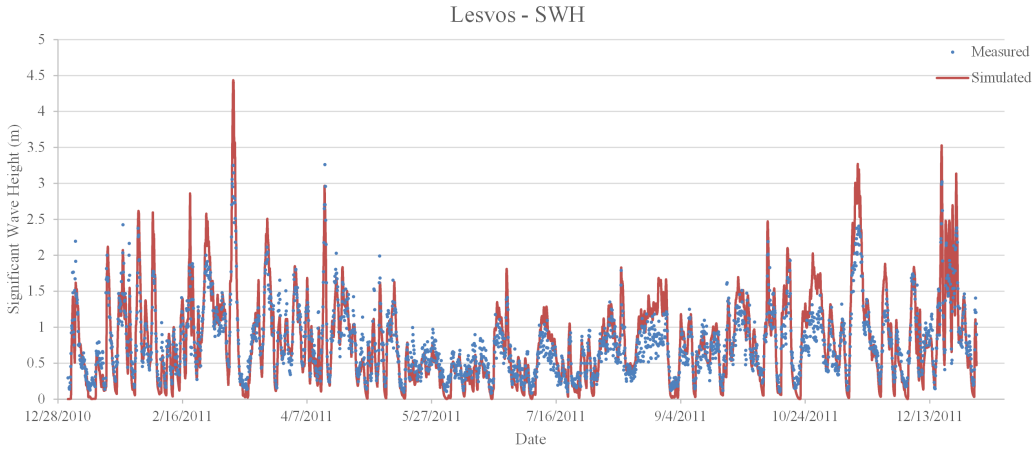

Figure 3.10: Comparison of the simulated and measured significant wave height for Lesvos station.

simulation result for this station shows that the simulation has reached the maximum points of measured data.

Most of the values of simulated and measured data are matching together with high accuracy in this station. The sudden variations are predicted by the simulations with a high accuracy. Figure 3.12 shows both data values and their date from January 1st to December 31st of 2011. The results of simulated data with measured data is quite good.

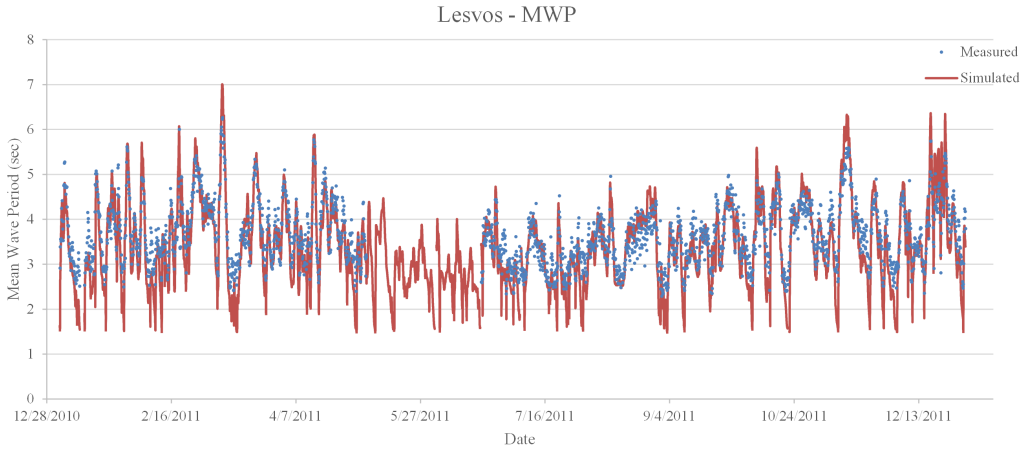

Figure 3.11: Comparison of the simulated and measured mean wave period for Lesvos station.

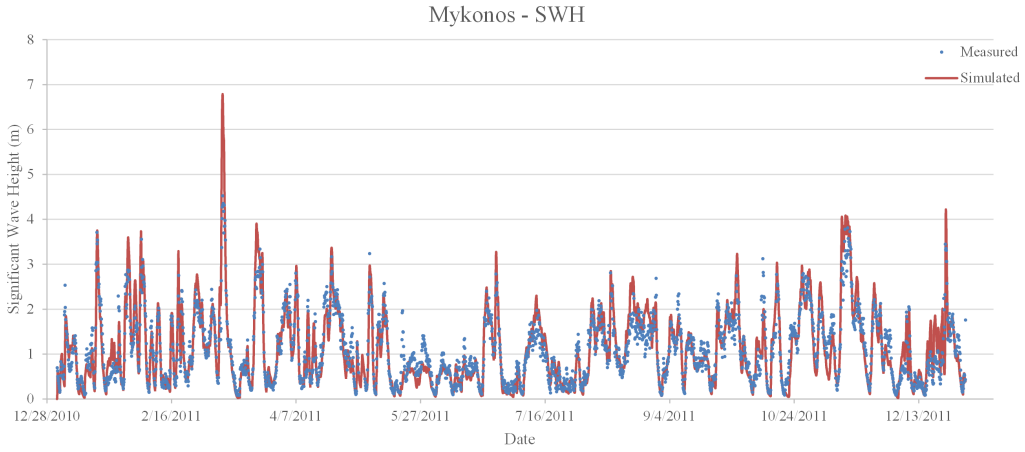

Figure 3.12: Comparison of the simulated and measured significant wave height for Mykonos station.

The closeness of the simulated to measured MWP for Mykonos is high as shown in Figure 3.13. There is data vacancy for 2nd of May to 20th of June for mean wave period in this station.

Same figures are mentioned for other stations and most of them show a good agreement with measured data.

The question of whether an oceanic model is able to reproduce the mean oceanic state, or its variability, is often referred to model validation, or model testing one cant test the model if it is near to reality situation or not by the comparison of the model results

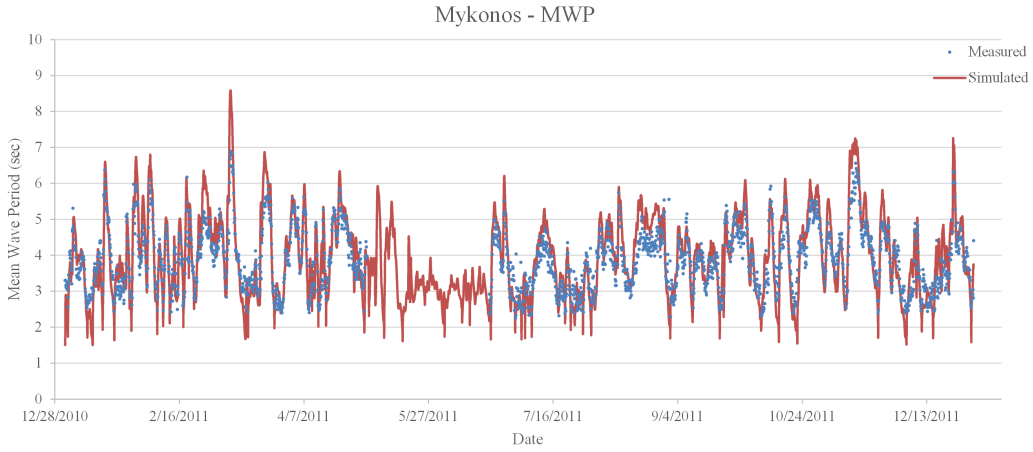

Figure 3.13: Comparison of the simulated and measured mean wave period for Mykonos station.

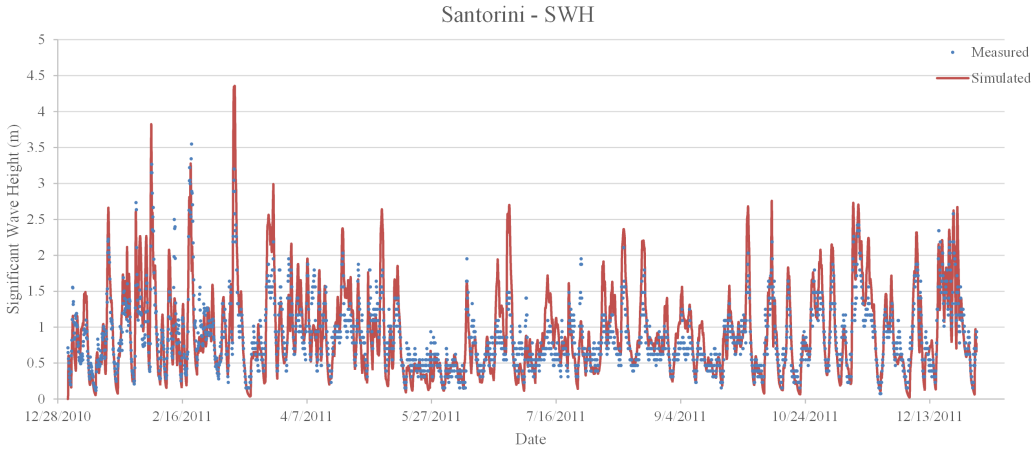

Figure 3.14: Comparison of the simulated and measured significant wave height for Santorini station.

with the observations. In this aspect there is statistical parameters which could be used for model validity and the closeness of the model results and observations.

Statistical evaluation of model took place by synchronization of the observed and simulated data for each time step. In this study 4 different statistical parameter is taken into account and calculated. It should be mentioned that for the scattered observed data which were not regular it was a must to write a program to match the times of the two data for the comparison.

Root Mean Square Error (RMSE) is on of the common measure of differences between values predicted and values observed. Basically RMSE shows the sample standard

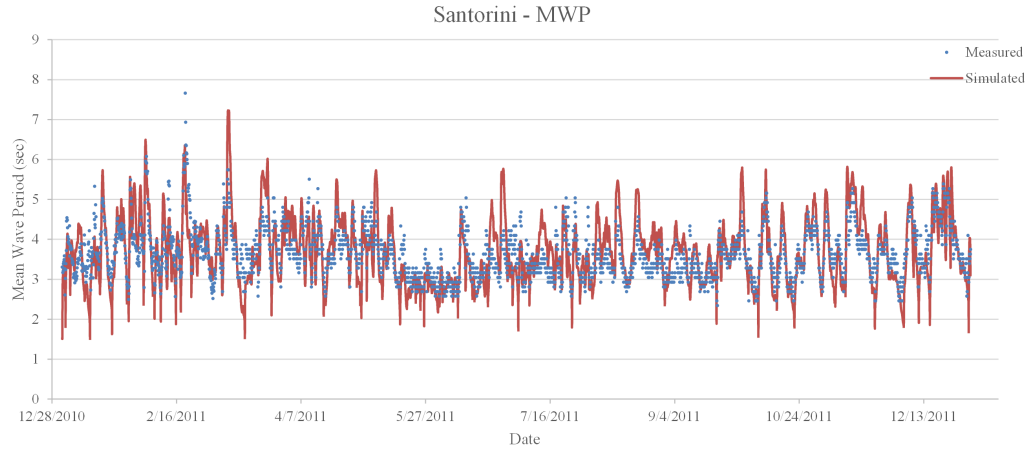

Figure 3.15: Comparison of the simulated and measured mean wave period for Santorini station.

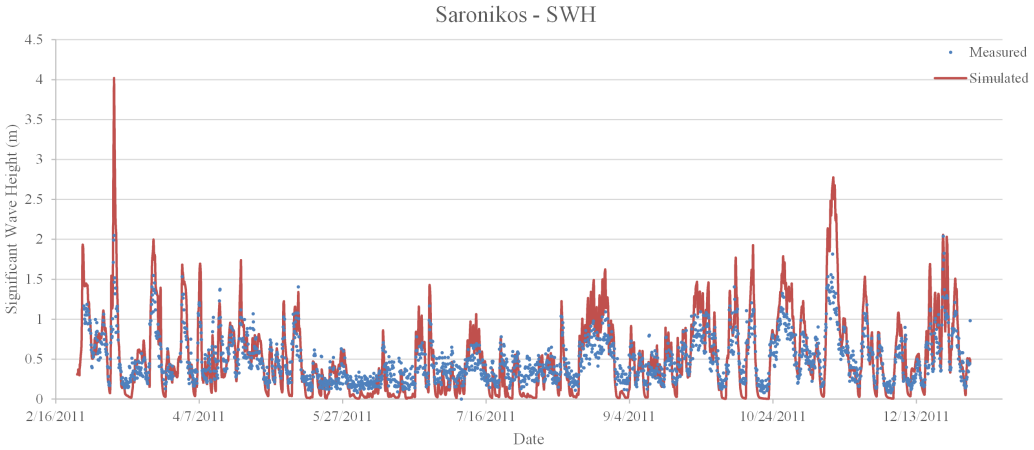

Figure 3.16: Comparison of the simulated and measured significant wave height for Saronikos station.

deviation of the difference between predicted ad observed values. These individual differences are called residuals when the calculations are performed over the data sample that was used for estimation and are called prediction errors when computed out-of-sample.

$$RMSE = \sqrt{\frac{\sum_{i=1}^{N}(P_i - O_i)^2}{N}} \tag{3.55}$$

The most familiar measure of dependence between two values is the Pearson product-moment correlation coefficient, or it is called correlation coefficient. It is

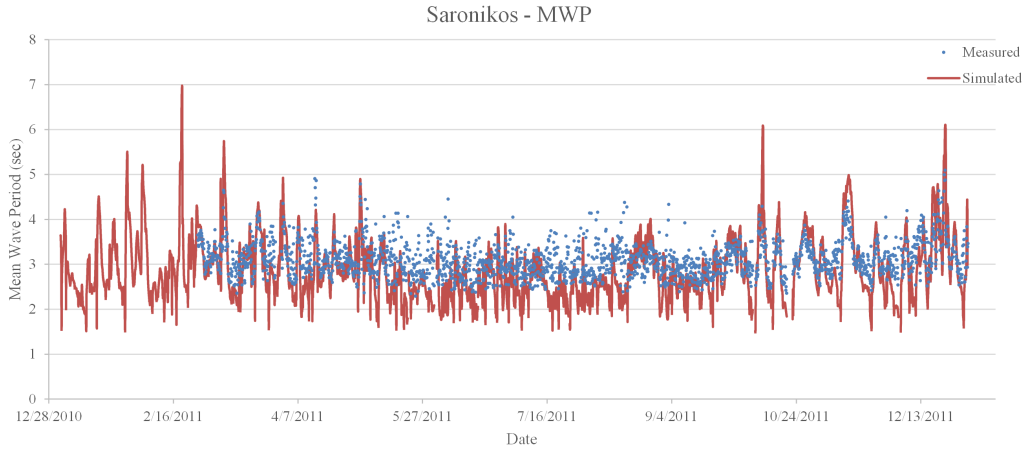

Figure 3.17: Comparison of the simulated and measured mean wave period for Saronikos station.

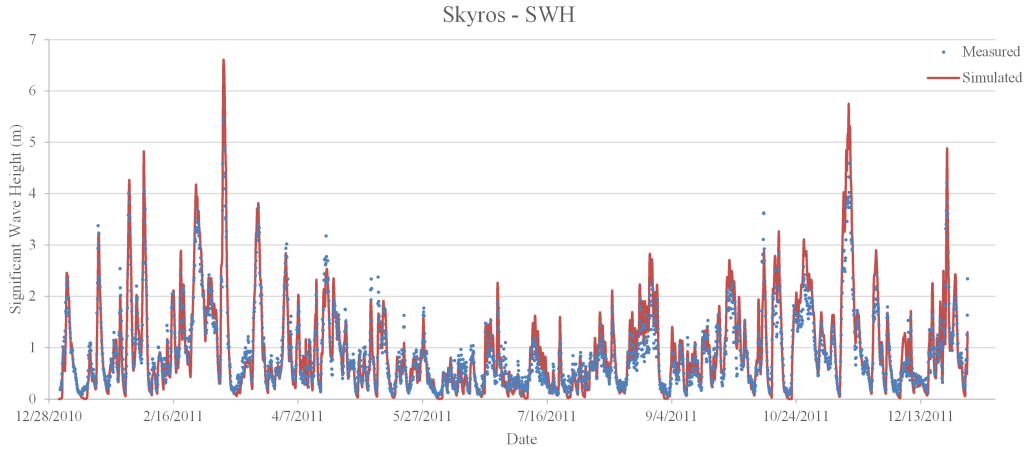

Figure 3.18: Comparison of the simulated and measured significant wave height for Skyros station.

obtained by dividing the covariance of the two variables by the product of their standard deviations.

$$R = \frac{\sum_{i=1}^{N}(P_i - \bar{P})(O_i - \bar{O})}{\sqrt{\sum_{i=1}^{N}(P_i - \bar{P})^2 \sum_{i=1}^{N}(O_i - \bar{O})^2}} \tag{3.56}$$

In statistics the difference between the estimation values and the real values which is observed or measured could be compared with different measures, BIAS is one of these formulas for measurement of the values' closeness.

$$BIAS = \sum_{i=1}^{N} \frac{1}{N}(P_i - O_i) \tag{3.57}$$

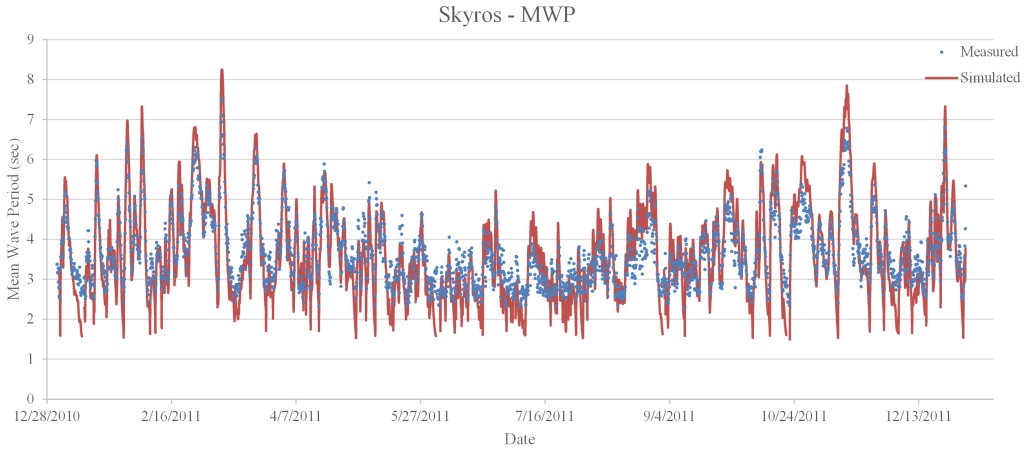

Figure 3.19: Comparison of the simulated and measured mean wave period for Skyros station.

Scattering index is one of the statistical measures for comparison of the 2 data sets which are occurred in the same time. These values could be the simulation results or estimations from a model with the observations or the reality values of a phenomena.

$$SI = \frac{\sqrt{\frac{1}{N}\sum_{i=1}^{N}(P_i - O_i)^2}}{\frac{1}{N}\sum_{i=1}^{N} O_i} 100 \tag{3.58}$$

By the introduction of the statistical measures used in this study the model validation results could be found for Significant Wave Height (H_s) and Mean Wave Period (T_{01}) as shown in Table 3.2 and Table 3.3.

As shown Table 3.2 Correlation Coefficients resulted from the model validation is logical and shows the high accuracy of the model.

Table 3.2: Statistical Evaluations on Significant Wave Height.

Station	Significant Wave Height (H_s)			
	R	RMSE	BIAS	SI
Athos	0.94	0.28	0.03	32.75
Bozcaada	0.76	0.3	0.05	52.38
Dalaman	0.88	0.29	0.16	51.85
E1M3A	0.89	0.37	-0.07	34.9
Lesvos	0.91	0.27	-0.03	34.37
Mykonos	0.91	0.35	-0.01	30.99
Santorini	0.85	0.33	-0.06	38.24
Saronikos	0.87	0.28	-0.04	56.25
Skyros	0.95	0.31	-0.05	33.21
Average	0.88	0.31	0.00	40.55

Table 3.3: Statistical evaluations on Mean Wave Period.

Station	Mean Wave Period (T_{01})			
	R	RMSE	BIAS	SI
Athos	0.87	0.68	0.46	18.02
Bozcaada	0.67	0.5	0.06	17.22
Dalaman	0.64	0.84	0.37	15.61
E1M3A	0.79	0.68	-0.12	16.15
Lesvos	0.88	0.49	0.18	13.37
Mykonos	0.90	0.54	-0.12	13.93
Santorini	0.73	0.57	-0.04	15.65
Saronikos	0.54	0.63	0.27	20.14
Skyros	0.91	0.53	0.04	14.46
Average	0.77	0.61	0.12	16.06

4. RESULTS AND DISCUSSIONS

In this thesis the simulations are taken place spanning from 1999 to 2013 for a 15 years duration. For this long time simulation a computer with 16 GB RAM and 2.2 GHz CPU speed used which for every year the computation time has taken 30 hours. Total simulations have taken nearly one month.

The simulations were conducted in yearly spans, so that the huge data analysis could be easier. Also the leap years having different time steps have taken into account for more precise simulations.

On the data extraction, monthly data was driven from yearly simulations. This was done with the Data Extraction Tool of MIKE Zero. Table 4.1 shows the time steps for data extraction for each year, while leap years (intercalary or bissextile year) having one day more than normal years, the time steps are calculated to make the analysis more accurate.

Table 4.2 shows the time steps and start and end of the each month by number of time steps for leap years.

The simulations are done with 10 minutes interval so as to catch the extreme points and get a higher temporal resolution for further investigations. The results of simulations will be shown and discussed with a completely detailed annotations.

This study could be called as an encyclopedia of Aegean Sea's wave behavior in last 15 years.

4.1 Temporal Analyses

The simulation's results are categorized in different time spans and time steps. This point should be taken into consideration that for every temporal analysis, mean wave characteristics are good measures for the area.

Figure 4.1 shows the mean significant wave height for Aegean Sea for a 15 years time span. This figure has been prepared by taking the average of 15 year data. The figure shows that the most frequent higher wave heights are occurring in the middle and southern parts of the domain.

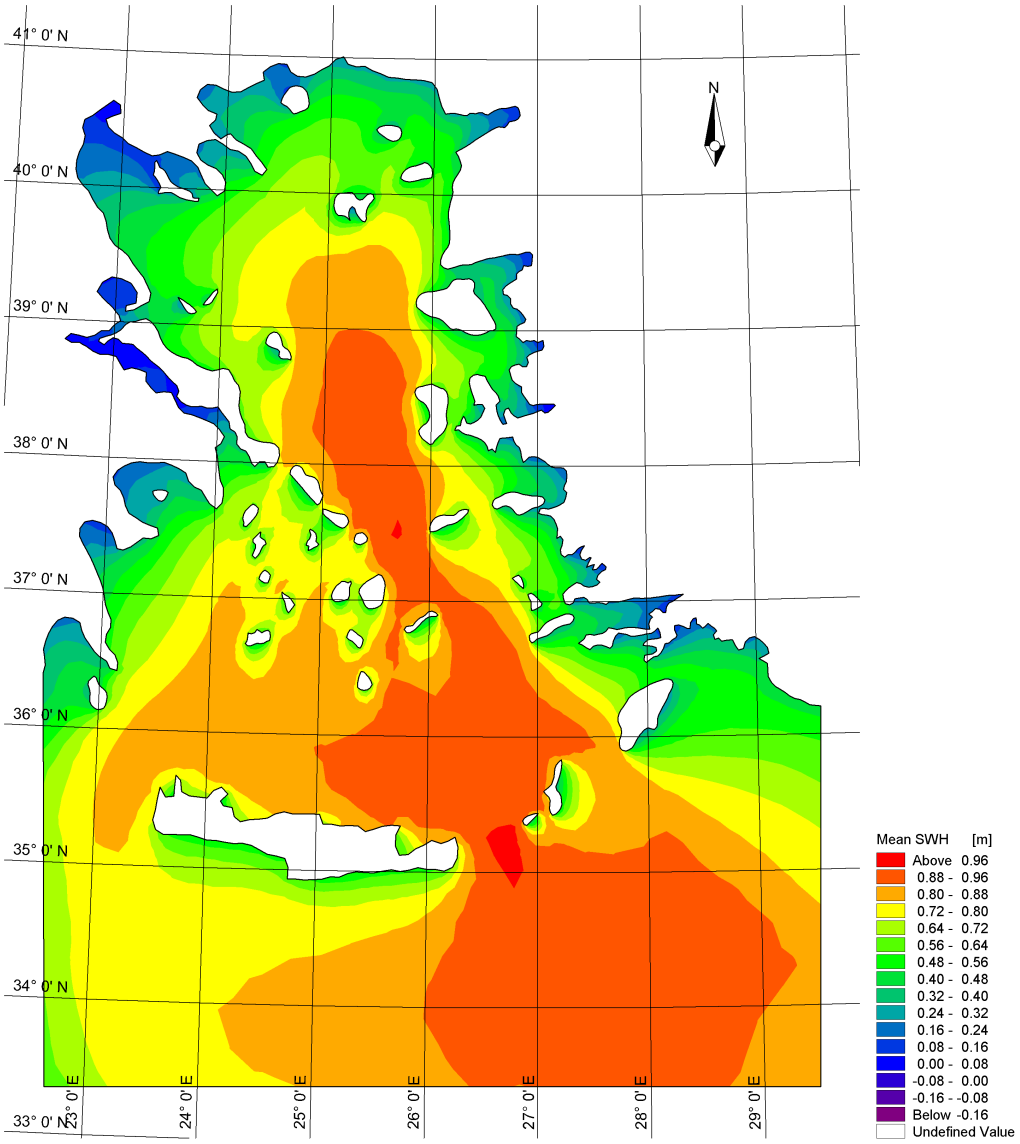

Figure 4.1: Fifteen-year mean significant wave height for Aegean Sea.

In the middle parts of Aegean Sea wave power reaches $5.2 kW/m$. Maximum values of the wave power is located in $37°N - 38°N$ and $25°E - 26°E$.

4.1.1 Monthly analysis

Monthly analysis is essential for having a deeper knowledge of the behavior of the domain. Each month could have different wave climate, so that in this Section every month's significant wave heights and wave power will be discussed and comments will be given.

- January
  - Significant Wave Height

    As shown in Figure 4.3, the maximum mean wave height is located in $37°N - 39°N$ and $25°E - 26°E$. In this parts of the model mean significant wave height reaches $1.3m$. In January area having H_s values between $1.2m - 1.3m$ is biggest part of the model area.

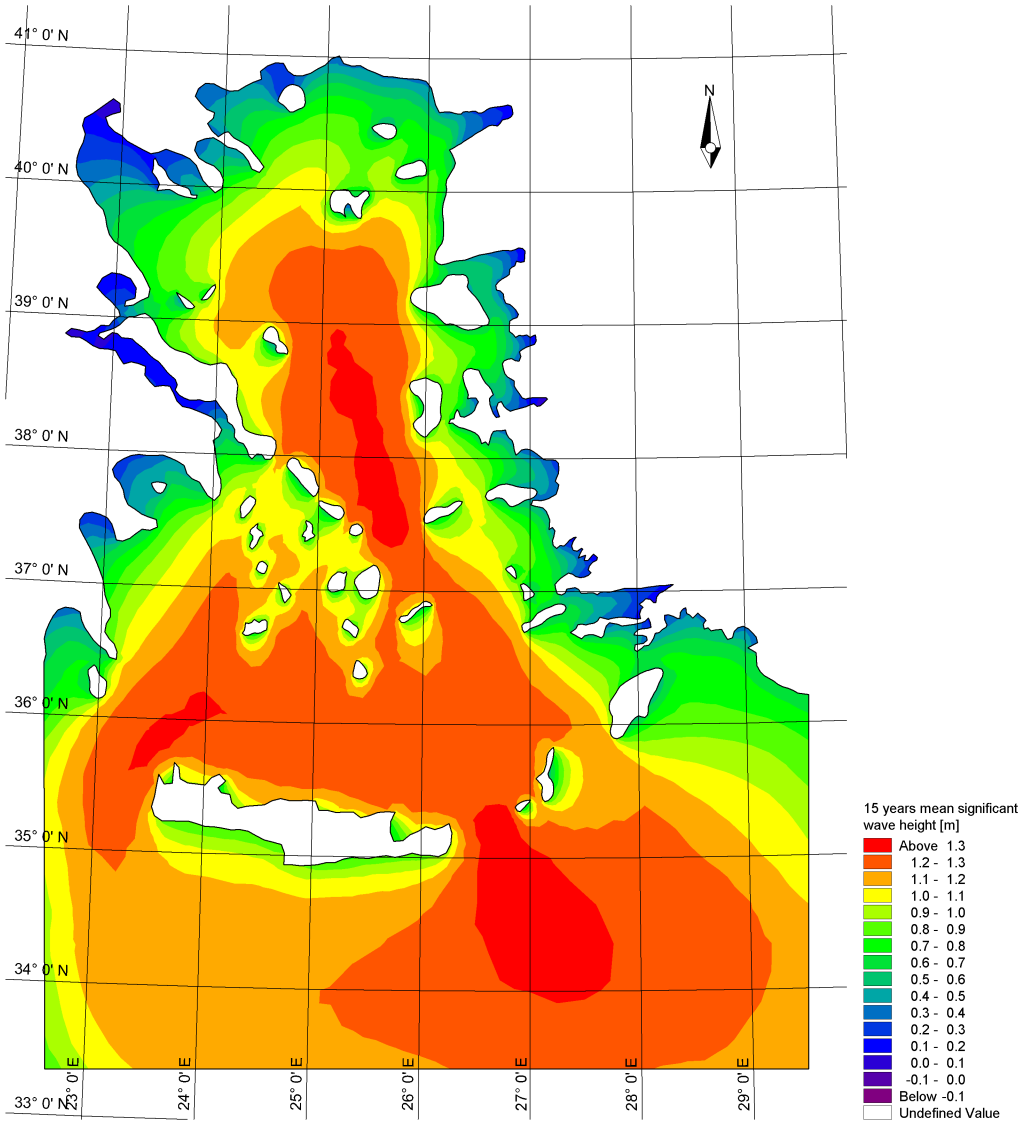

Figure 4.3: Fifteen-year mean significant wave height for January.

– Mean Wave Power

  Mean wave power in this month has higher magnitude in the middle northern part of the domain. In this part wave power is more than 8.4 kW/m. Figure 4.4 shows a mean wave power in January months of 15 years.

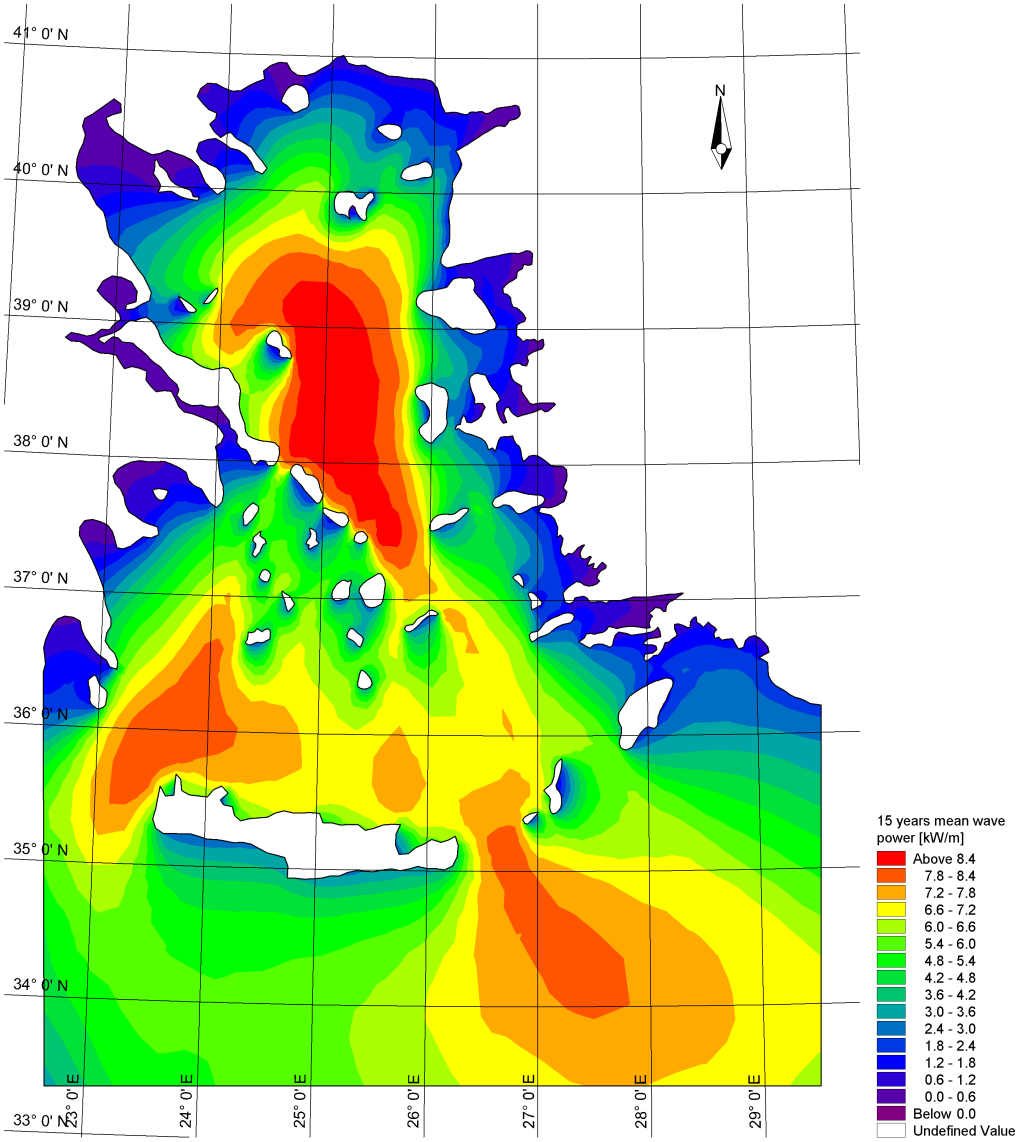

Figure 4.4: Fifteen-year mean wave power for January.

- February

  - Significant Wave Height

    In Figure 4.5, it can be obviously seen that most of the study region is covered with an area that has more than 1.2 m significant wave heights. Though this values which are shown in the Figure 4.5 are the mean values which are simulated.

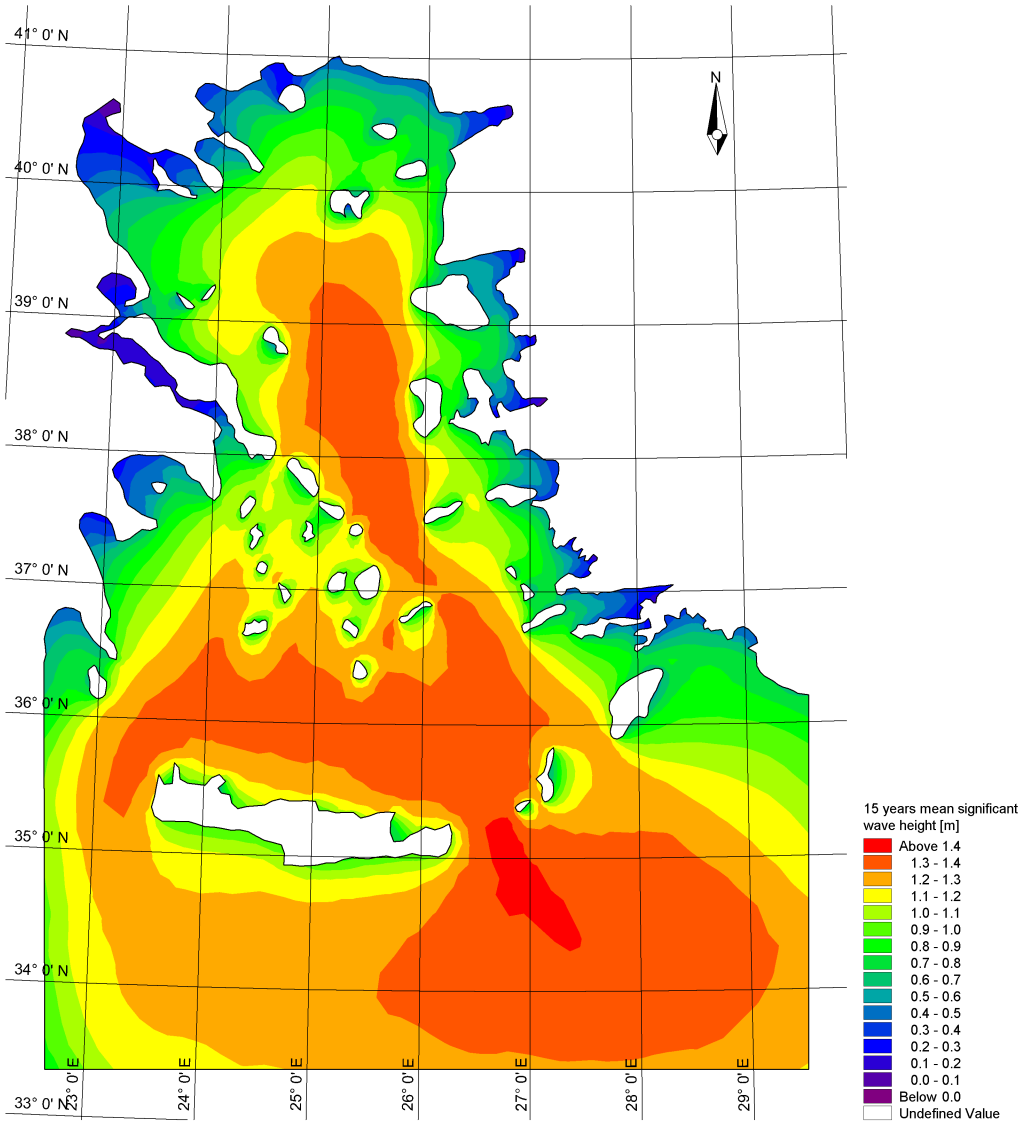

Figure 4.5: Fifteen-year mean significant wave height for February.

– Mean Wave Power

  Having half a glance to maps of wave power for other months it can be concluded from the Figure 4.6 that in this month the mean wave power has increased significantly in contrast to other months, until it reaches to 9 kw/m in some small parts of the Aegean Sea.

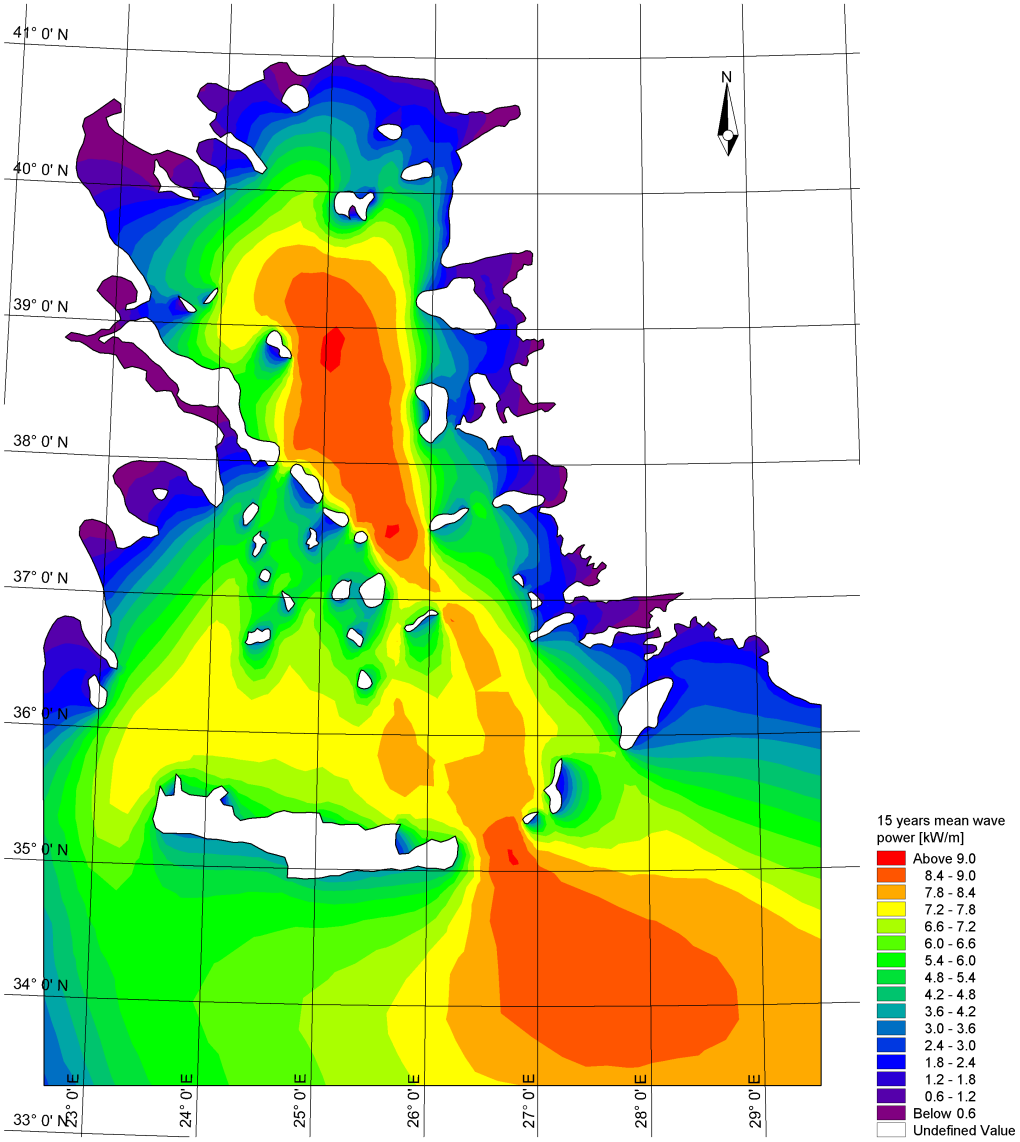

Figure 4.6: Fifteen-year mean wave power for February.

- March
  - Significant Wave Height

    While it can be seen from Figure 4.7 that wave heights have decreased in comparison with the previous month.

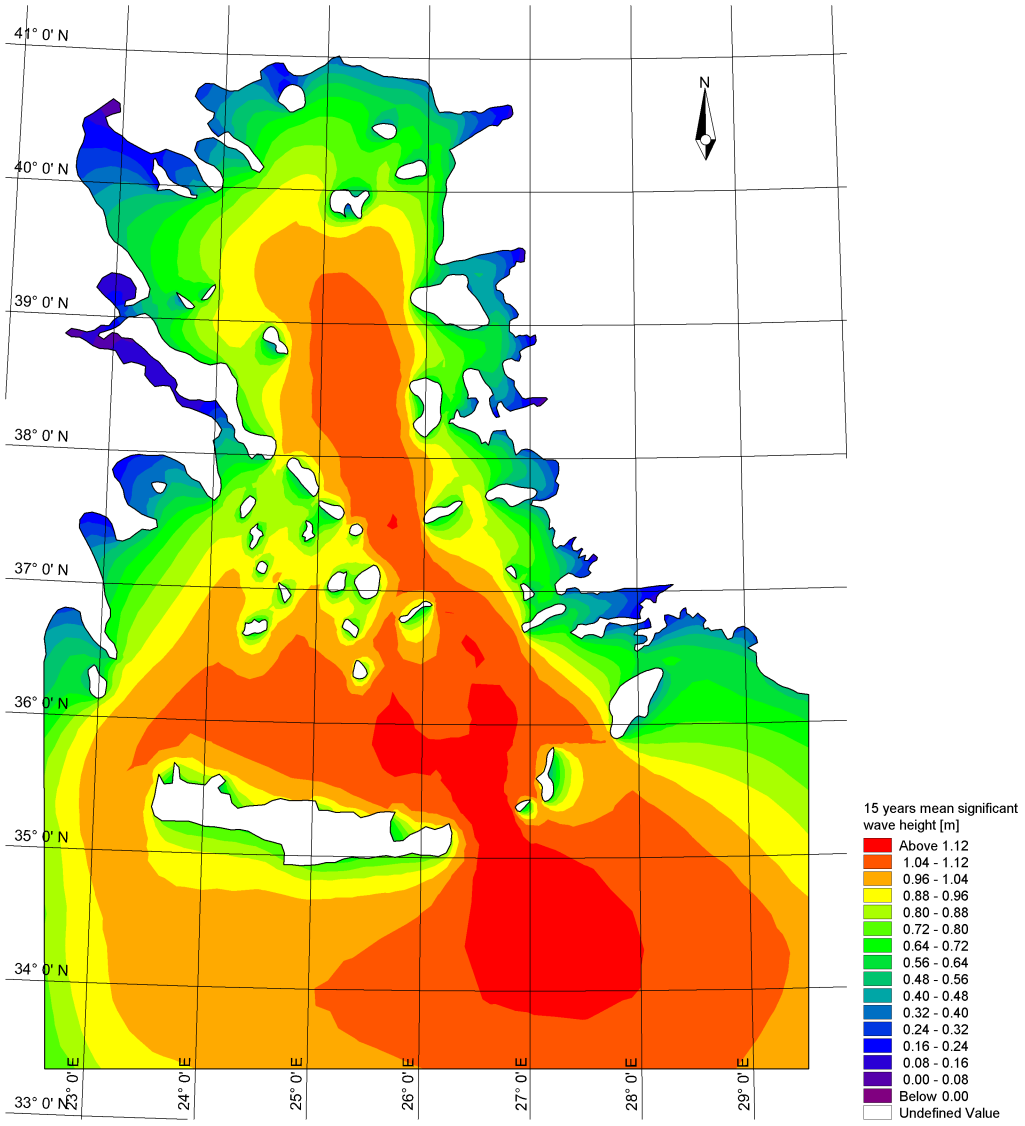

Figure 4.7: Fifteen-year mean significant wave height for March.

– Mean Wave Power

Figure 4.8 shows the mean wave power of March months from 1999-2013. The wave power in this month has decreased considerably, while the main part of the domain is covered with a mean wave power values more exceeding 4 kw/m

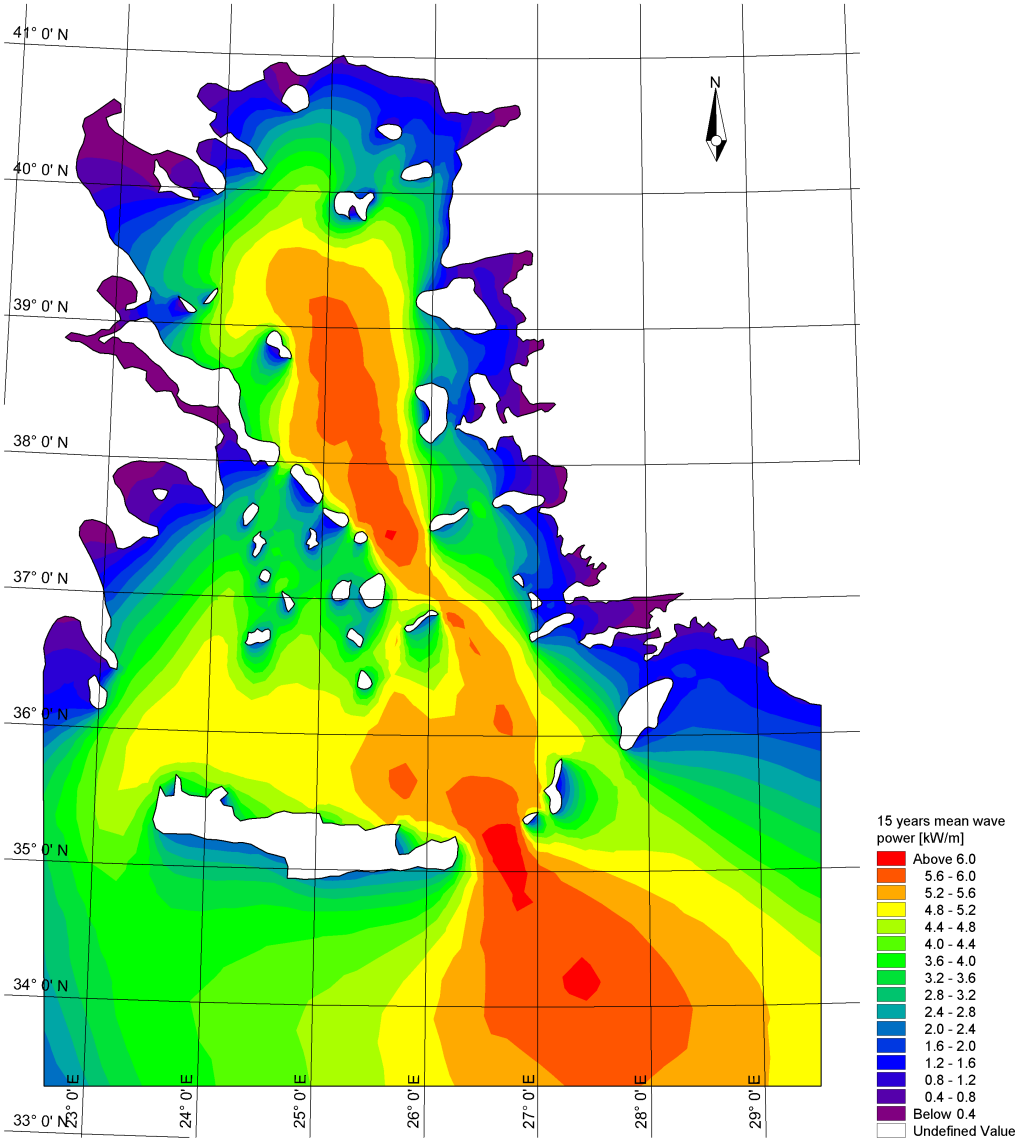

Figure 4.8: Fifteen-year mean wave power for March.

- April

  - Significant Wave Height

    Main percentages of the higher waves are located in the southern parts of the Aegean Sea in this month and Figure 4.9 shows it. The middle part of the Aegean Sea which had higher wave heights has a displacement to area between $26°E - 28°E$ and $34°N - 38°N$ coordinates.

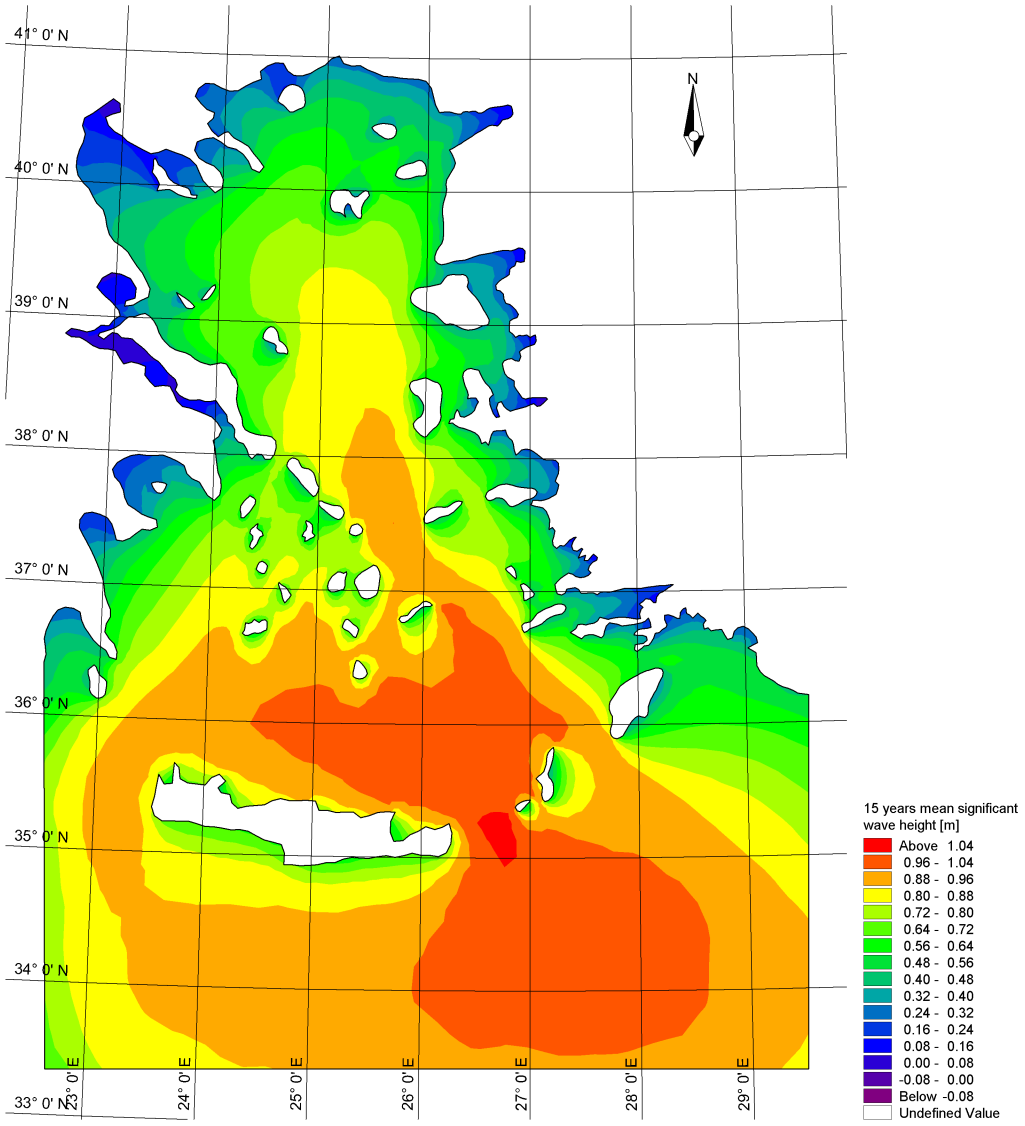

Figure 4.9: Fifteen-year mean significant wave height for April.

– Mean Wave Power

  As shown in Figure 4.10, for a 15 years mean wave power equal to 2 kW/m it has the biggest area. Also a decline has happened from the previous month to April. So it can be concluded that in April the mean wave power is lower than previous months.

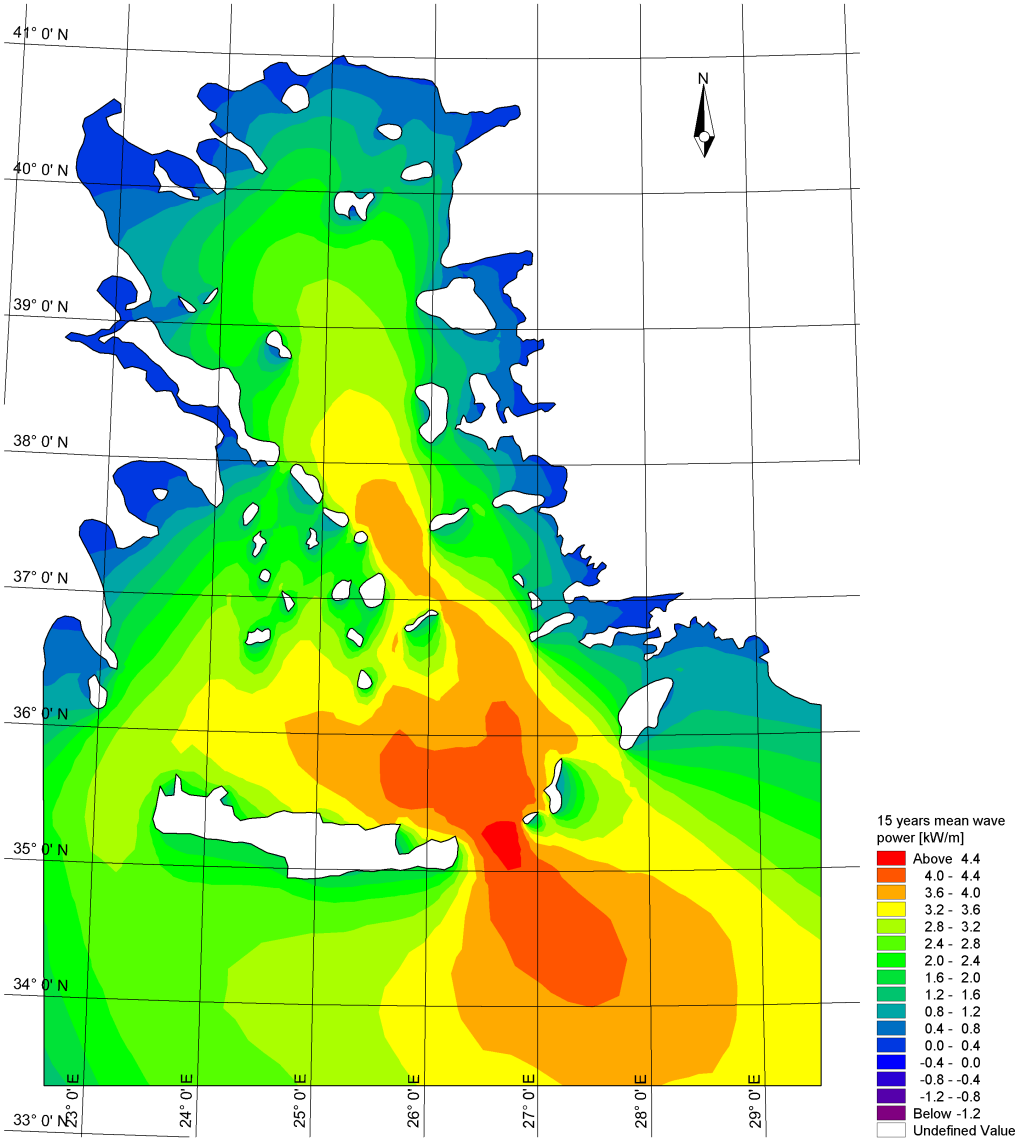

Figure 4.10: Fifteen-year mean wave power for April.

- May

  - Significant Wave Height

    In this month the higher magnitudes of the wave happen in the southern part of the domain which is shown in the Figure 4.11.

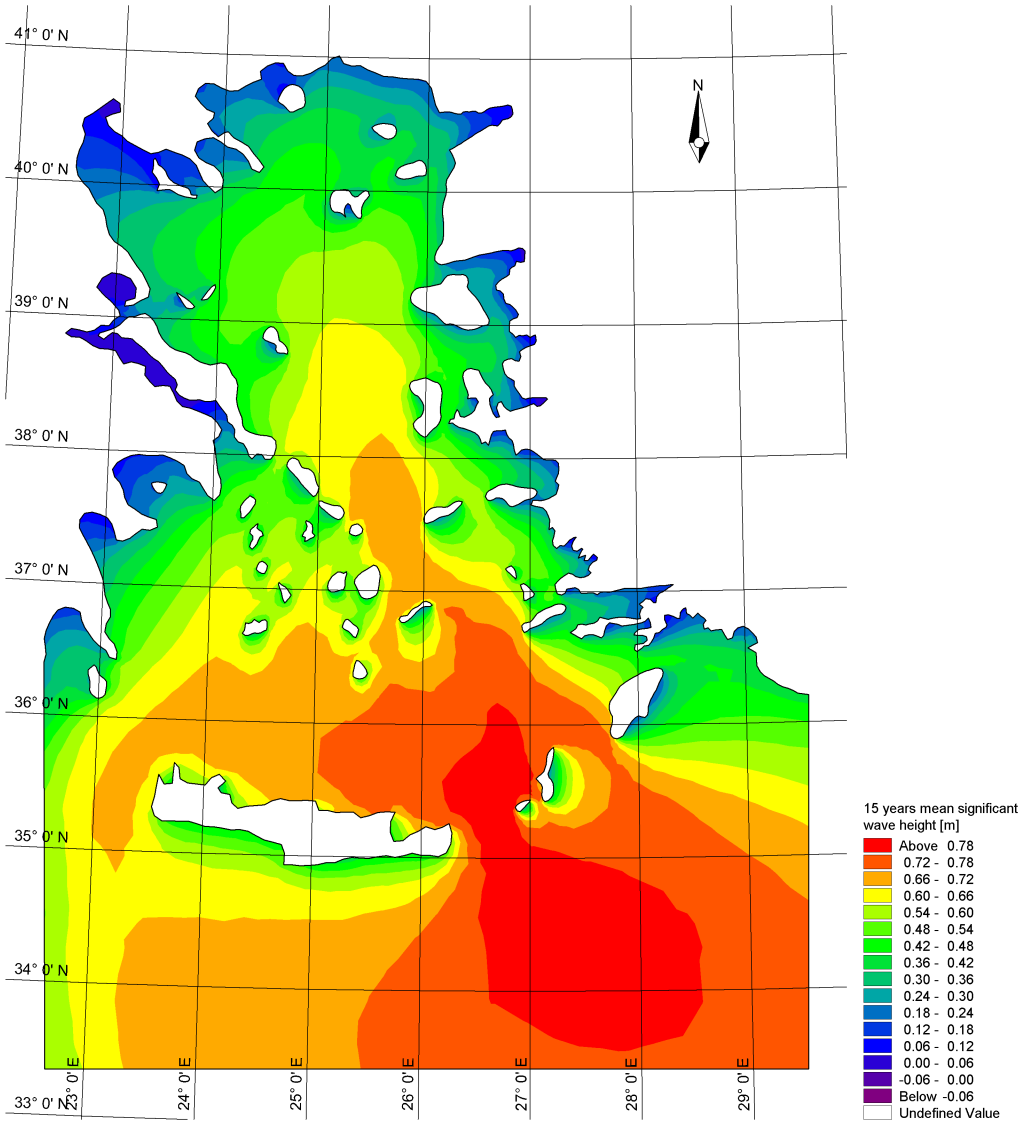

Figure 4.11: Fifteen-year mean significant wave height for May.

– Mean Wave Power

In contrast to the April mean values of wave power,Figure 4.12 indicate that in this month the wave power values have got half the last month. The main part of the domain has a wave power between 0.3 - 2.25 kw/m.

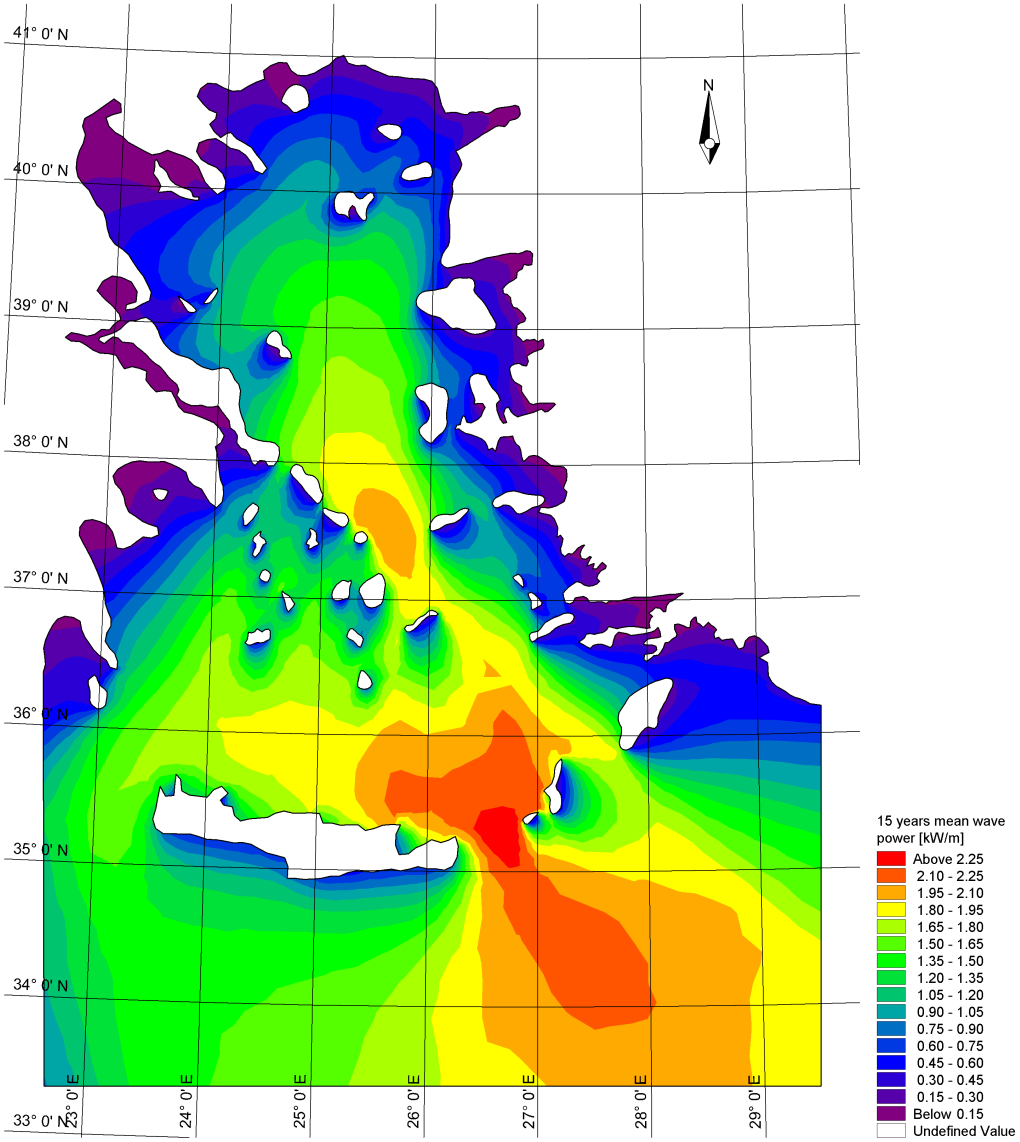

Figure 4.12: Fifteen-year mean wave power for May.

- June

  - Significant Wave Height

    Greater significant wave heights have happened in South West part of domain.

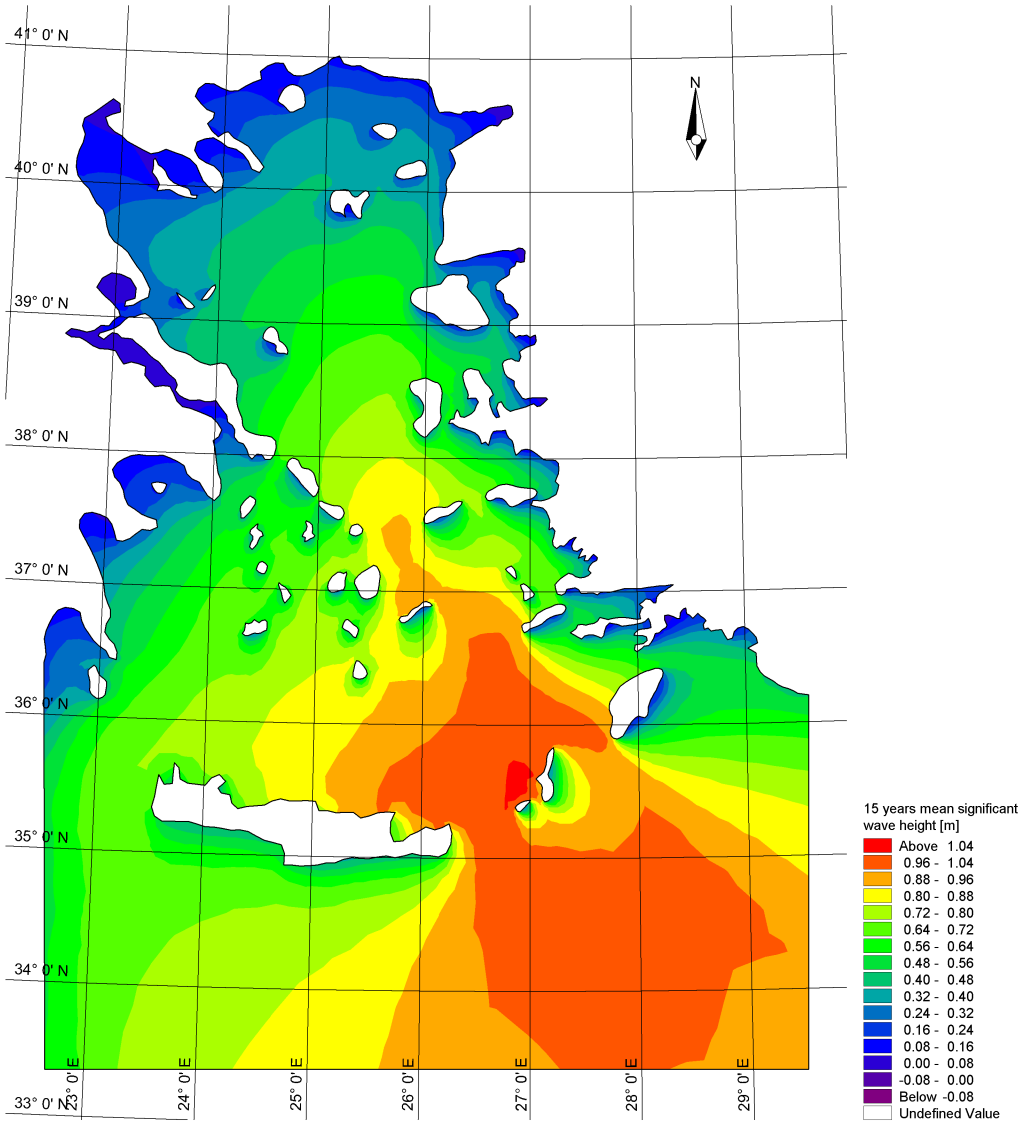

Figure 4.13: Fifteen-year mean significant wave height for June.

– Mean Wave Power

Figure 4.14 shows that in this month the wave power is declining to the minimum values by comparing it to previous months or the next months of the year. This month has the least wave power result from the simulations done for 15 years.

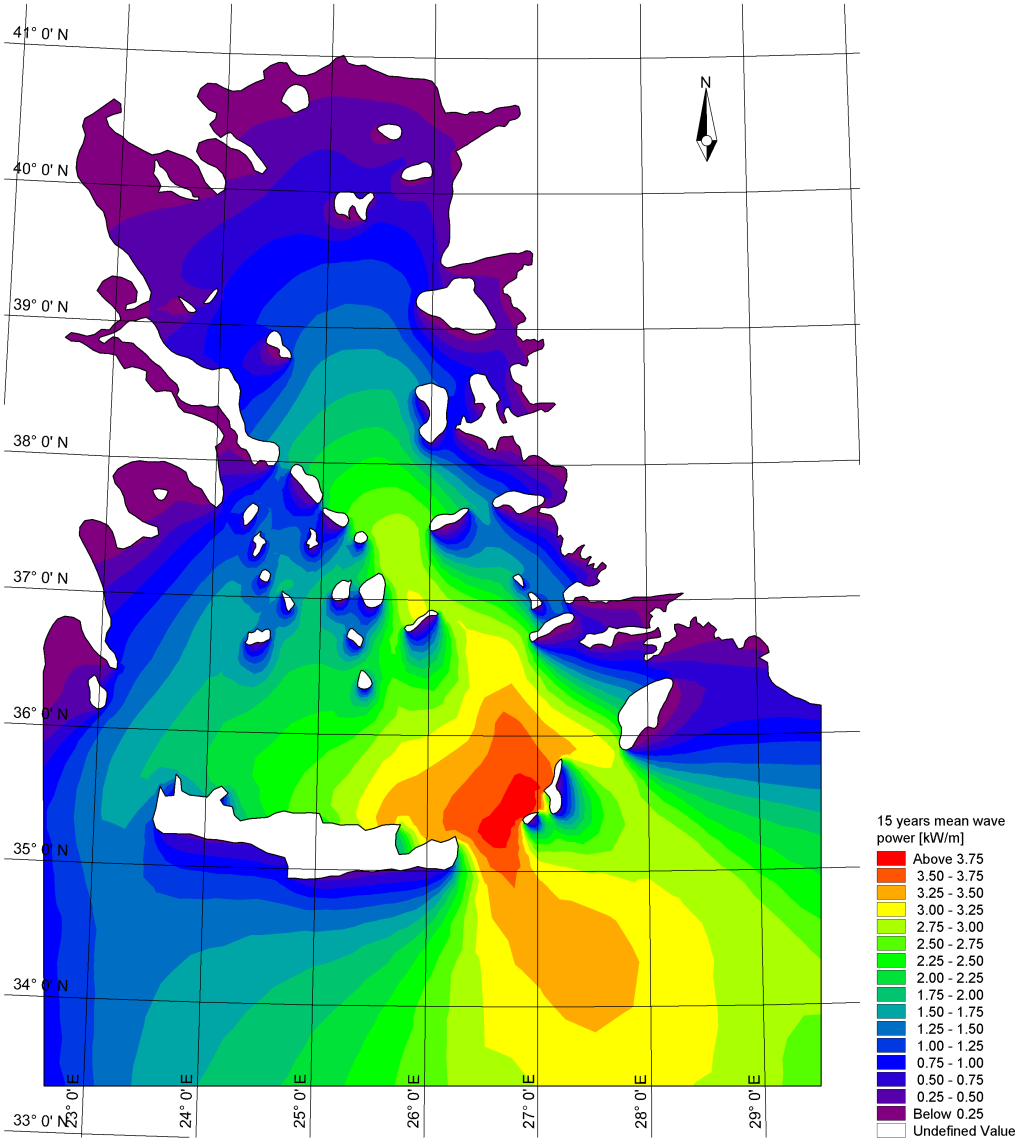

Figure 4.14: Fifteen-year mean wave power for June.

- July
  - Significant Wave Height

    Higher significant wave heights are located in the middle part of the domain between Crete and Kasos islands which is named Cretan Trough. Figure 4.15 shows significant wave height map in July.

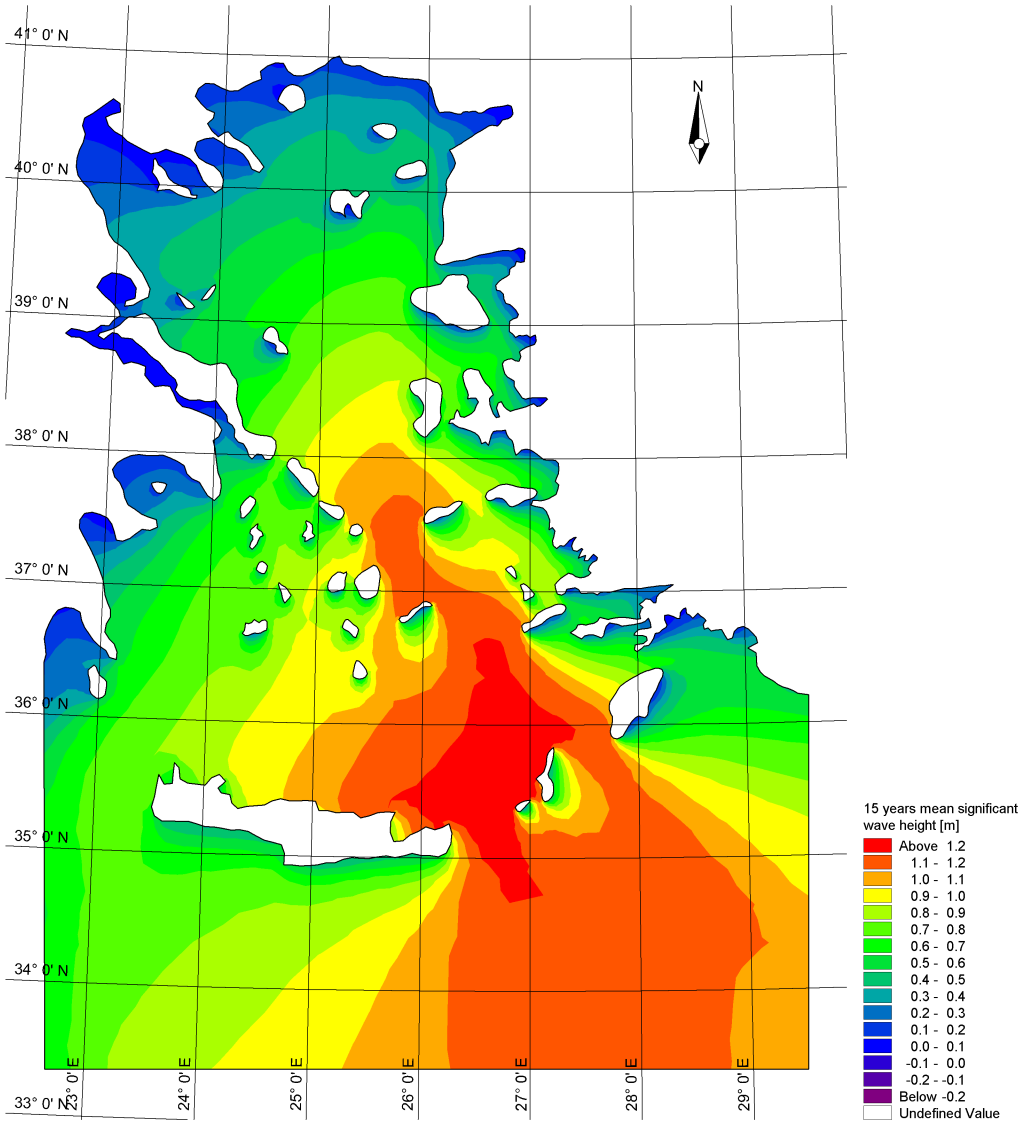

Figure 4.15: Fifteen-year mean significant wave height for July.

– Mean Wave Power

The fifteen-year mean wave power which is shown in Figure 4.16 demonstrate a wave power above 4.8 kW/m in Cretan Sea near Karpathos and Kasos islands.

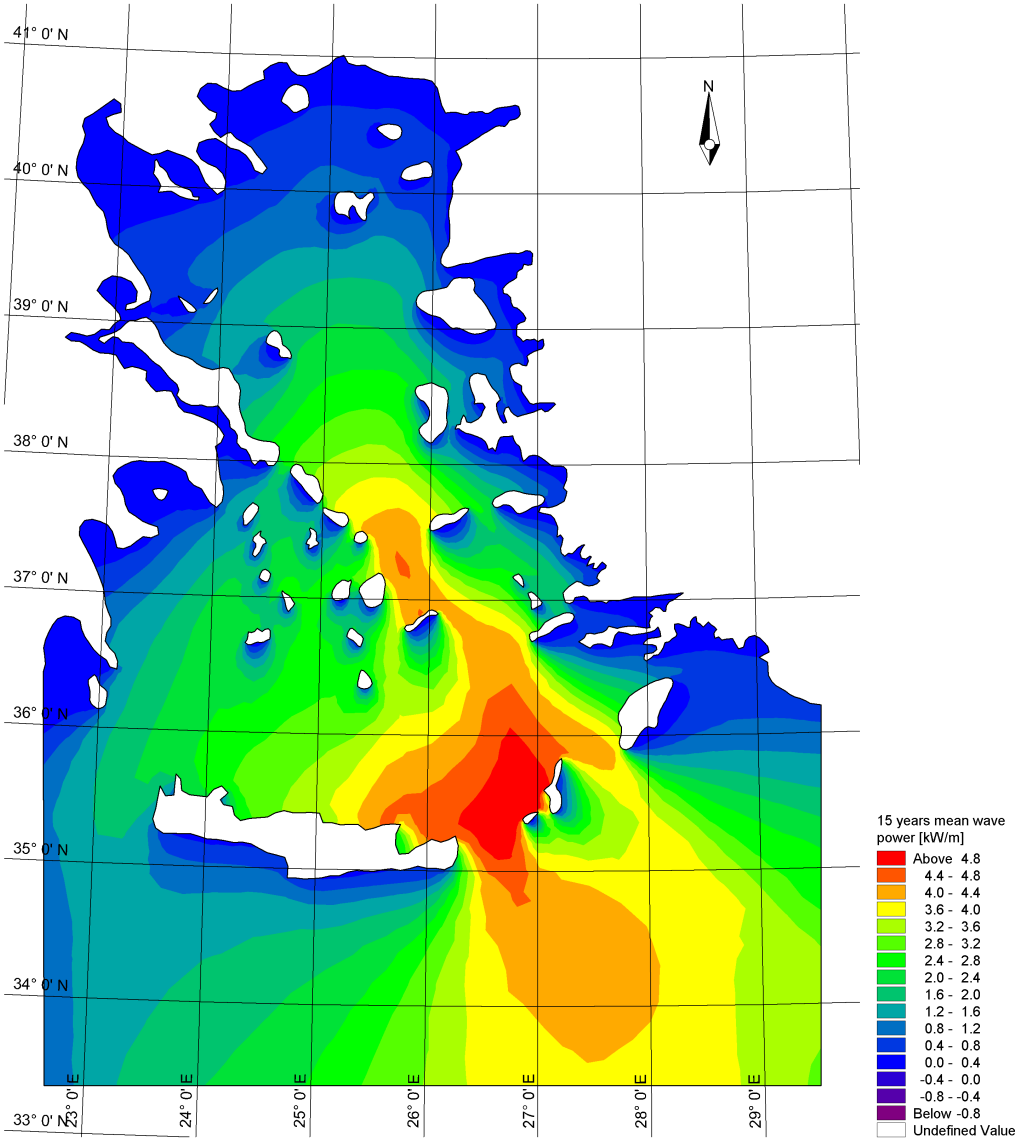

Figure 4.16: Fifteen-year mean wave power for July.

- August

  - Significant Wave Height

    In this month as shown in Figure 4.17 the frequent wave direction is North-South, while the highest values of significant wave heights occur in the middle part of the Aegean Sea, between Aegialis Amorgos, Naxos, Mykonos and Ikaria islands.

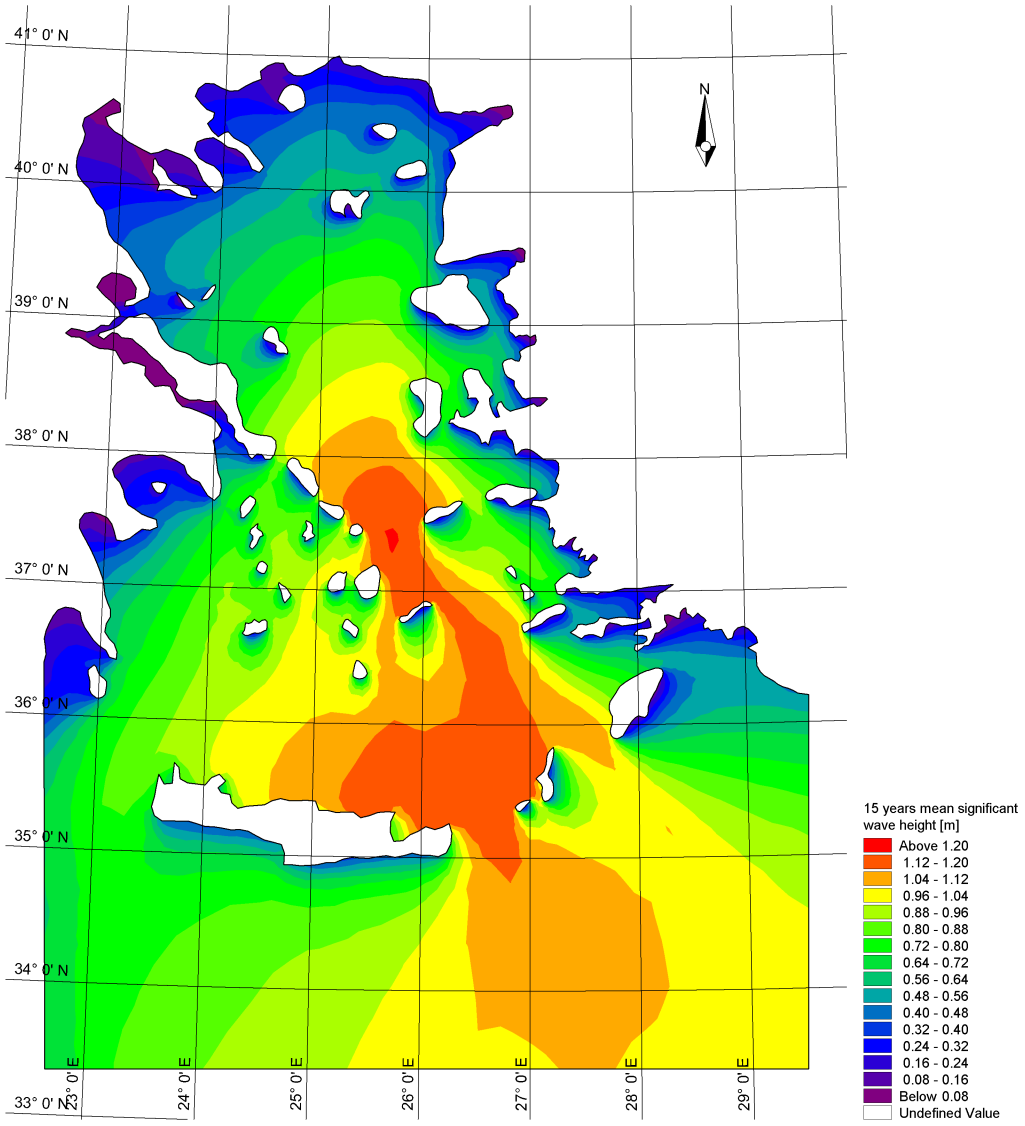

Figure 4.17: Fifteen-year mean significant wave height for August.

– Mean Wave Power

  Higher wave power magnitudes are observable in Cretan Trough and South-West Ikaria basin with 4.8 kW/m. Figure 4.18 obviously shows that the wave power is not high in the coastal parts of the Aegean Sea both in east and west coasts.

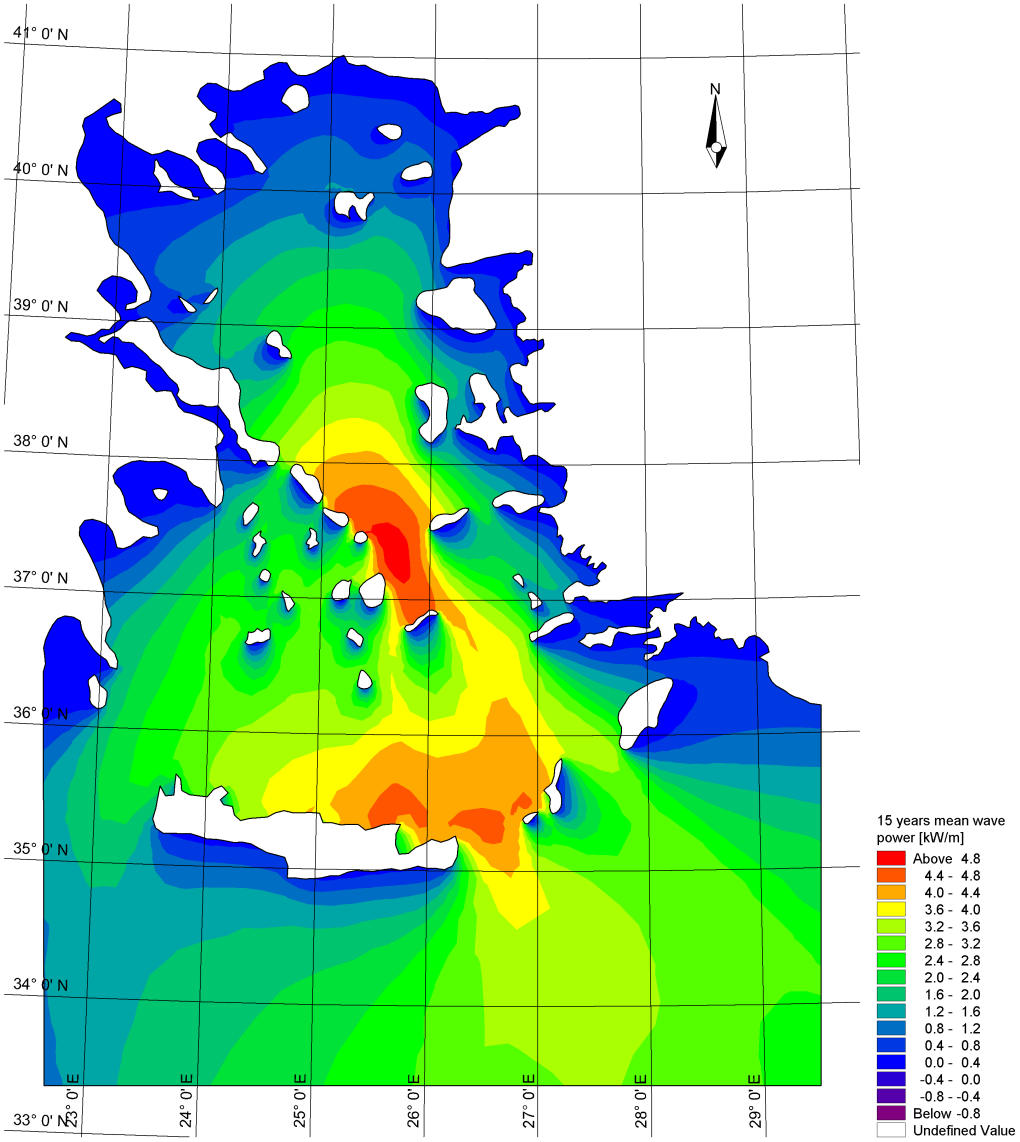

Figure 4.18: Fifteen-year mean wave power for August.

- September

  - Significant Wave Height

    Significant wave heights in this month shows that most of the island's southern coasts face lower waves. Waves facing islands, decline in magnitude until they reach to coasts i.e. islands are like an obstacle for waves for Aegean Sea's coasts.

Table 4.1: Time steps and duration of every month for normal year.

Month	Start	End	Time Steps	Days
January	0	4463	4463	31
February	4464	8495	4031	28
March	8496	12959	4463	31
April	12960	17279	4319	30
May	17280	21743	4463	31
June	21744	26063	4319	30
July	26064	30527	4463	31
August	30528	34991	4463	31
September	34992	39311	4319	30
October	39312	43775	4463	31
November	43776	48095	4319	30
December	48096	52524	4463	31

Table 4.2: Time steps starts and end and duration of each month for a leap year.

Month	Start	End	Time Steps	Days
January	0	4463	4463	31
February	4464	8639	4175	29
March	8640	13103	4463	31
April	13104	17423	4319	30
May	17424	21887	4463	31
June	21888	26207	4319	30
July	26208	30671	4463	31
August	30672	35135	4463	31
September	35136	39455	4319	30
October	39456	43919	4463	31
November	43920	48239	4319	30
December	48240	52703	4463	31

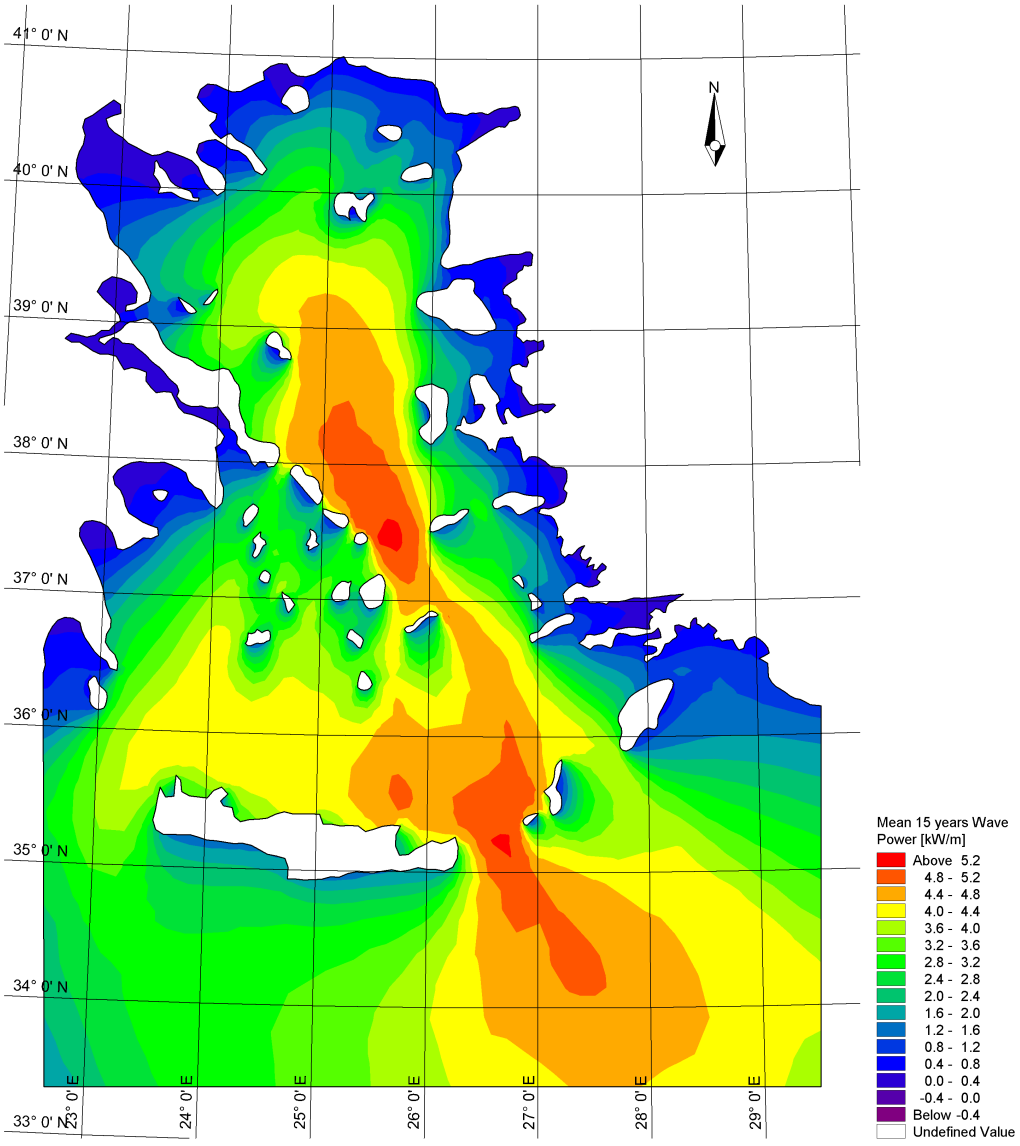

Figure 4.2: Fifteen-year mean wave power for Aegean Sea.

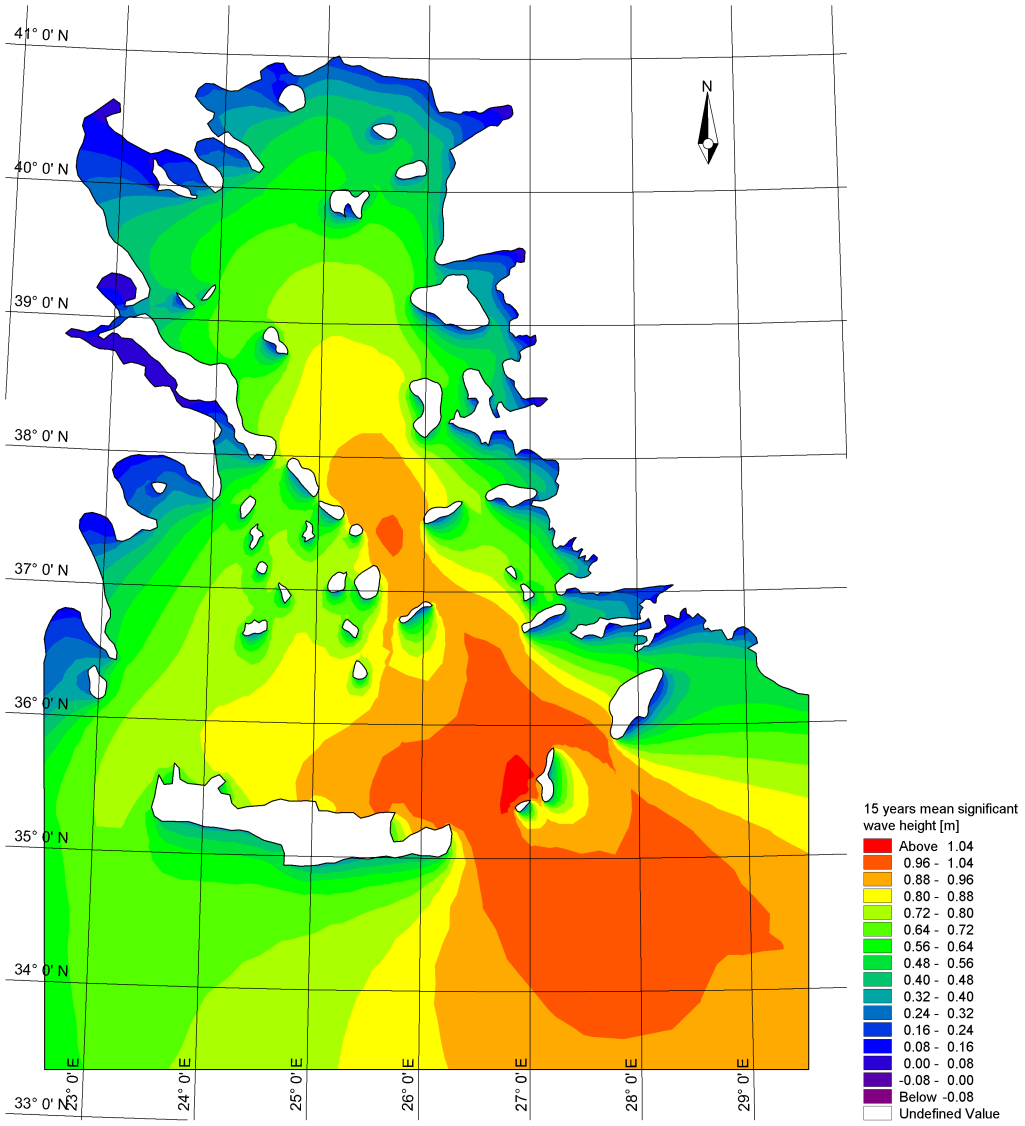

Figure 4.19: Fifteen-year mean significant wave height for September.

– Mean Wave Power

  September has a higher mean wave power than August which is a sign of a wave climate change. The mean wave power map for 15 years is shown in Figure 4.20.

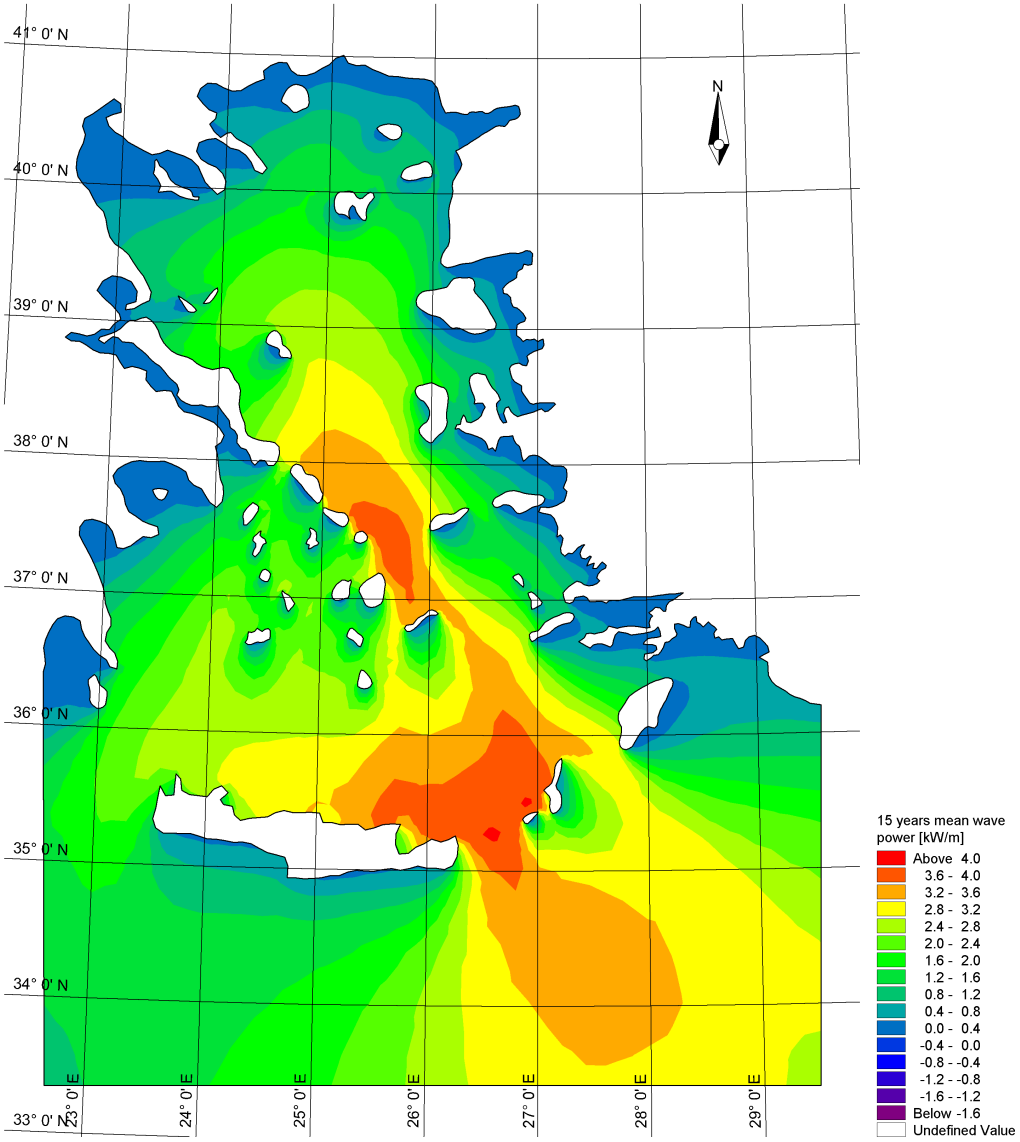

Figure 4.20: Fifteen-year mean wave power for September.

- October

  - Significant Wave Height

    The magnitude of the higher significant wave heights have changed from September to October as shown in Figure 4.21, also the coverage area of higher significant wave heights has increased and and spread to higher latitudes between Chios and Skyros islands while the bigger wave heights remain in the same location as it was for September.

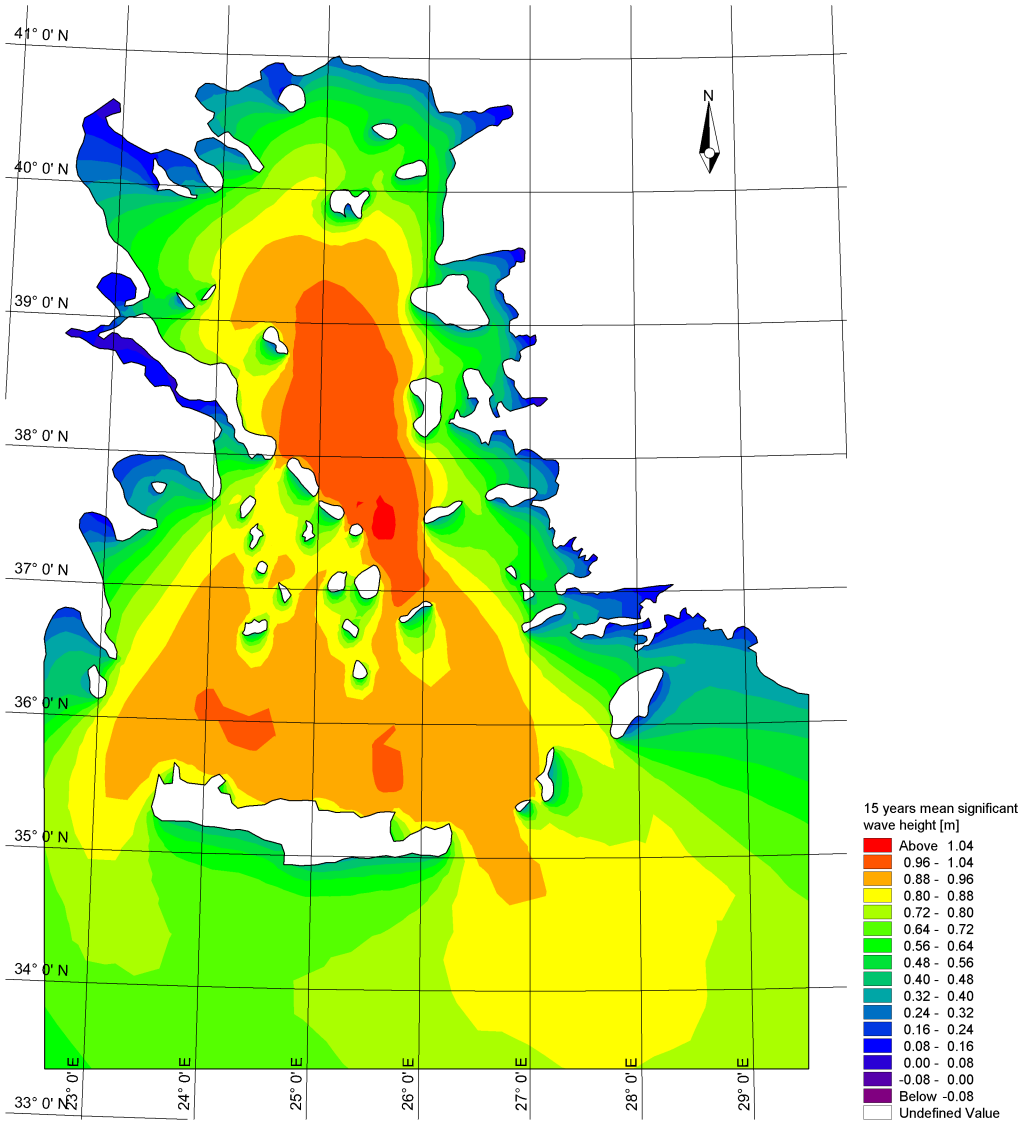

Figure 4.21: Fifteen-year mean significant wave height for October.

– Mean Wave Power

  Maximum mean wave power of 15 years is located in the northern part of the domain in east of Mykonos, Tinos, and Andros islands. As shown in Figure 4.22 the maximum wave power location has moved to northern latitudes between $37°N - 39°N$.

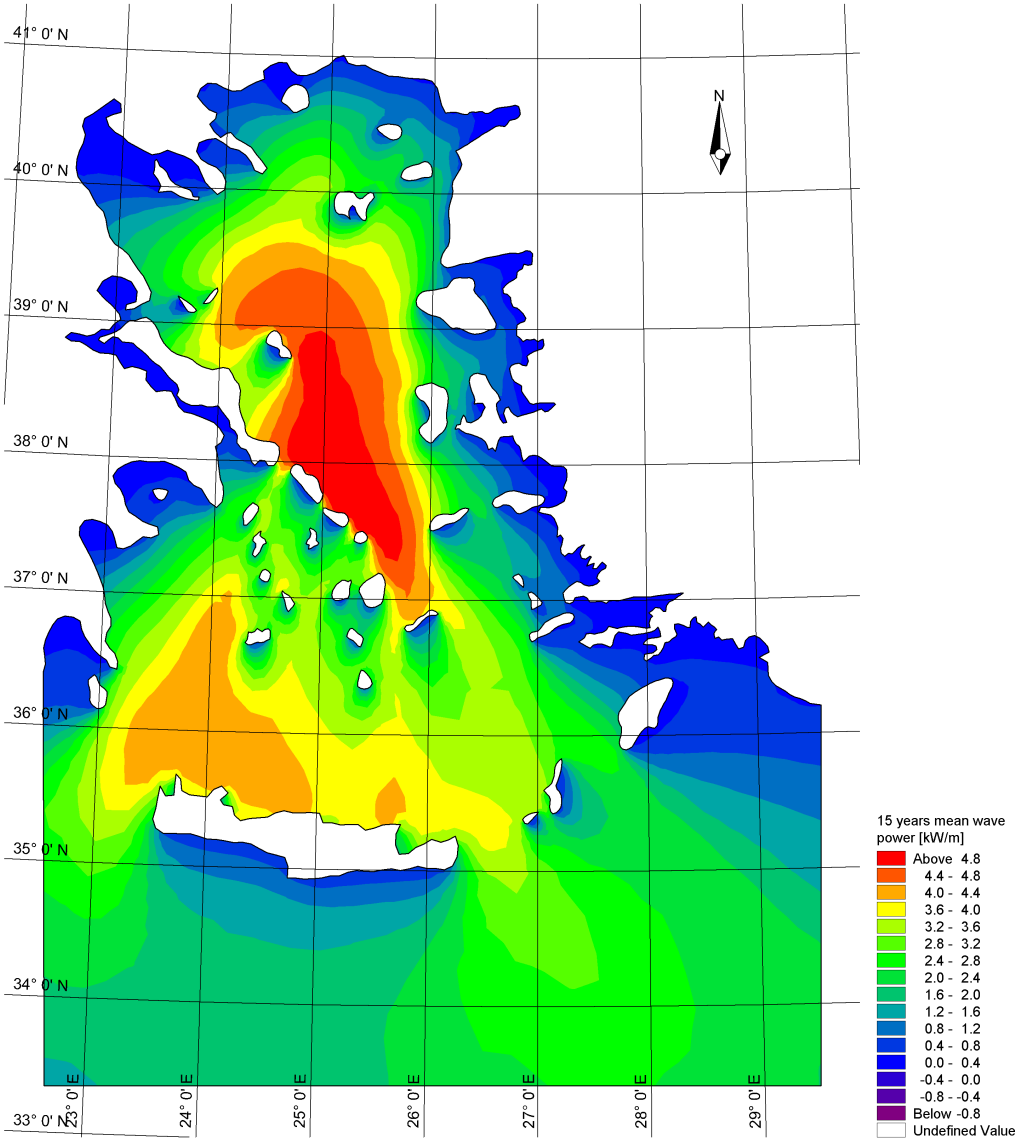

Figure 4.22: Fifteen-year mean wave power for October.

- November

  - Significant Wave Height

    Coverage area of the higher significant wave height values has increased in contrast to previous month, Figure 4.23 demonstrate a fifteen-year mean significant wave height for November.

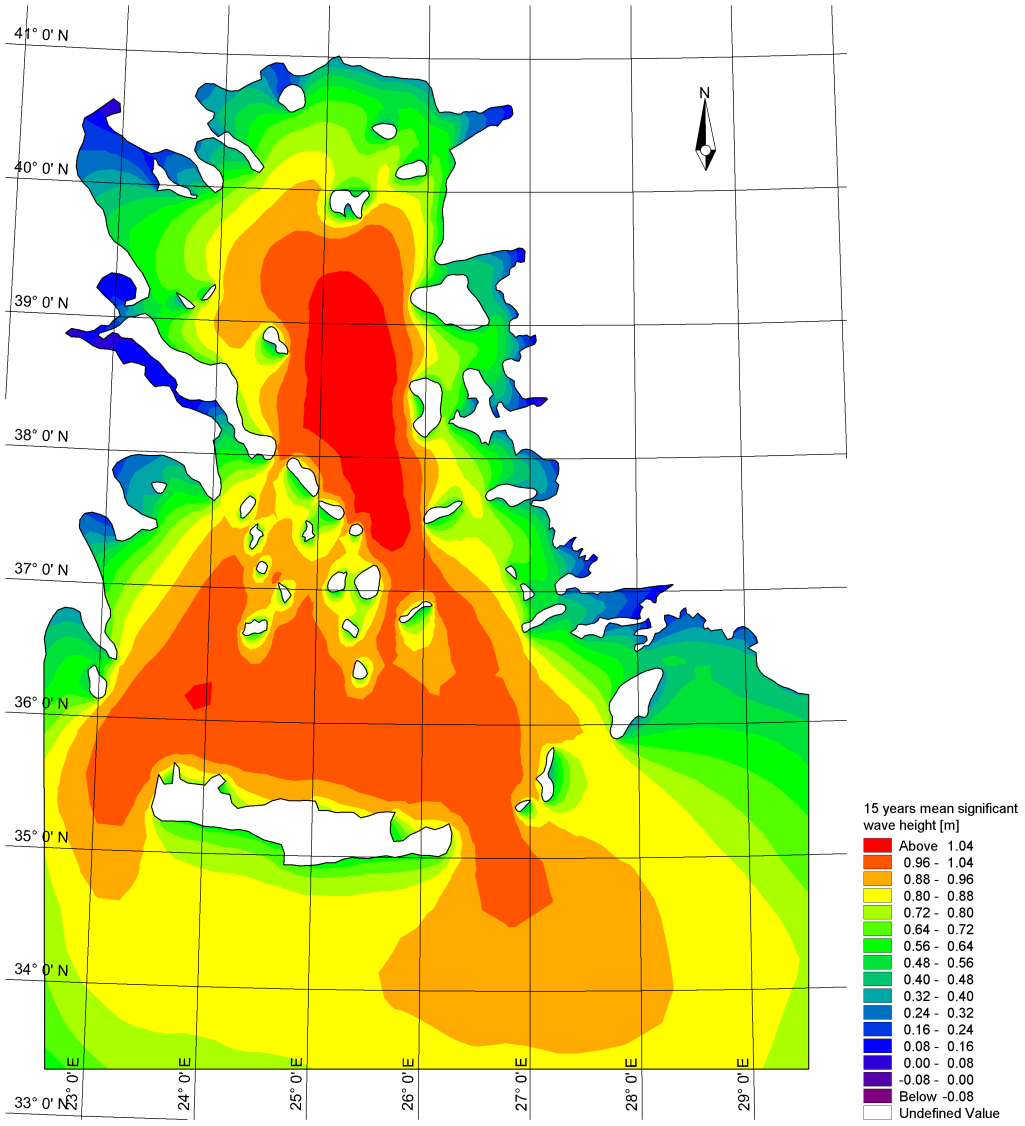

Figure 4.23: Fifteen-year mean significant wave height for November.

– Mean Wave Power

  Displacement of maximum wave power area to north ($38°N - 40°N$ is noticeable for this month in comparison with October (Figure 4.21).

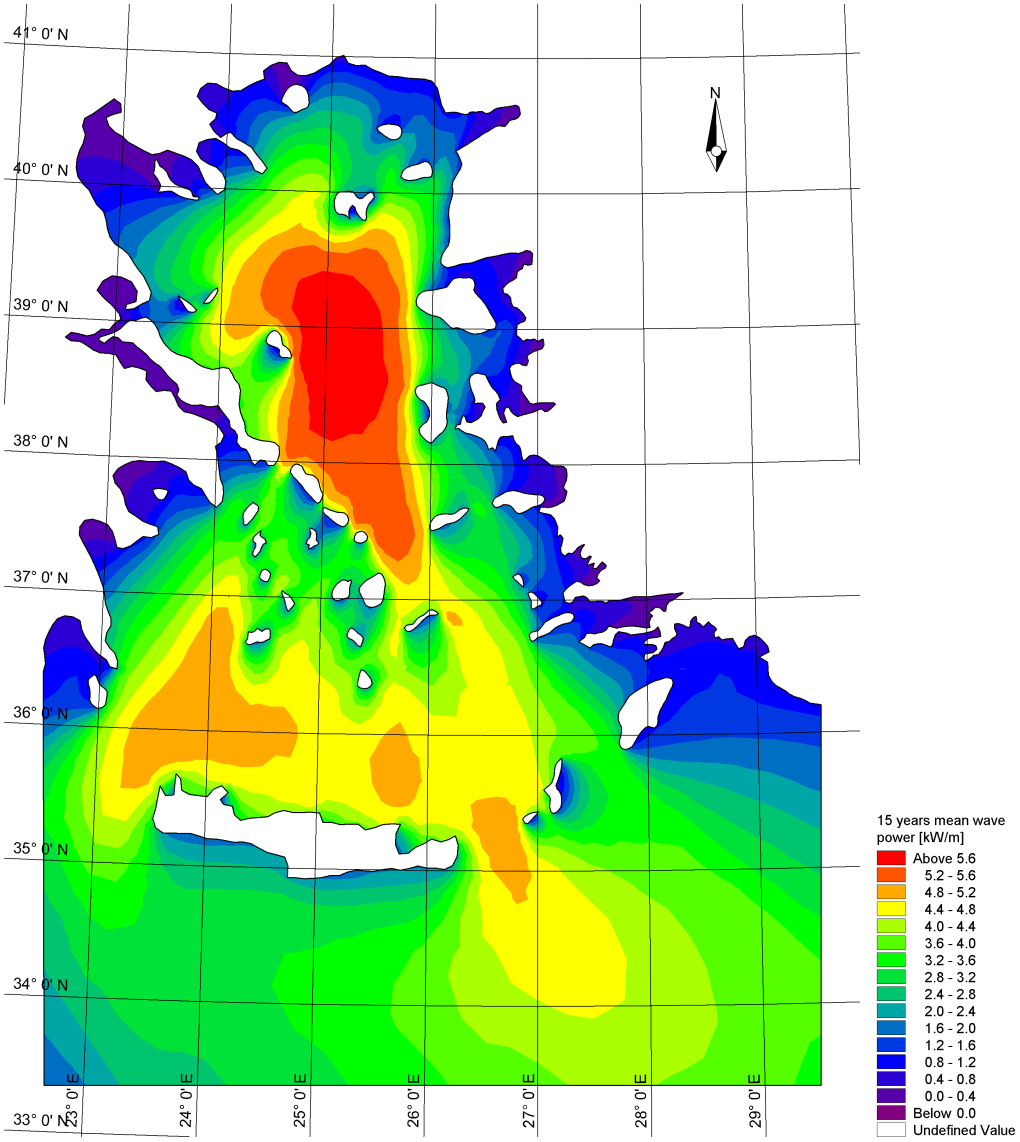

Figure 4.24: Fifteen-year mean wave power for November.

- December
  - Significant Wave Height

    The increase in significant wave heights are obvious in this month relative to previous month. In Figure 4.25 values of SWH have increased while covering more area of the north Aegean Sea.

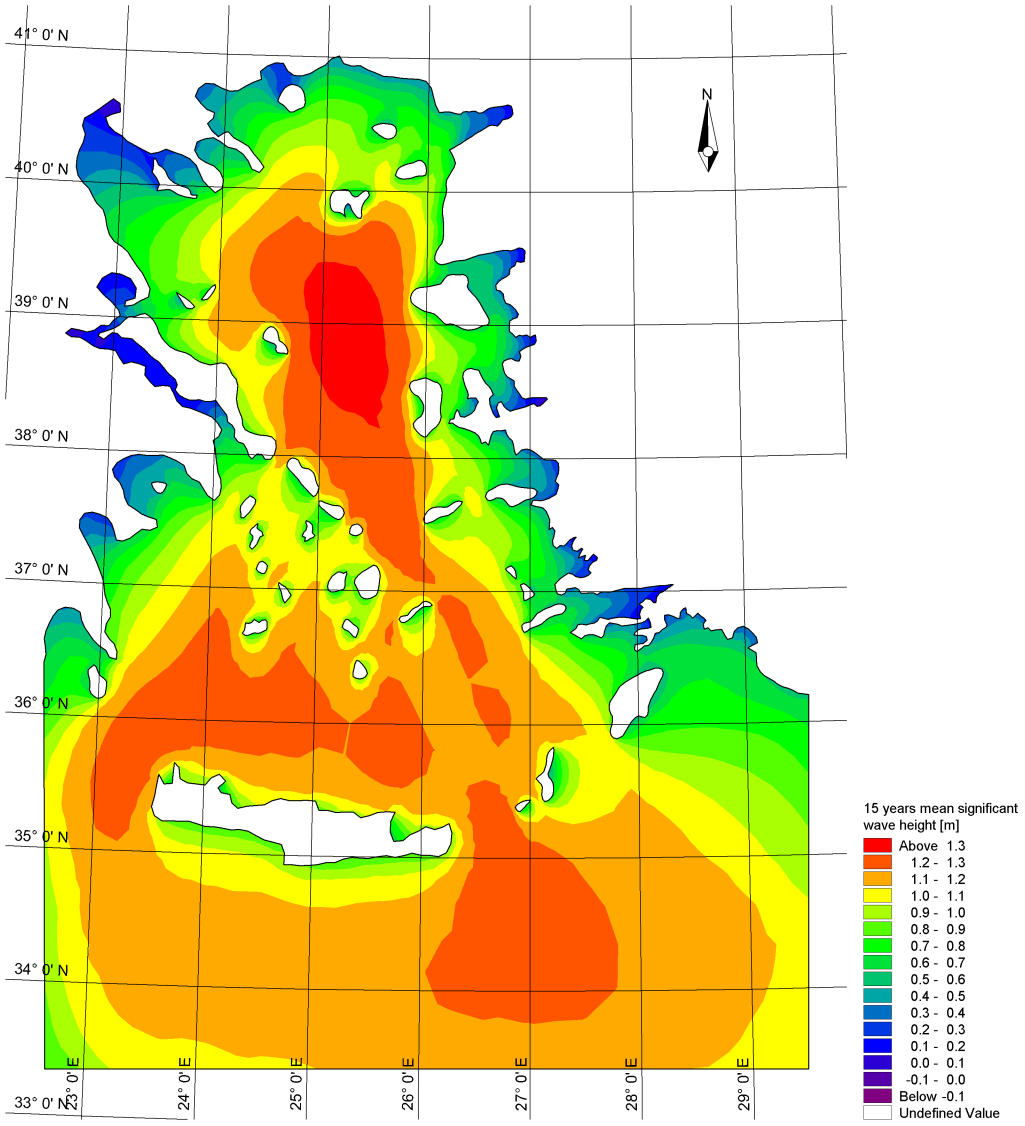

Figure 4.25: Fifteen-year mean significant wave height for December.

– Mean Wave Power

  Magnitude of maximum wave power for December has rose in comparison to November distinctly. Figure 4.26 shows that maximum wave power values are located in North Skyros Basin.

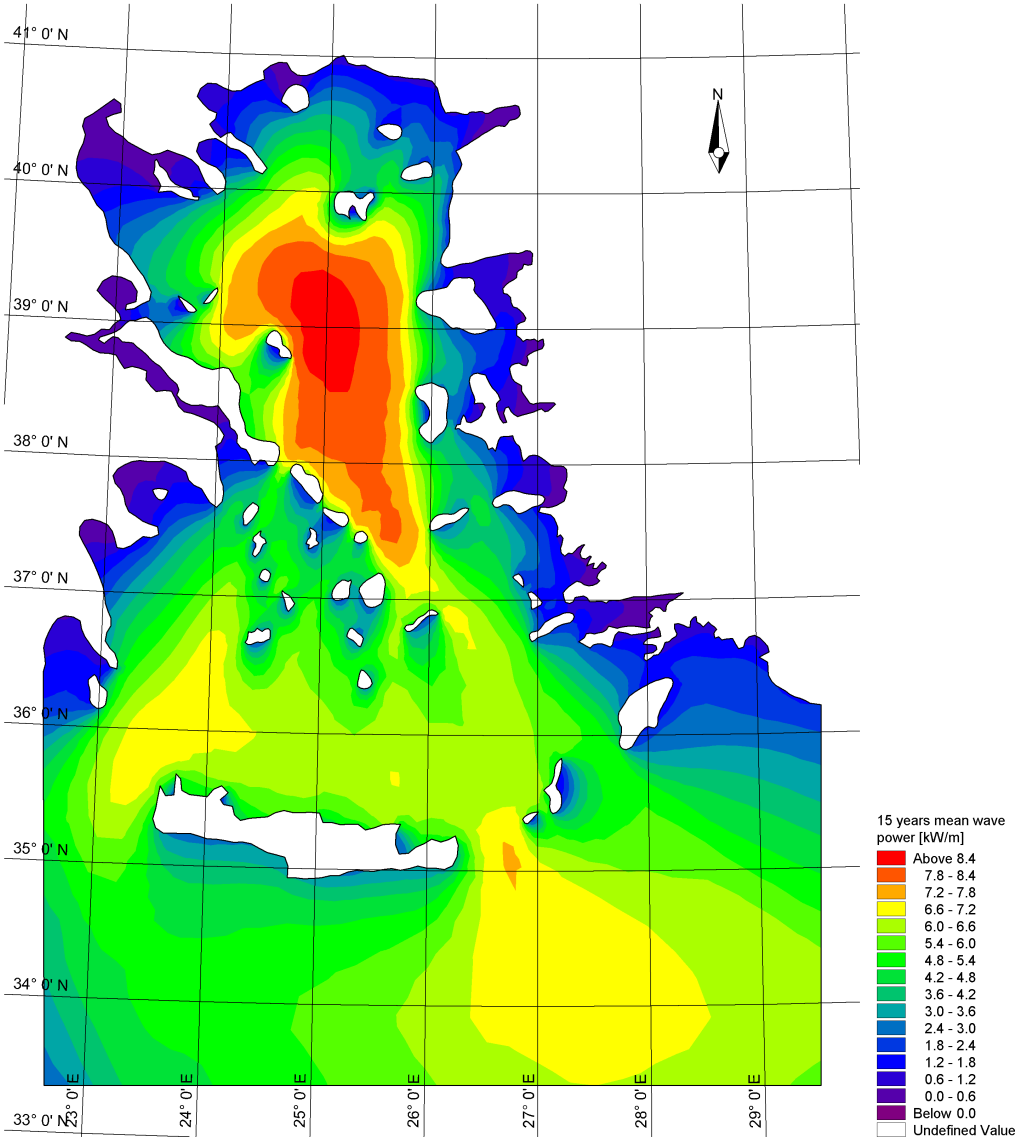

Figure 4.26: Fifteen-year mean wave power for December.

4.1.2 Seasonal analysis

Season change and its effect on the wave climate is an important subject and it is discussed in this study, for this purpose significant wave height and wave power maps were produced by calculation of mean value of the whole domain in that season.

- Significant Wave Height

Figure 4.27 shows mean wave heights for Spring, and for summer Figure 4.28 was prepared and for two other seasons Figure 4.29 and Figure 4.30 shows their mean significant wave height in that season.

The displacements of the maximum wave heights can be traced from these four figures mentioned in here. The maximum wave heights occur in southern part of Aegean Sea in Spring while this continues for Summer with a little shift of the maximum points to north. But in Fall season the maximum parts of the domain has increased from one to 2 parts, one in the middle-north and one occurring in 1° lower in Latitude coordinates.

Also by having a deeper look to the maps of the seasonal results this can be concluded that in fall and winter the area covering higher significant wave heights are greater than other 2 seasons. From Figure 4.30, it is concluded that higher wave heights occur than other seasons.

- Mean Wave Power

  Mean wave power is calculated for each season to show the difference of the wave climate in different seasons. It can be seen from figures shown that wave power magnitudes in Fall and Winter are more than Spring and Summer. The least powerful season for Aegean sea is Summer shown in Figure 4.32 and Spring, Fall and Winter has higher wave power potential respectively.

  High wave power magnitudes in Spring is accumulated in middle and southern parts of Aegean Sea, specifically maximum wave power can be observable in 2 locations. First of them which has bigger area is located between Kasos and Crete islands. Th second maximum wave power point is between Ikaria and Mykonos islands. However the magnitudes of wave power in this season is not as high as winter but major area of the domain is faced with medium-high wave powers. A fifteen-year mean wave power map for Spring is shown in Figure 4.31.

  In Summer a small part of the middle Aegean Sea is encountered with high wave powers which is located in northern part of Kasos island. Summer could be called as a calm season for wave power potential that does not include high wave powers relative to Spring.

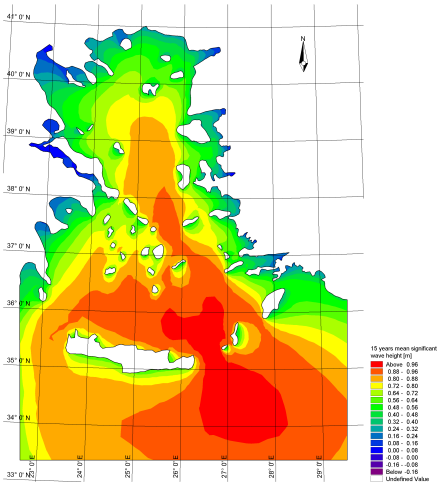

Figure 4.27: Mean significant wave height for Spring.

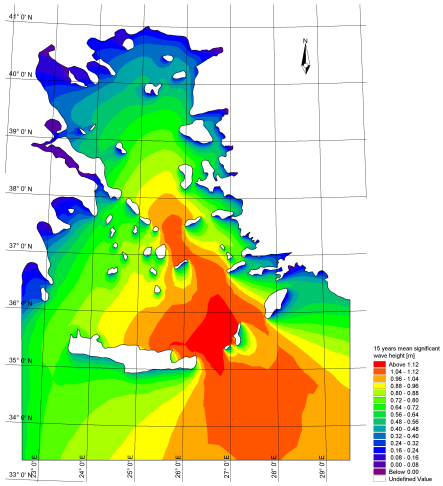

Figure 4.28: Mean significant wave height for Summer.

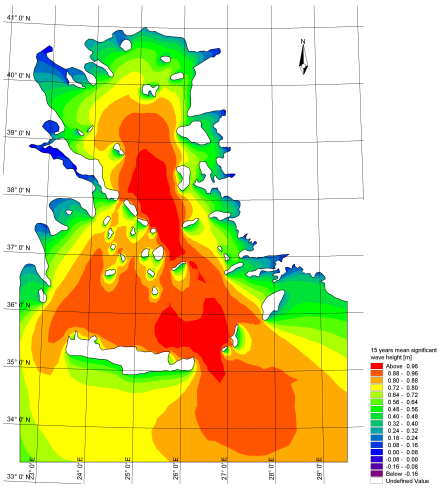

Figure 4.29: Mean significant wave height for Fall.

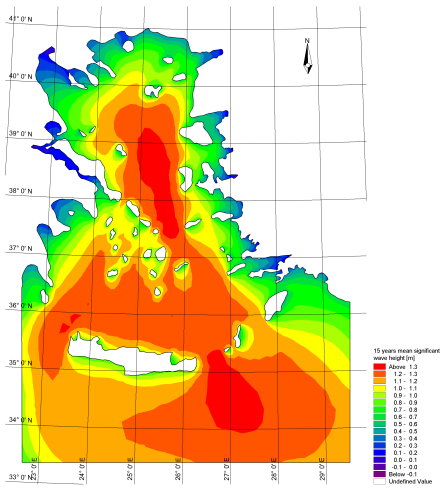

Figure 4.30: Mean significant wave height for Winter.

Mean wave power for Fall is shown in Figure 4.33, the shift of maximum wave power points to north, between Chios and Skyros islands, is obviously observable. This second most powerful waves take place in this season having more than 4.4 kW/m.

The most powerful wave potential is found to be happening in Winter as a result of 15 years simulation and calculation of each year's winter wave power values. As demonstrated in Figure 4.34, the points having maximum wave power potential are concentrated at the northern part of the domain. Maximum wave power potential possible which is estimated by the model for winter season is more 8.4 kW/m. An important point which should be noted by considering Figure 4.34 is that the whole domain is facing more wave power than other seasons.

4.1.3 Yearly analysis

In this part of the thesis the data which shows simulation's mean values will be given as a reference which shows the change of the wave characteristics each year. As it mentioned before the simulations have taken place for a fifteen years time span.

The simulation results are given in Chapter A. These figures are shown as a reference for further analyses in this thesis. In these figures every year's significant wave height and wave power maps are shown.

4.2 Spatial Analyses

4.2.1 Overall area-based analysis

Analysis of the area percentage which is not shown in the figures had to be calculated by hand. The area consisting each interval of values are first found from each map by image processing and the percentages are then calculated using excel. Analysis of this section will give a useful information of the domain with quantitative results for the area coverage of each significant wave height and wave power's interval.

Table 4.3 demonstrates percentages of the 15-year mean significant wave height ($\bar{H}_s$) and mean wave power ($\bar{P}_{wave}$) in whole study area.

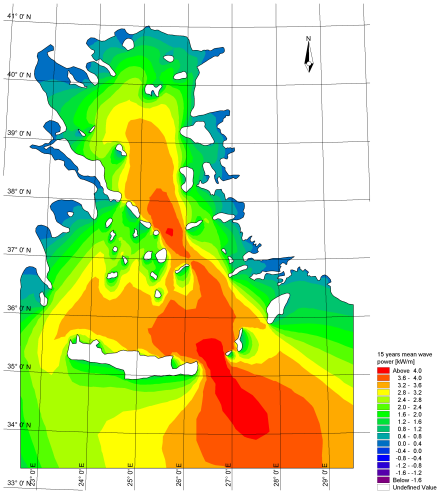

Figure 4.31: Mean wave power for Spring.

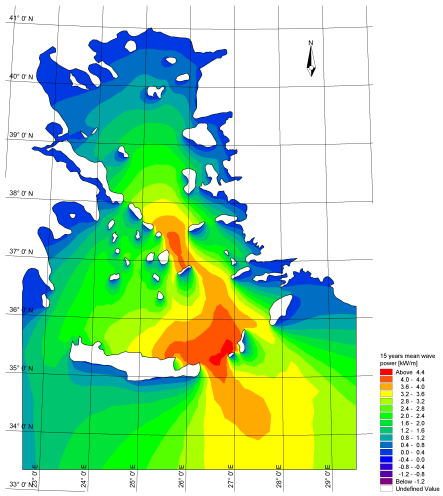

Figure 4.32: Mean wave power for Summer.

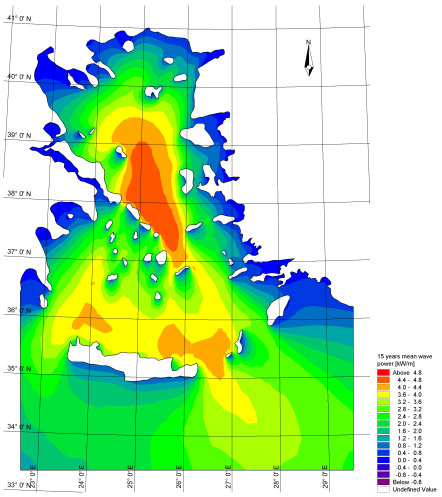

Figure 4.33: Mean wave power for Fall.

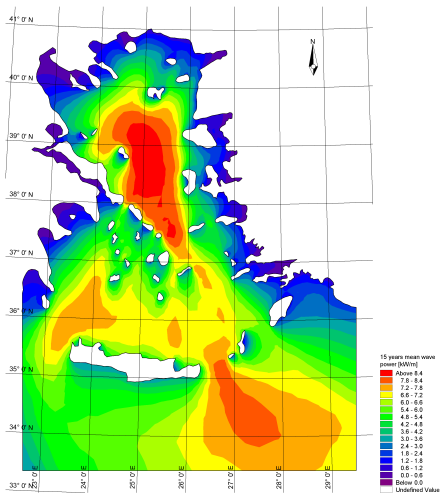

Figure 4.34: Mean wave power for Winter.

Table 4.3: Fifteen-year mean significant wave height and mean wave power area percentages in domain.

SWH (m)	(%)	Wave Power (kW/m)	(%)
Above 0.96	0.17%	Above 5.2	0.24%
0.88-0.96	11.80%	4.8-5.2	4.08%
0.80-0.88	11.03%	4.4-4.8	13.19%
0.72-0.80	9.16%	4.0-4.4	16.15%
0.64-0.72	4.83%	3.6-4.0	9.90%
0.56-0.64	3.12%	3.2-3.6	8.81%
0.48-0.56	2.76%	2.8-3.2	12.50%
0.40-0.48	53.42%	2.4-2.8	8.36%
0.32-0.40	1.40%	2.0-2.4	6.00%
0.24-0.32	1.07%	1.6-2.0	4.92%
0.16-0.24	0.66%	1.2-1.6	4.57%
0.08-0.16	0.39%	0.8-1.2	4.45%
0.00-0.08	0.19%	0.4-0.8	3.88%
		0.0-0.4	2.94%

4.2.1.1 Seasonal area-based analysis

Seasonal mean wave heights and wave power values are calculated for the importance of the season changes in wave climate and making a good reference for whom needed these discussions.

Table 4.4 shows every interval's percentage on the map. The highest percentage of the H_s has occurred in wave heights between $0.88-0.96$, on the other hand this table shows that in most of the study domain, H_s values are more than $0.64m$, the most frequent wave power in this domain is more than 2.4 kW/m. The tables shown in this part of the thesis are based on 15 years simulations for the season being discussed.

For summer, Table 4.5 shows the highest percentage of area for $2.8-3.6kW/m$ wave power. On the other hand the biggest area of the domain has a H_s between $0.96-1.12m$.

In Table 4.6 as it can be seen it is shown that the percentages of the lower wave powers have decreased in comparison with the summer percentages. Also on this season the highest percentage of the area has increased in contrast to summer. So that it shows that the distribution of the area having the same wave power has shifted to the higher wave power values.

Table 4.4: Significant wave height and wave power percentages based on 15 years spring season simulation data.

SWH (m)	(%)	Wave Power (kW/m)	(%)
Above 0.96	8.70%	Above 4.0	3.12%
0.88-0.96	24.37%	3.6-4.0	14.50%
0.80-0.88	23.56%	3.2-3.6	17.63%
0.72-0.80	11.70%	2.8-3.2	13.80%
0.64-0.72	8.68%	2.4-2.8	14.52%
0.56-0.64	6.18%	2.0-2.4	9.70%
0.48-0.56	5.55%	1.6-2.0	6.95%
0.40-0.48	3.94%	1.2-1.6	5.60%
0.32-0.40	2.80%	0.8-1.2	5.82%
0.24-0.32	2.16%	0.4-0.8	4.71%
0.16-0.24	1.28%	0.0-0.4	3.66%
0.08-0.16	0.69%		
0.00-0.08	0.39%		

Table 4.5: Significant wave height and wave power percentages based on 15 years summer simulation data.

SWH	(%)	Wave Power (kW/m)	(%)
Above 1.12	2.37%	Above 4.4	0.35%
1.04-1.12	15.17%	4.0-4.4	2.72%
0.96-1.04	12.82%	3.6-4.0	6.16%
0.88-0.96	9.14%	3.2-3.6	11.93%
0.80-0.88	10.31%	2.8-3.2	10.15%
0.72-0.80	11.83%	2.4-2.8	7.37%
0.64-0.72	9.33%	2.0-2.4	9.04%
0.56-0.64	6.44%	1.6-2.0	11.02%
0.48-0.56	5.79%	1.2-1.6	13.09%
0.40-0.48	5.09%	0.8-1.2	8.81%
0.32-0.40	3.94%	0.4-0.8	9.70%
0.24-0.32	2.85%	0.0-0.4	9.66%
0.16-0.24	2.46%		
0.08-0.16	1.60%		
0.00-0.08	0.84%		

Table 4.6: Significant wave height and wave power percentages based on fall season simulation.

SWH (m)	(%)	Wave Power (kW/m)	(%)
Above 0.96	6.73%	Above 4.8	0.07%
0.88-0.96	22.88%	4.4-4.8	2.98%
0.80-0.88	20.53%	4.0-4.4	5.61%
0.72-0.80	19.28%	3.6-4.0	11.99%
0.64-0.72	8.82%	3.2-3.6	12.72%
0.56-0.64	5.63%	2.8-3.2	14.65%
0.48-0.56	4.68%	2.4-2.8	9.26%
0.40-0.48	4.19%	2.0-2.4	14.08%
0.32-0.40	2.65%	1.6-2.0	8.39%
0.24-0.32	2.14%	1.2-1.6	5.56%
0.16-0.24	1.29%	0.8-1.2	5.40%
0.08-0.16	0.83%	0.4-0.8	5.60%
0.00-0.08	0.35%	0.0-0.4	3.69%

While having half a glance to the Table 4.6 and then comparing with the values in the Table 4.7 it can be concluded that the percentage of area facing higher H_s values has increased intensively. As a result, in winter times the area facing higher wave power values is greater than other seasons.

4.2.2 Nearshore analysis

In this thesis different analysis was designed and implemented so as to make a complete reference Aegean Sea's wave climate in last 15 years. Significant wave height and wave power is calculated through the lines parallel shape of the Aegean Sea's east coast.

The goal of this investigation was to have complete information of the Aegean Seas's wave characteristics in different aspects. so that it was decided to get the wave parameters in 4 different distances from coastal line, the points of these lines were calculated in a way to not be located in the islands near eastern coast.

The parallel coastal lines with 1, 5, 10 and 20 *km* spans from coastal line of the Turkey is drawn and was decided to get 2 results from model. Significant wave height and wave power values were derived from model for 15 years as an average value for each point spanning with the distances mentioned. For demonstration of the values for each parallel line, mean value on that line is calculated.

Table 4.7: Significant wave height and wave power percentages based winter season simulation.

SWH (m)	(%)	Wave Power (kW/m)	(%)
Above 1.3	6.16%	Above 8.4	2.44%
1.2-1.3	32.53%	7.8-8.4	5.98%
1.1-1.2	23.44%	7.2-7.8	13.57%
1.0-1.1	10.74%	6.6-7.2	15.23%
0.9-1.0	6.85%	6.0-6.6	10.11%
0.8-0.9	5.06%	5.4-6.0	11.52%
0.7-0.8	4.65%	4.8-5.4	10.02%
0.6-0.7	3.21%	4.2-4.8	6.45%
0.5-0.6	2.27%	3.6-4.2	5.08%
0.4-0.5	1.97%	3.0-3.6	4.11%
0.3-0.4	1.34%	2.4-3.0	3.71%
0.2-0.3	0.93%	1.8-2.4	3.53%
0.1-0.2	0.69%	1.2-1.8	3.04%
0.0-0.1	0.17%	0.6-1.2	2.86%
		0.0-0.6	2.34%

Table 4.8: Mean significant wave height and mean wave power on the parallel shape of the east coast of Aegean Sea.

Significant wave height (m)				Wave Power (kW/m)			
1 km	5 km	10 km	20 km	1 km	5 km	10 km	20 km
0.29	0.37	0.46	0.55	0.52	0.74	1.06	1.56

This should be annotated that for calculations in this part was not done as easily as other analysis. First of all, the coastline data was converted into a format which could be imported to Autocad, then the Poly-lines were drawn using offset command to make parallel lines then the shapes with the edited points were imported to MIKE Zero data extraction tool and values were taken out of simulations result for 15 years.

The results of this nearshore investigation is shown in Table 4.8. The 2 main columns referring to $\bar{H}_s$ and $\bar{P}_{wave}$ and the values shown in second raw shows the distance of the parallel shapes of the Aegean Sea from Turkish coast. Row 3 shows the mean values of each poly-line's points for each distance.

From the values derived from calculations in each distance of the coastline; It is easily concluded that by going further from coast the wave heights and wave power are increasing.

Table 4.9: Coordinates of the selected points for in-depth investigations.

	UTM-35		WGS84			
	Meter		Decimal Degree		DMS	
	Lon.	Lat.	Lon.	Lat.	Lon.	Lat.
1	408388.3	4405714	25.92994	39.79646	25°55′48”	39°47′47”
2	243225.9	4391681	24.00793	39.63639	24°0′29”	39°38′11”
3	345777.7	4301003	25.22292	38.84434	25°13′23”	38°50′40”
4	384639.5	4159590	25.69357	37.57613	25°41′37”	37°34′34”
5	656671.6	4038686	28.74893	36.48068	28°44′56”	36°28′50”
6	236749	4025733	24.06685	36.34069	24°4′1”	36°20′26”
7	434296.1	4014938	26.26843	36.27715	26°16′6”	36°16′38”
8	463442.4	3901591	26.59812	35.25676	26°35′53”	35°15′24”
9	570312.2	3804437	27.76479	34.37892	27°45′53”	34°22′44”
10	187092.3	3793642	23.60292	34.23686	23°36′10”	34°14′13”

4.2.3 Point series analysis

This part of thesis investigates the behavior of waves in 10 different points of the domain. Some of the points are located in a high magnitude wave heights and some are located in nearshore. Selected points' geographical coordinates are given in Table 4.9 for both UTM-35 and World Mercator systems.

Figure 4.35 shows the positions of the points in the domain. every point is labeled with a number from 1 to 10 to easy recognition of the further analyses.

4.2.3.1 Frequency analysis

Frequency diagrams of the wave heights versus wave period intervals are shown in Appendix B, horizontal axis shows mean wave period (T_{01}) and vertical axis demonstrates significant wave height (H_s) values. Intervals are shown with 0.5 difference for each wave characteristic to have high resolution. The main aim of this part of analysis is to determine the most frequent wave height-wave period magnitudes for each of selected points in the Aegean Sea. These values are derived from 10-minutes simulations and shows the number of occurrences for each interval.

Figure B.1 shows the distributions of the significant wave height with mean wave period for Point 1, in this figure it can be observable that most frequent interval for wave heights and wave periods is located between $1.5 \leq T_{01} < 2$ (sec) and $H_s < 0.5$(m).

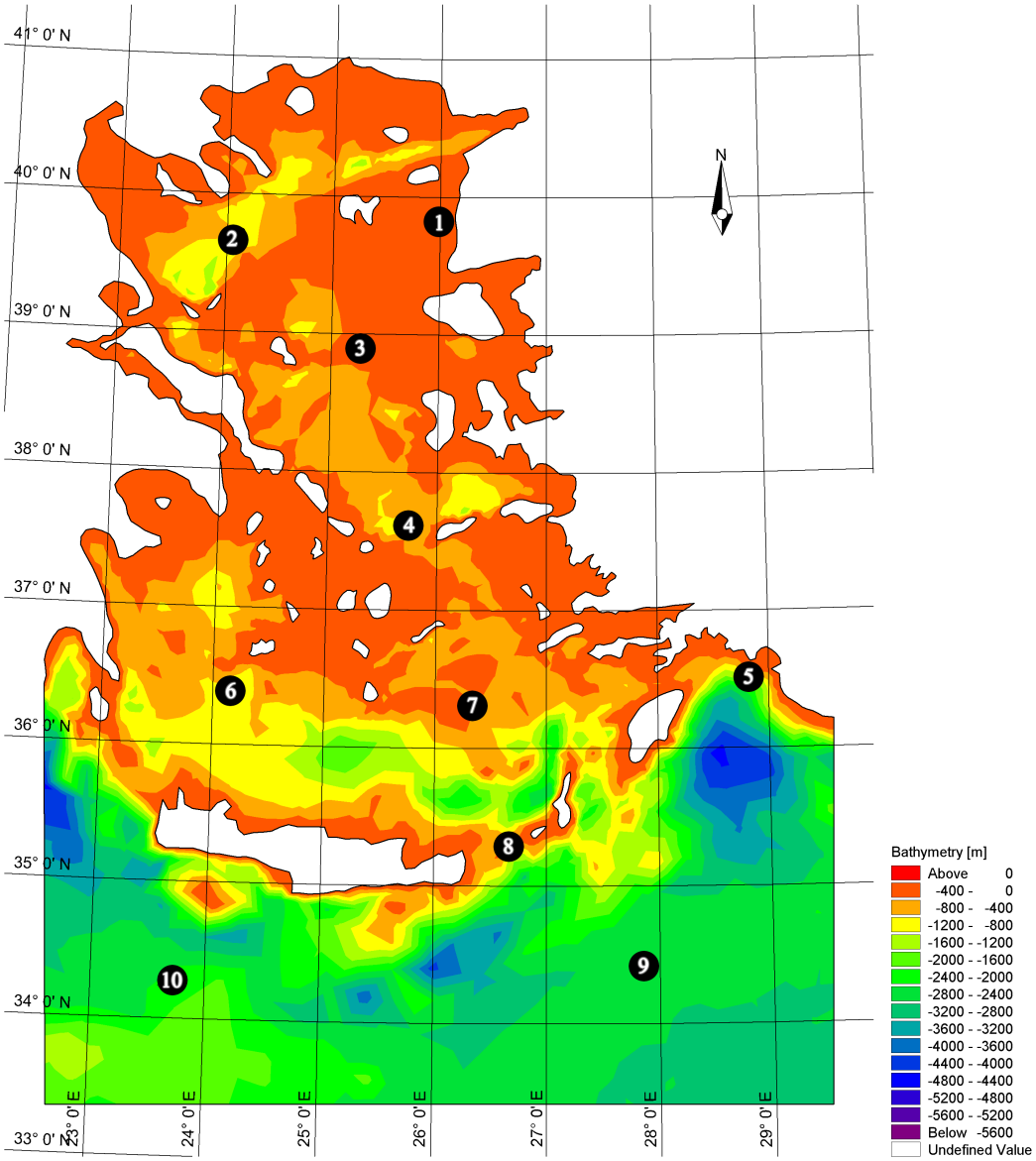

Figure 4.35: Selected points in Aegean Sea.

Same wave frequency analyses are done for other 9 points and the results of the comparisons show that for points in nearshore parts of the domain, the most frequent interval is in lower wave heights and wave periods. In contrast to nearshore points, offshore points' frequent wave height-wave period interval has a higher values for these wave characteristics.

4.2.3.2 Monthly mean time series

In this part of this thesis the focus is on difference of the wave heights and wave periods for each selected point in study area. Comparisons of wave characteristics are conducted by figures for the same points. Figures show the variations of the wave height and wave periods magnitudes by time. The aim of this section is to investigate the behavior of waves in different locations of the domain.

Deep analysis of wave heights for different locations of the domain is definitely indispensable for a study in this scale. Monthly mean significant wave height values are calculated from simulations for selected points. The values shown in Figure 4.36 has 15 years span with monthly intervals. For every point, a color is given in the figure to be recognized easily.

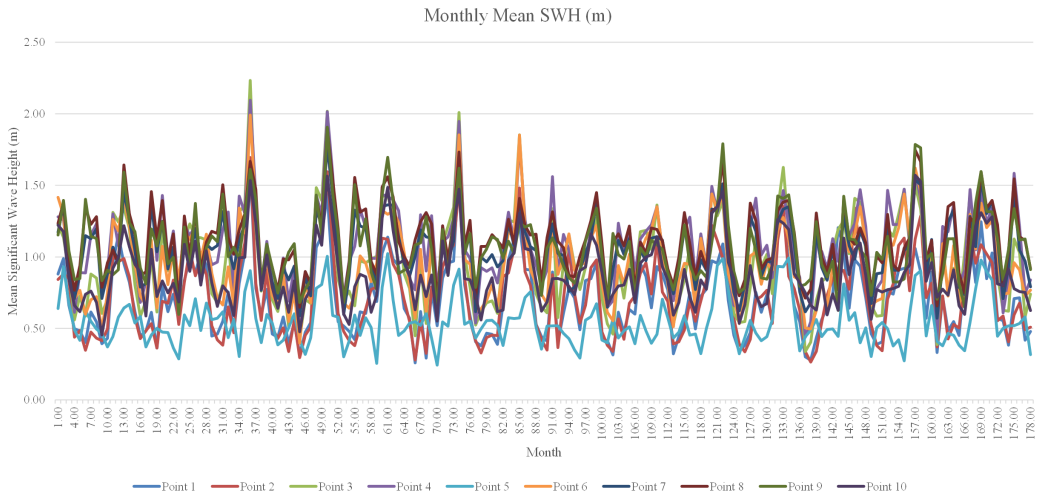

Figure 4.36: Monthly mean significant wave heights for selected points.

As shown in Figure 4.36 also mean wave characteristics are shown in Table 4.10, the least wave height is found to be in Point 5 through selected points, whilst the least mean wave period refers to Point 1. On the other hand, the maximum significant wave

Table 4.10: Fifteen-year mean wave height and wave period values for selected points.

Point	Significant wave height H_s (m)	Mean wave period T_{01} (sec)
1	0.70	3.07
2	0.72	3.36
3	0.97	3.58
4	1.09	3.83
5	0.54	3.27
6	0.97	3.68
7	1.05	3.82
8	1.12	4.02
9	1.07	4.03
10	0.88	3.54

height is detected for Point 8 which is between Crete and Kasos islands. It has to be taken into consideration that Point 9 and Point 8 have a relatively close wave height values.

Monthly mean wave periods for in-depth analysis points are shown in Figure 4.37, by studying this figure it could be concluded that Point 1 is has least monthly mean wave period relative to other points. Figure 4.37 demonstrate that points located in offshore have higher magnitudes of wave periods.

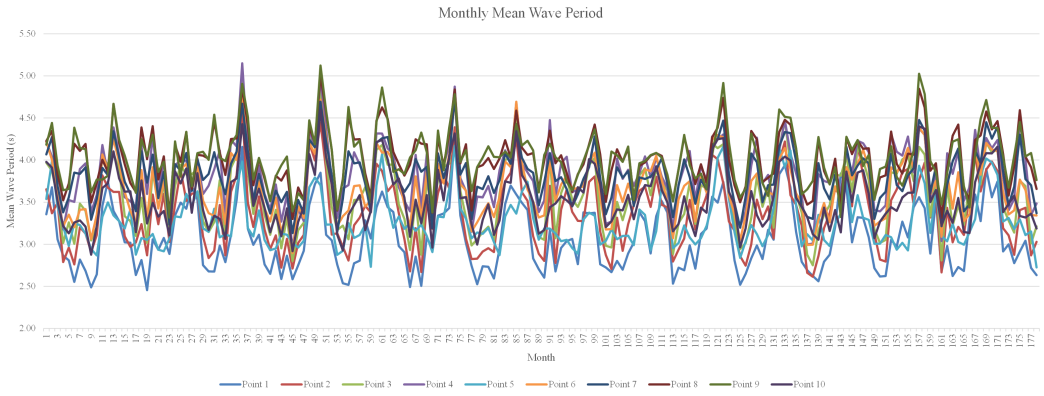

Figure 4.37: Monthly mean wave periods for selected points.

The minimum and maximum values of 15-year mean wave heights and mean wave periods are specified by one underline and two underlines. The maximum wave period refers to Point 9.

4.2.3.3 Wave rose analysis

Wave power magnitudes corresponding to the wave directions are one of the most important facts that should be analyzed in wave power review of study region. Selected points are used in this stage for derivation of the wave power and directions in 10 points.

This part of thesis focuses on the behavior of the waves in 10 points which are selected to cover all of the Aegean Sea's area. Different patterns are revealed by the data obtained from simulations. Wave roses for these 10 points are shown in Figure 4.38. The map shows the frequency of a wave power and wave directions in each point. Wave power values are divided into 6 intervals from 0.5 kW/m to above 4 kW/m wave power potential.

The term "Calm" is used for the wave powers lower than 0.5 kW/m which is shown in center point of each wave rose figure on map. Percentage of each wave power value interval is shown by percentage and scale shows determines 10% scale for recognition of the values shown on figures.

The map of the wave rose figures shows that for coastal parts of the model greater proportion of the waves are in low magnitude. Point 1, Point 2 and Point 5 have the highest percentage of lower magnitudes of wave powers.

It can be inferred from Figure 4.38 that most of the high magnitude waves approach to middle parts of the domain from south-east corner of the Aegean Sea. Higher wave powers in north-west direction in Point 9 proves the fact that higher wave heights are taking place in this point. The most frequent direction in Point 9 is north-west direction.

Point 8 is one of the points in the domain which has a high wave power potential among other points and is one of the most powerful points. In this point wave powers less than 0.5 kW/m form 21.5% of the total waves in this point. For Point 9 there is only one high frequent direction which is north-west, while for Point 8 it could be interpreted as a division of most frequent wave powers into 2 directions in that point. The most occurring wave direction in this point is in north and north-west orientation.

The calm waves' percentage is increasing by approaching to the middle parts of the Aegean Sea as it can be seen from wave rose of Point 7. The most frequent wave direction belongs to south to north waves.

As a conclusion to this section of the study, waves can be traced in the domain that south to north waves for lower part of the domain and south-west to north-east waves in higher altitudes are the most frequent waves.

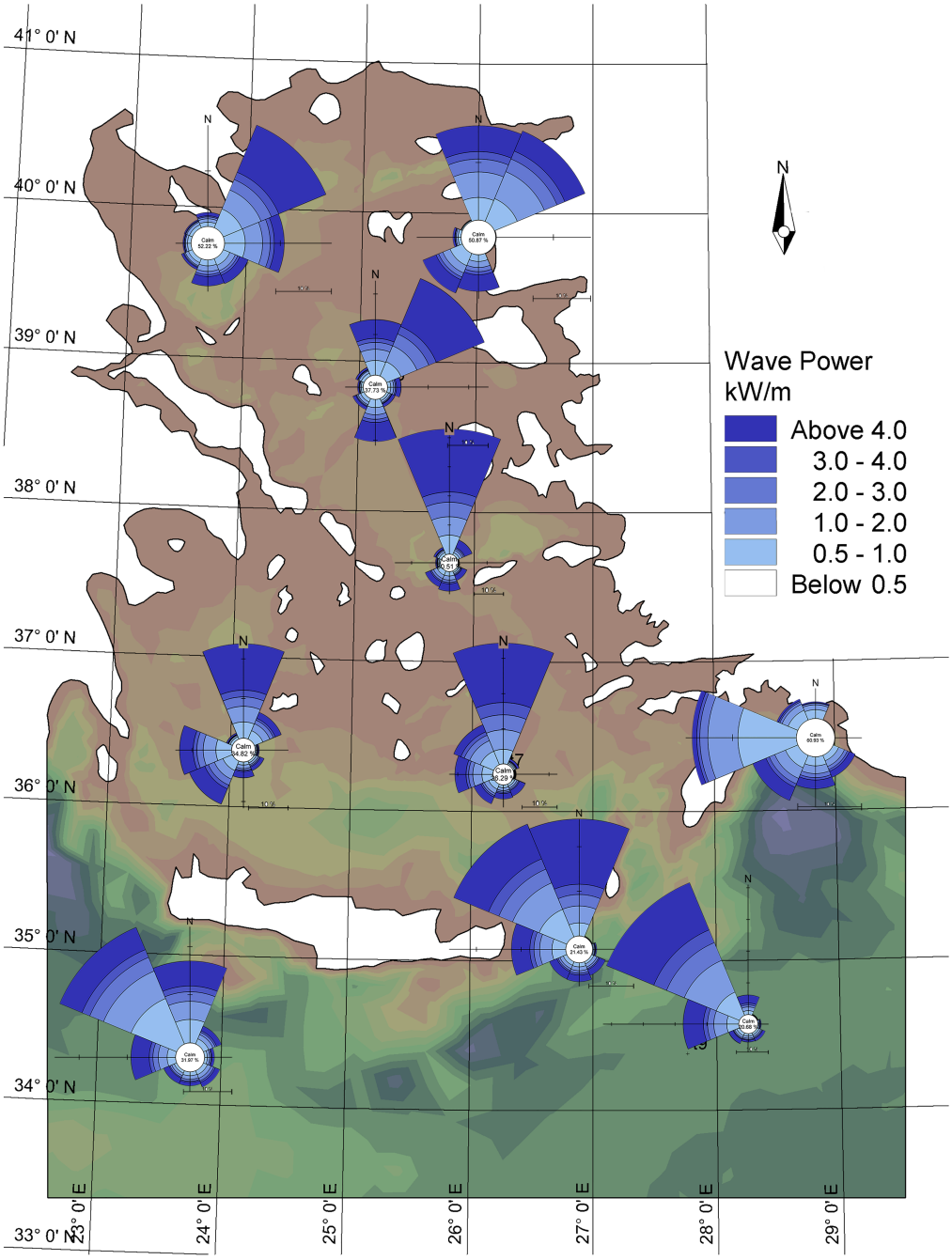

Figure 4.38: Wave rose diagrams for selected points.

5. CONCLUSION

In this study significant wave characteristics are simulated for Aegean Sea from 1999 to 2013 using MIKE 21 SW. Model parameters have been calibrated by 3 wave buoy station measurements. The high correlation coefficients and other statistical measures shows a good agreement between model and observation data which proves the model for the long-time simulations.

Wave simulations have a 10-minutes temporal resolution which it applies to both significant wave heights and mean wave period. In analyses, significant wave heights and wave powers are mentioned as a wave characteristics which takes place for monthly, seasonal and yearly analyses. The results of the analyses is presented as maps in this study and comments have been given. Under all analyses and results which are mentioned in the Chapter 4, conclusions can be listed as below:

- In the model results, spatial and temporal changes of wave characteristics have been taken into account. According to these analyses wave heights and wave power values are changing by time and place. These changes were significant and very obvious. In order to understand this behavior different analyses were done.
- In Winter, significant wave heights and wave powers have higher magnitudes in comparison with the other seasons. The least wave power in the study region was in Summer.
- Having a glance to the monthly analysis of this study which was prepared from 15-year data, this could be concluded that the most powerful waves are in February, reaching a wave power potential of 9 kW/m, in contrast the least powerful waves occur in June and August.
- Islands located in the Aegean Sea, prevent wave from reaching to the nearshore with their full energy, therefore in areas having less islands the wave powers are higher.

- Most energetic points in the domain is located in the offshore.
- Higher wave powers and significant wave heights occurring in Crete Sea, southern part of the Aegean Sea, in Spring and Summer. In Winter this part of the Aegean Sea has the highest wave powers.
- The wave rose analysis of this thesis has shown that different points have different frequent wave directions with the same wave power ranges. By taking all of the wave rose diagrams into consideration, most frequent wave directions are from south-east to north-west and from middle part of the domain the main direction changes to north-east and north.
- According to the frequency diagrams of mean wave period and mean wave height for selected points. The points located in middle and offshore parts of the domain have a wider ranges of significant wave height and mean wave period values. The most frequent intervals are placed between $0.5 < H_s < 2$ and $2 < T_{01} < 3.5$.
- For Turkish coasts these conclusions can be taken out of this study:
  - For the Turkish coast it was seen that the shading effect had decreased the wave energy for this regions. Though there were some locations which had a higher wave power potential compared with other parts of east coast of Aegean Sea.
  - In a glance to the 15-year mean significant wave height map it was seen that high wave potential is available in Northern part of Aegean Sea specially in Bozcaada, Gökçeada and Baba Burnu. In this part mean wave power is between 1.0 - 2.8 kW/m.
  - For middle-Aegean Sea, Karaburun and Çesme have a 2.0 kW/m of wave power potential.
  - As a result of data derivated from parallel coastline to east coast of Aegean Sea, it can be concluded that by going further from shoreline to deep water the wave heights and wave power is increasing.

REFERENCES

[1] **Arinaga, R.A. and Cheung, K.F.** (2012). Atlas of global wave energy from 10 years of reanalysis and hindcast data, *Renewable Energy*, 39(1), 49–64.

[2] **Yamaguchi, M.**, **Hatada, Y. and Utsunomiya, Y.** (1987). A shallow water wave prediction model at a single location and its applicability, *Jour. JSCE*, 381, 151–160.

[3] **Hatada, Y. and Yamaguchi, M.** (1998). A long term wave hindcast system using ECMWF winds, *Coastal Engineering Proceedings*, 1(26).

[4] **Golshani, A.**, **Nakhaee, A.**, **Taebi, S.**, **Chegini, V. and Alaee, M.J.** (2005). Wave Hindcast Study of the Caspian Sea, *Journal of Marine Engineering*.

[5] **Jose, F. and Stone, G.W.** (2006). Forecast of nearshore wave parameters using MIKE-21 Spectral wave model, *Journal of Physical Oceanography*.

[6] **Janssen, P.A.** (1989). Wave-induced stress and the drag of air flow over sea waves, *Journal of Physical Oceanography*, 19(6), 745–754.

[7] **Komen, G.**, **Hasselmann, K. and Hasselmann, K.** (1984). On the existence of a fully developed wind-sea spectrum, *Journal of Physical Oceanography*, 14(8), 1271–1285.

[8] **Moeini, M. and Etemad-Shahidi, A.** (2007). Application of two numerical models for wave hindcasting in Lake Erie, *Applied Ocean Research*, 29(3), 137–145.

[9] **Komen, G.J.**, **Cavaleri, L.**, **Donelan, M.**, **Hasselmann, K.**, **Hasselmann, S. and Janssen, P.** (1996). *Dynamics and modelling of ocean waves*, Cambridge University Press.

[10] **Holthuijsen, L.**, **Booij, N. and Herbers, T.** (1989). A prediction model for stationary, short-crested waves in shallow water with ambient currents, *Coastal Engineering*, 13(1), 23–54.

[11] **Kazeminezhad, M.**, **Etemad-Shahidi, A. and Mousavi, S.** (2007). Evaluation of Neuro fuzzy and numerical wave prediction models in Lake Ontario, *Journal of Coastal Research*, 317–321.

[12] **Jacob, D.**, **Podzun, R. and Claussen, M.** (1995). REMO-A model for climate research and weather prediction, *International workshop on limited-area and variable resolution models, Beijing, China*, pp.273–278.

[13] **Jacob, D. and Podzun, R.** (1997). Sensitivity studies with the regional climate model REMO, *Meteorology and Atmospheric Physics*, 63(1-2), 119–129.

[14] **Sotillo, M.**, **Ratsimandresey, A.**, **Carretero, J.**, **Bentamy, A.**, **Valero, F. and González-Rouco, F.** (2005). A high-resolution 44-year atmospheric hindcast for the Mediterranean Basin: contribution to the regional improvement of global reanalysis, *Climate Dynamics*, 25(2-3), 219–236.

[15] **Cherneva, Z.**, **Andreeva, N.**, **Pilar, P.**, **Valchev, N.**, **Petrova, P. and Guedes Soares, C.** (2008). Validation of the WAMC4 wave model for the Black Sea, *Coastal Engineering*, 55(11), 881–893.

[16] **Janssen, P.A.** (1991). Quasi-linear theory of wind-wave generation applied to wave forecasting, *Journal of Physical Oceanography*, 21(11), 1631–1642.

[17] **Hasselmann, K.** (1974). On the spectral dissipation of ocean waves due to white capping, *Boundary-Layer Meteorology*, 6(1-2), 107–127.

[18] **van Vledder, G.P. and Hurdle, D.P.** (2002). Performance of formulations for whitecapping in wave prediction models, *ASME 2002 21st International Conference on Offshore Mechanics and Arctic Engineering*, American Society of Mechanical Engineers, pp.155–163.

[19] **Yan, L.** (1987). *An improved wind input source term for third generation ocean wave modelling*, KNMI.

[20] **Henrique, J.**, **Alves, G. and Banner, M.L.** (2003). Performance of a saturation-based dissipation-rate source term in modeling the fetch-limited evolution of wind waves., *Journal of Physical Oceanography*, 33(6).

[21] **Rusu, E.** (2009). Wave energy assessments in the Black Sea, *Journal of Marine Science and Technology*, 14(3), 359–372.

[22] **Booij, N.**, **Ris, R. and Holthuijsen, L.H.** (1999). A third-generation wave model for coastal regions: 1. Model description and validation, *Journal of Geophysical Research: Oceans (1978–2012)*, 104(C4), 7649–7666.

[23] **Iglesias, G. and Carballo, R.** (2009). Wave energy potential along the Death Coast (Spain), *Energy*, 34(11), 1963–1975.

[24] **Bourke, W.** (1972). An efficient, one-level, primitive-equation spectral model, *Monthly Weather Review*, 100(9), 683–689.

[25] **Contento, G.**, **Lupieri, G.**, **Venturi, M. and Ciuffardi, T.** (2011). A medium-resolution wave hindcast study over the Central and Western Mediterranean Sea, *Journal of Marine Science and Technology*, 16(2), 181–201.

[26] **Musić, S. and Nicković, S.** (2008). 44-year wave hindcast for the Eastern Mediterranean, *Coastal Engineering*, 55(11), 872–880.

[27] **Cavaleri, L.**, **Ferraris, L. and Crapolicchio, R.** (2005). The wind and wave atlas of the Mediterranean Sea–the calibration phase., *Advances in Geosciences*, 2.

[28] **Liberti, L.**, **Carillo, A. and Sannino, G.** (2013). Wave energy resource assessment in the Mediterranean, the Italian perspective, *Renewable Energy*, 50, 938–949.

[29] **Ayat, B.** (2013). Wave power atlas of Eastern Mediterranean and Aegean Seas, *Energy*, 54, 251–262.

[30] **Aydoğan, B.**, **Ayat, B. and Yüksel, Y.** (2013). Black Sea wave energy atlas from 13 years hindcasted wave data, *Renewable Energy*, 57, 436–447.

[31] **Zodiatisa, G.**, **Galanisa, G.**, **Nikolaidisa, A.**, **Kalogeric, C.**, **Hayesa, D.**, **Georgioua, G.C.**, **Chud, P.C. and Kallosc, G.** (2014). Wave Energy Potential in the Eastern Mediterranean Levantine Basin. An integrated 10-year study, *Renewable Energy*.

[32] **Young, I.R.** (1999). *Wind generated ocean waves*, volume 2, Elsevier.

[33] **Dean, R.G. and Dalrymple, R.A.** (1991). Water wave mechanics for scientists and engineers, *Advanced Series on Ocean Engineering, World Scientific*, 2.

[34] **Vilsmeier, R. and Hänel, D.** (1996). Adaptive solutions for unsteady laminar flows on unstructured grids, *International Journal for Numerical Methods in Fluids*, 22(2), 85–101.

[35] **Weber, N.** (1991). Bottom friction for wind sea and swell in extreme depth-limited situations, *Journal of Physical Oceanography*, 21(1), 149–172.

[36] **Jonsson, I.G.** (1966). Wave boundary layers and friction factors, *Coastal Engineering*, 127–148.

APPENDICES

APPENDIX A : Mean Significant Wave Heights and Wave power Maps
APPENDIX B : Frequency Analysis Charts

APPENDIX A

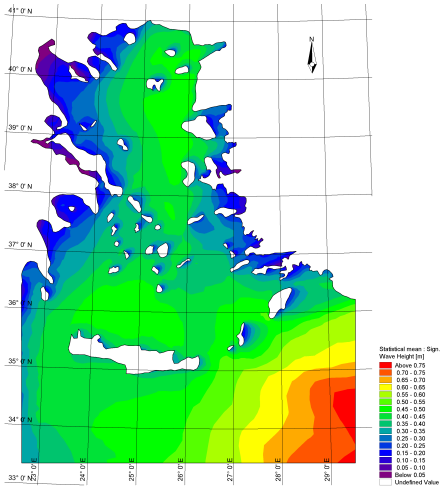

Figure A.1: Mean SWH - 1999.

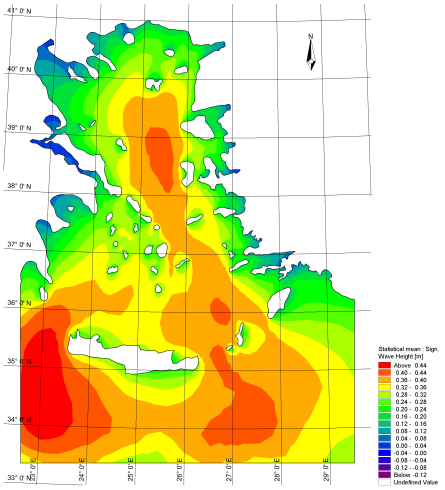

Figure A.2: Mean SWH - 2000.

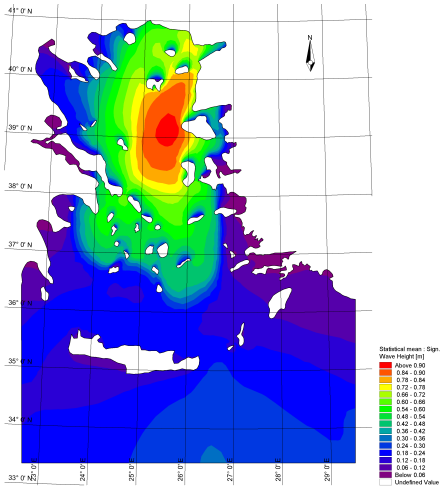

Figure A.3: Mean SWH - 2001.

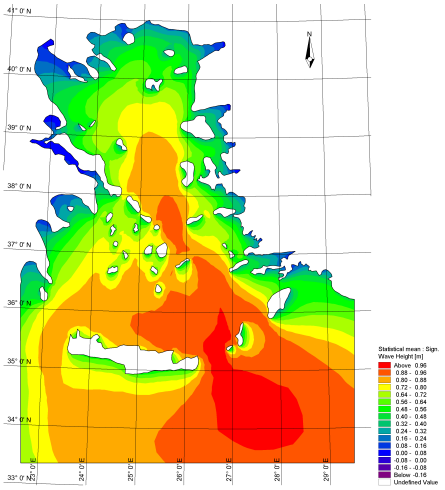

Figure A.4: Mean SWH - 2002.

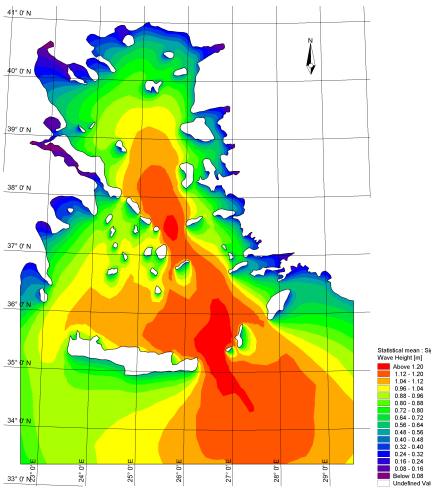

Figure A.5: Mean SWH - 2003.

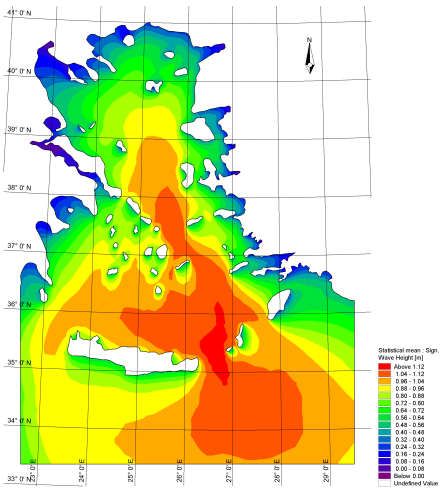

Figure A.6: Mean SWH - 2004.

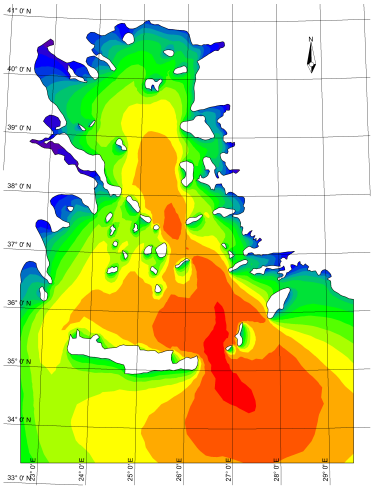

Figure A.7: Mean SWH - 2005.

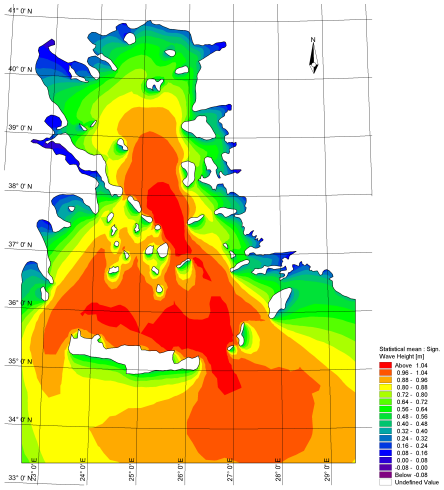

Figure A.8: Mean SWH - 2006.

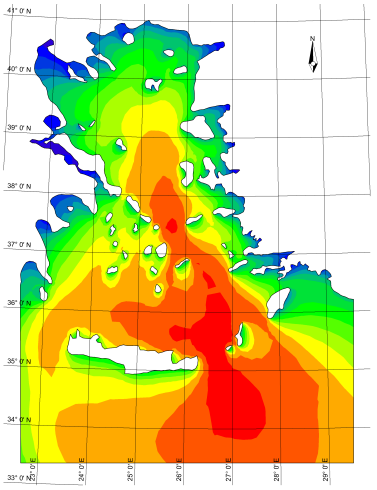

Figure A.9: Mean SWH - 2007.

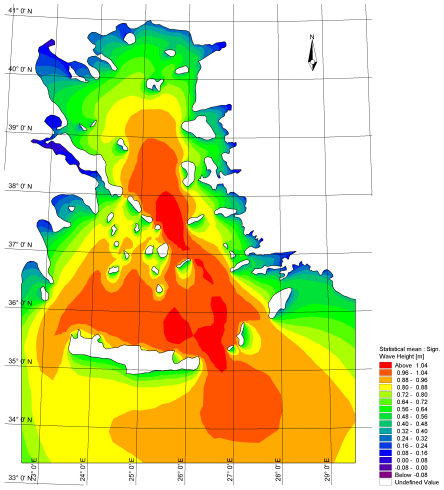

Figure A.10: Mean SWH - 2008.

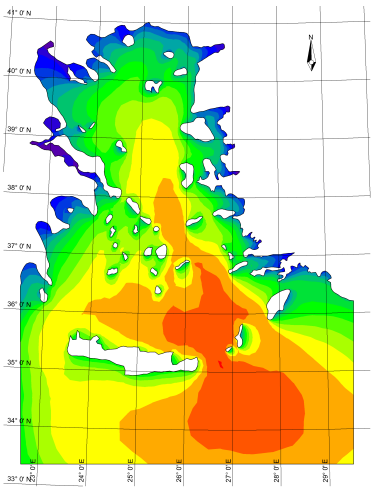

Figure A.11: Mean SWH - 2009.

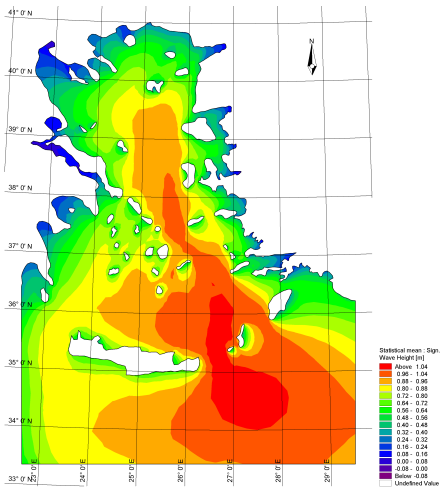

Figure A.12: Mean SWH - 2010.

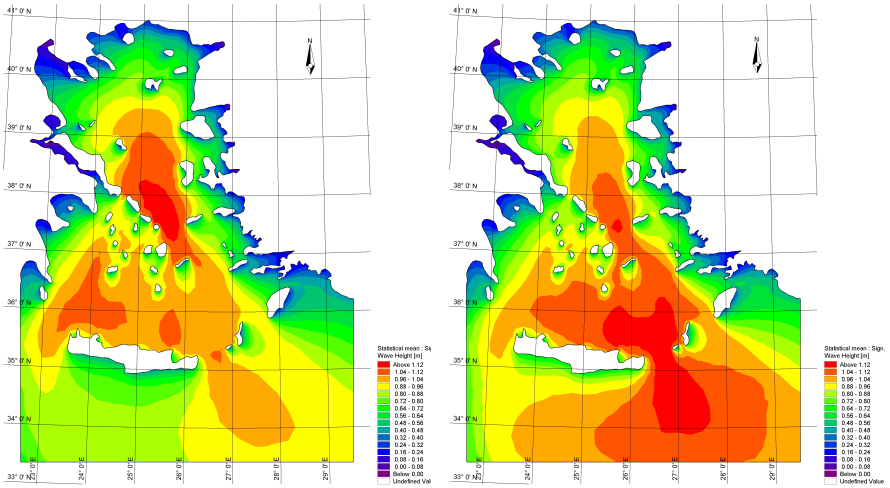

Figure A.13: Mean SWH - 2011. **Figure A.14**: Mean SWH - 2012.

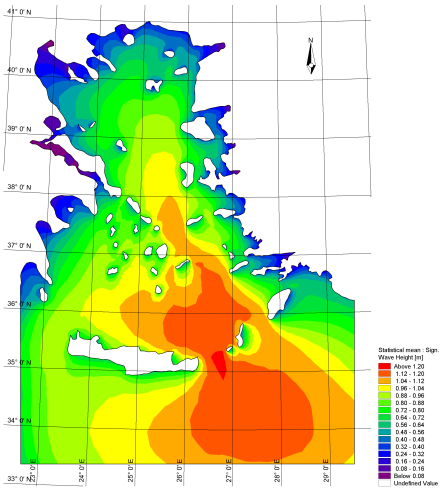

Figure A.15: Mean SWH - 2013.

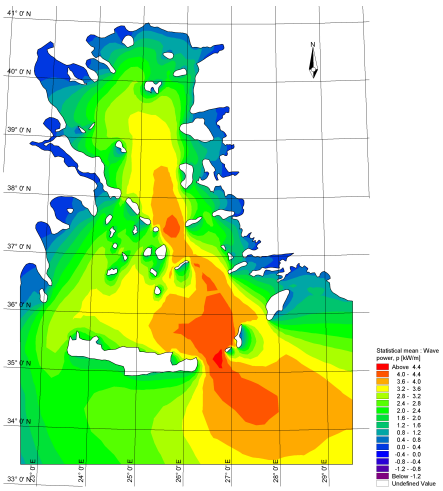

Figure A.16: Mean wave power - 1999.

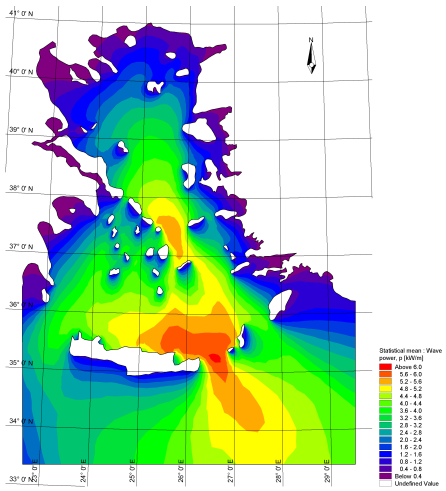

Figure A.17: Mean wave power - 2000.

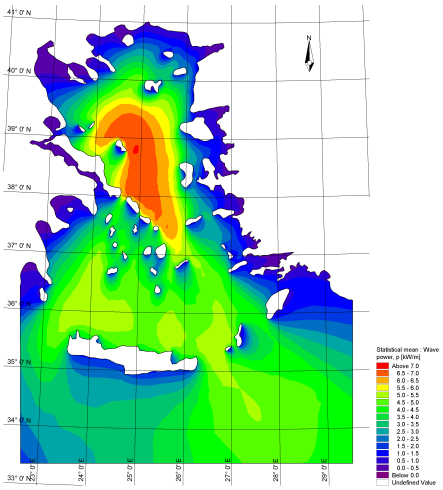

Figure A.18: Mean wave power - 2001.

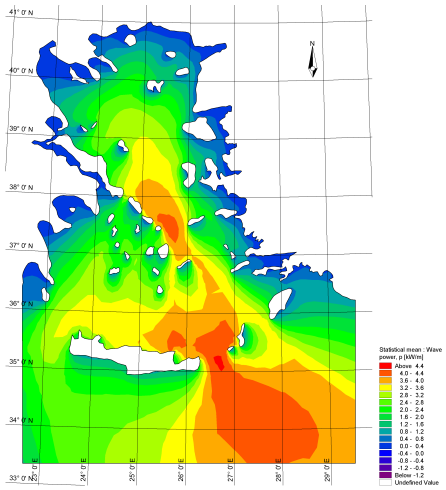

Figure A.19: Mean wave power - 2002.

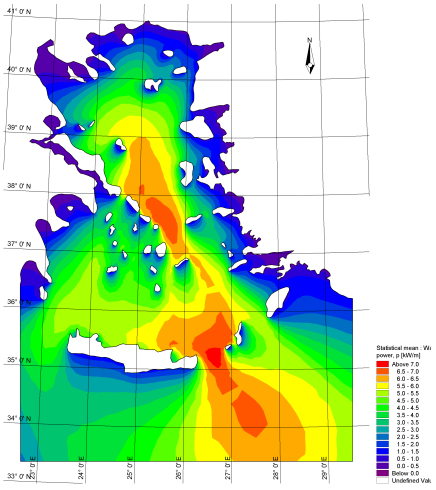

Figure A.20: Mean wave power - 2003.

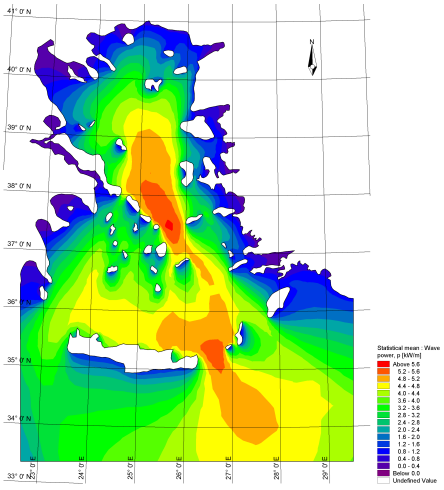

Figure A.21: Mean wave power - 2004.

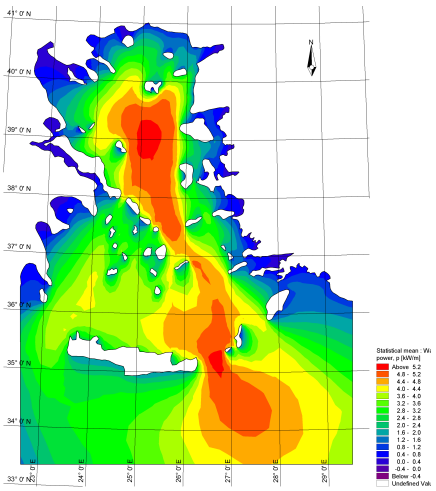

Figure A.22: Mean wave power - 2005.

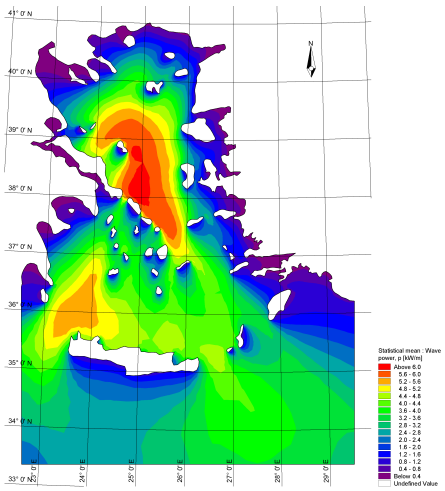

Figure A.23: Mean wave power - 2006.

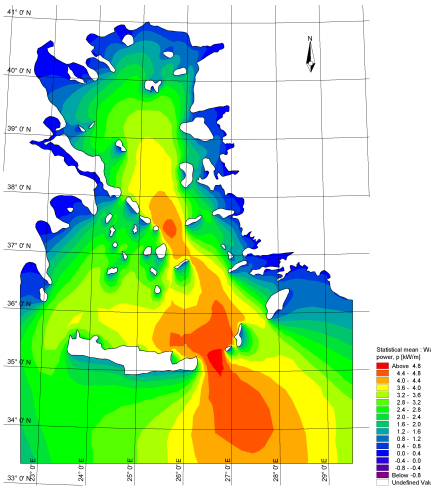

Figure A.24: Mean wave power - 2007.

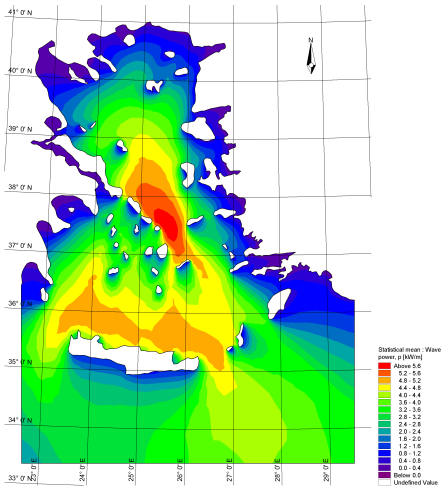

Figure A.25: Mean wave power - 2008.

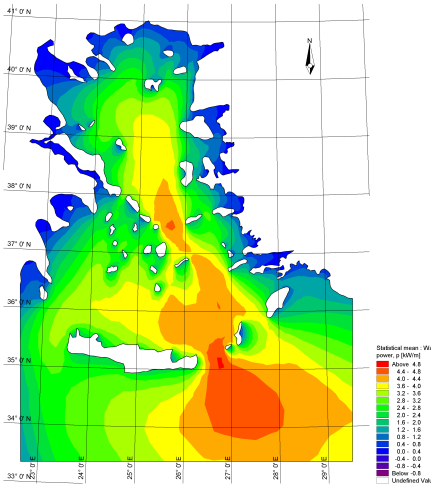

Figure A.26: Mean wave power - 2009.

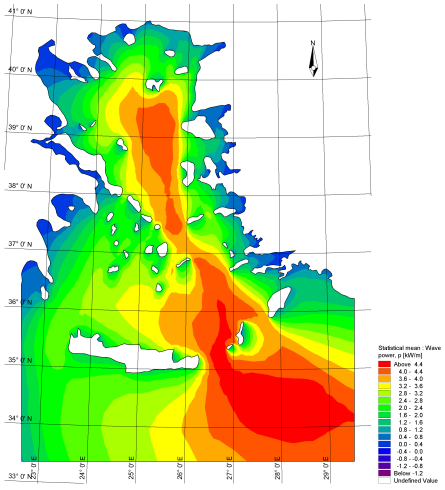

Figure A.27: Mean wave power - 2010.

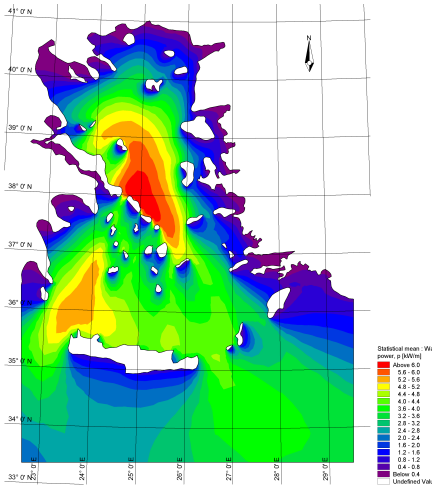

Figure A.28: Mean wave power - 2011.

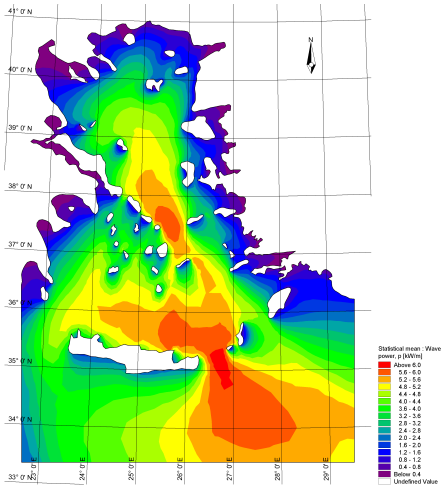

Figure A.29: Mean wave power - 2012.

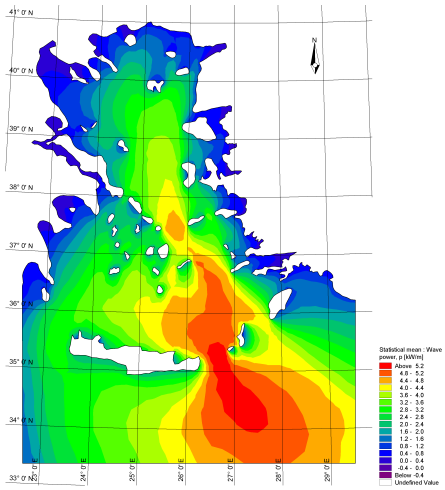

Figure A.30: Mean wave power - 2013.

APPENDIX B

	< 1.5	1.5	2.0	2.5	3.0	3.5	4.0	4.5	5.0	5.5	6.0	6.5	7.0	7.5	8.0	8.5
< 0.5	2048	58728	128864	98176	28002	9317	1914	319	69	36	27	29	11	2	0	0
0.5	0	103	1355	95004	105156	18245	5715	1486	337	42	0	0	0	0	0	0
1.0	0	0	0	83	19627	64167	16578	4091	855	329	32	0	0	0	0	0
1.5	0	0	0	0	1	5250	25428	10255	2460	421	91	41	0	0	0	0
2.0	0	0	0	0	0	0	2363	9515	6358	1826	148	19	0	0	0	0
2.5	0	0	0	0	0	0	0	1814	3440	4096	614	31	0	0	0	0
3.0	0	0	0	0	0	0	0	0	1313	1571	2413	100	0	0	0	0
3.5	0	0	0	0	0	0	0	0	6	986	989	750	7	0	0	0
4.0	0	0	0	0	0	0	0	0	0	235	146	473	79	0	0	0
4.5	0	0	0	0	0	0	0	0	0	0	28	52	65	11	0	0
5.0	0	0	0	0	0	0	0	0	0	0	0	1	48	33	0	0
5.5	0	0	0	0	0	0	0	0	0	0	0	0	7	77	0	0
>= 6	0	0	0	0	0	0	0	0	0	0	0	0	0	0	0	0

Figure B.1: Significant wave height and mean wave period frequency diagram for point 1.

	< 1.5	1.5	2.0	2.5	3.0	3.5	4.0	4.5	5.0	5.5	6.0	6.5	7.0	7.5	8.0	8.5	9	9.5
< 0.5	291	40540	104383	134377	69677	17441	1851	144	0	0	0	0	0	0	0	0	0	0
0.5	0	19	774	39888	77995	73837	20489	3281	1534	419	28	0	0	0	0	0	0	0
1.0	0	0	0	21	1582	22298	46531	13714	2209	989	387	81	0	0	0	0	0	0
1.5	0	0	0	0	3	159	6754	26491	8217	1043	383	221	63	0	0	0	0	0
2.0	0	0	0	0	0	1	42	2045	15970	4146	359	117	39	62	0	0	0	0
2.5	0	0	0	0	0	0	0	23	1158	9014	1747	111	21	50	19	0	0	0
3.0	0	0	0	0	0	0	0	0	13	1085	4351	463	46	0	0	0	0	0
3.5	0	0	0	0	0	0	0	0	0	15	1271	2129	84	0	0	0	0	0
4.0	0	0	0	0	0	0	0	0	0	0	26	1139	459	26	0	0	0	0
4.5	0	0	0	0	0	0	0	0	0	0	0	86	796	72	0	0	0	0
5.0	0	0	0	0	0	0	0	0	0	0	0	1	312	328	4	0	0	0
5.5	0	0	0	0	0	0	0	0	0	0	0	0	15	273	29	0	0	0
6.0	0	0	0	0	0	0	0	0	0	0	0	0	0	28	129	11	0	0
7	0	0	0	0	0	0	0	0	0	0	0	0	0	0	35	0	0	0
>= 7	0	0	0	0	0	0	0	0	0	0	0	0	0	0	0	0	0	0

Figure B.2: Significant wave height and mean wave period frequency diagram for point 2.

	< 1.5	1.5	2.0	2.5	3.0	3.5	4.0	4.5	5.0	5.5	6.0	6.5	7.0	7.5	8.0	> 8.5
< 0.5	271	27389	82729	102122	30809	7061	1265	223	4	0	0	0	0	0	0	0
0.5	0	32	818	57548	112107	51742	6621	1394	304	80	0	0	0	0	0	0
1.0	0	0	0	26	1024	59251	61346	5518	1221	332	67	2	0	0	0	0
1.5	0	0	0	0	1	125	22137	48676	4096	576	256	49	1	0	0	0
2.0	0	0	0	0	0	0	27	7645	31749	2593	445	108	19	0	0	0
2.5	0	0	0	0	0	0	0	3	4636	15484	1063	179	53	3	0	0
3.0	0	0	0	0	0	0	0	0	4	4095	7013	347	85	17	0	0
3.5	0	0	0	0	0	0	0	0	0	7	3496	2612	108	11	0	0
4.0	0	0	0	0	0	0	0	0	0	0	39	2263	574	30	0	0
4.5	0	0	0	0	0	0	0	0	0	0	0	274	1193	56	0	0
5.0	0	0	0	0	0	0	0	0	0	0	0	0	425	407	5	0
5.5	0	0	0	0	0	0	0	0	0	0	0	0	13	570	20	0
6.0	0	0	0	0	0	0	0	0	0	0	0	0	0	128	179	0
6.5	0	0	0	0	0	0	0	0	0	0	0	0	0	0	58	0
7.0	0	0	0	0	0	0	0	0	0	0	0	0	0	0	21	5
7.5	0	0	0	0	0	0	0	0	0	0	0	0	0	0	2	6
8.0	0	0	0	0	0	0	0	0	0	0	0	0	0	0	0	12
>= 8.5	0	0	0	0	0	0	0	0	0	0	0	0	0	0	0	6

Figure B.3: Significant wave height and mean wave period frequency diagram for point 3.

	< 1.5	1.5	2.0	2.5	3.0	3.5	4.0	4.5	5.0	5.5	6.0	6.5	7.0	7.5	8.0	8.5	9.0	9.5
< 0.5	103	11616	45978	85482	41857	15639	3142	412	0	0	0	0	0	0	0	0	0	0
0.5	0	31	691	45597	103288	56930	12409	3570	1446	205	29	0	0	0	0	0	0	0
1.0	0	0	0	13	1070	59453	74525	10844	2523	905	457	174	17	0	0	0	0	0
1.5	0	0	0	0	0	96	24379	61668	9613	1319	418	192	53	28	5	0	0	0
2.0	0	0	0	0	0	0	18	8752	38641	6107	566	245	76	35	63	0	0	0
2.5	0	0	0	0	0	0	0	6	4074	16082	2886	352	151	61	32	1	0	0
3.0	0	0	0	0	0	0	0	0	5	3068	8732	1138	231	102	3	2	0	0
3.5	0	0	0	0	0	0	0	0	0	38	2408	2730	298	12	4	0	0	0
4.0	0	0	0	0	0	0	0	0	0	0	43	1712	956	101	2	0	0	0
4.5	0	0	0	0	0	0	0	0	0	0	0	106	1093	184	2	0	0	0
5.0	0	0	0	0	0	0	0	0	0	0	0	0	140	306	107	2	0	0
5.5	0	0	0	0	0	0	0	0	0	0	0	0	6	336	127	11	0	0
6.0	0	0	0	0	0	0	0	0	0	0	0	0	0	50	75	8	2	0
6.5	0	0	0	0	0	0	0	0	0	0	0	0	0	0	56	7	6	0
7.0	0	0	0	0	0	0	0	0	0	0	0	0	0	0	9	17	14	11
>= 7.5	0	0	0	0	0	0	0	0	0	0	0	0	0	0	0	0	0	0

Figure B.4: Significant wave height and mean wave period frequency diagram for point 4.

	< 1.5	1.5	2	2.5	3	3.5	4	4.5	5	5.5	6	6.5	7	7.5	8	8.5
< 0.5	71	12854	64570	184125	104708	47188	12154	1267	190	13	8	0	0	0	0	0
0.5	0	10	297	60316	126909	48575	17135	8585	3714	897	111	2	0	0	0	0
1	0	0	0	3	1445	21326	16421	8781	4645	2324	726	171	71	0	0	0
1.5	0	0	0	0	0	114	3739	6215	4446	2219	1234	326	185	7	0	0
2	0	0	0	0	0	0	17	744	2460	1720	762	391	175	90	0	0
2.5	0	0	0	0	0	0	0	0	246	935	637	245	106	61	0	0
3	0	0	0	0	0	0	0	0	0	93	451	329	112	56	0	0
3.5	0	0	0	0	0	0	0	0	0	0	1	124	155	68	4	0
4	0	0	0	0	0	0	0	0	0	0	0	1	58	49	0	0
>= 4.5	0	0	0	0	0	0	0	0	0	0	0	0	5	35	0	0

Figure B.5: Significant wave height and mean wave period frequency diagram for point 5.

	< 1.5	1.5	2	2.5	3	3.5	4	4.5	5	5.5	6	6.5	7	7.5	8	8.5	9
< 0.5	33	7208	40036	120913	57468	6262	491	64	0	0	0	0	0	0	0	0	0
0.5	0	18	370	43072	130831	79403	8591	1870	470	131	18	0	0	0	0	0	0
1	0	0	0	9	614	49620	70827	7649	857	299	140	0	0	0	0	0	0
1.5	0	0	0	0	0	42	15005	50482	6345	540	197	92	0	0	0	0	0
2	0	0	0	0	0	0	13	3713	31774	4161	294	123	33	0	0	0	0
2.5	0	0	0	0	0	0	2	8	1768	16988	1321	151	69	0	0	0	0
3	0	0	0	0	0	0	0	1	4	1683	7663	234	32	0	0	0	0
3.5	0	0	0	0	0	0	0	0	2	15	1705	2492	70	0	0	0	0
4	0	0	0	0	0	0	0	0	0	1	37	1718	611	1	0	0	0
4.5	0	0	0	0	0	0	0	0	0	0	2	81	1085	50	0	0	0
5	0	0	0	0	0	0	0	0	0	0	0	4	170	469	0	0	0
5.5	0	0	0	0	0	0	0	0	0	0	0	0	4	317	33	0	0
6	0	0	0	0	0	0	0	0	0	0	0	0	0	21	57	0	0
6.5	0	0	0	0	0	0	0	0	0	0	0	0	0	0	13	8	0
7	0	0	0	0	0	0	0	0	0	0	0	0	0	0	1	9	0
>= 7.5	0	0	0	0	0	0	0	0	0	0	0	0	0	0	0	0	0

Figure B.6: Significant wave height and mean wave period frequency diagram for point 6.

	< 1.5	1.5	2	2.5	3	3.5	4	4.5	5	5.5	6	6.5	7	7.5	8	8.5
< 0.5	27	4833	31180	82360	43032	10250	1021	324	178	72	34	0	0	0	0	0
0.5	0	17	418	38190	124526	83377	18804	3502	447	109	19	0	0	0	0	0
1	0	0	0	7	575	54837	92236	15203	2455	420	142	18	0	0	0	0
1.5	0	0	0	0	0	34	20205	62663	9438	1091	333	4	0	0	0	0
2	0	0	0	0	0	0	7	4828	32230	4763	582	72	3	0	0	0
2.5	0	0	0	0	0	0	0	5	2411	14197	2074	111	10	0	0	0
3	0	0	0	0	0	0	0	0	1	1808	6721	530	19	0	0	0
3.5	0	0	0	0	0	0	0	0	0	3	1888	1850	76	0	0	0
4	0	0	0	0	0	0	0	0	0	0	7	1070	396	0	0	0
4.5	0	0	0	0	0	0	0	0	0	0	0	33	486	118	0	0
5	0	0	0	0	0	0	0	0	0	0	0	0	123	180	3	0
5.5	0	0	0	0	0	0	0	0	0	0	0	0	1	82	20	0
6	0	0	0	0	0	0	0	0	0	0	0	0	0	54	5	0
>= 6.5	0	0	0	0	0	0	0	0	0	0	0	0	0	0	0	0

Figure B.7: Significant wave height and mean wave period frequency diagram for point 7.

	< 1.5	1.5	2	2.5	3	3.5	4	4.5	5	5.5	6	6.5	7	7.5	8	>= 8.5
< 0.5	64	3339	19019	59434	44623	13832	1415	334	83	36	15	0	0	0	0	0
0.5	0	25	363	25520	119488	98284	27375	5932	1063	284	47	0	0	0	0	0
1	0	0	0	9	441	32251	96106	32329	4954	922	205	0	0	0	0	0
1.5	0	0	0	0	0	23	9600	61756	23345	2371	674	94	24	9	0	0
2	0	0	0	0	0	0	4	1347	31725	14766	978	171	0	0	0	0
2.5	0	0	0	0	0	0	0	5	634	15246	6897	229	68	0	0	0
3	0	0	0	0	0	0	0	0	3	533	8220	2681	49	0	0	0
3.5	0	0	0	0	0	0	0	0	0	3	377	4628	549	6	0	0
4	0	0	0	0	0	0	0	0	0	0	8	349	1906	106	0	0
4.5	0	0	0	0	0	0	0	0	0	0	0	4	409	737	17	0
5	0	0	0	0	0	0	0	0	0	0	0	0	21	342	71	0
5.5	0	0	0	0	0	0	0	0	0	0	0	0	0	17	245	18
6	0	0	0	0	0	0	0	0	0	0	0	0	0	0	40	28
6.5	0	0	0	0	0	0	0	0	0	0	0	0	0	0	0	47
>= 7	0	0	0	0	0	0	0	0	0	0	0	0	0	0	0	40

Figure B.8: Significant wave height and mean wave period frequency diagram for point 8.

	< 1.5	1.5	2	2.5	3	3.5	4	4.5	5	5.5	6	6.5	7	7.5	8	>= 8.5
< 0.5	52	2219	18212	53723	44175	17321	3391	688	308	100	0	0	0	0	0	0
0.5	0	12	325	20833	113041	122106	38145	8367	1740	289	7	0	0	0	0	0
1	0	0	0	7	469	25365	96180	43002	7018	937	35	0	0	0	0	0
1.5	0	0	0	0	0	29	4806	47434	28686	3987	494	55	8	0	0	0
2	0	0	0	0	0	0	6	1019	19955	15635	1758	209	0	0	0	0
2.5	0	0	0	0	0	0	0	0	402	9272	8042	617	116	1	0	0
3	0	0	0	0	0	0	0	0	0	173	5726	3769	145	25	14	0
3.5	0	0	0	0	0	0	0	0	0	1	132	3702	986	40	0	0
4	0	0	0	0	0	0	0	0	0	0	2	153	1743	221	4	0
4.5	0	0	0	0	0	0	0	0	0	0	0	2	268	592	50	0
5	0	0	0	0	0	0	0	0	0	0	0	0	11	252	131	9
5.5	0	0	0	0	0	0	0	0	0	0	0	0	0	32	197	49
6	0	0	0	0	0	0	0	0	0	0	0	0	0	0	5	69
6.5	0	0	0	0	0	0	0	0	0	0	0	0	0	0	0	33
>= 7	0	0	0	0	0	0	0	0	0	0	0	0	0	0	0	12

Figure B.9: Significant wave height and mean wave period frequency diagram for point 9.

	< 1.5	1.5	2	2.5	3	3.5	4	4.5	5	5.5	6	6.5	7	>= 7.5
< 0.5	30	5923	44988	105319	30179	5360	558	135	41	0	0	0	0	0
0.5	0	15	480	78115	174337	77412	9331	2182	733	216	67	0	0	0
1	0	0	0	10	741	52783	69918	10440	1382	520	207	113	0	0
1.5	0	0	0	0	0	39	13724	40905	7126	646	179	92	2	0
2	0	0	0	0	0	0	13	3536	18200	3571	323	35	21	7
2.5	0	0	0	0	0	0	0	10	1692	8408	1466	67	10	0
3	0	0	0	0	0	0	0	0	9	1087	3029	355	8	0
3.5	0	0	0	0	0	0	0	0	0	13	576	1128	73	0
4	0	0	0	0	0	0	0	0	0	0	20	521	326	4
4.5	0	0	0	0	0	0	0	0	0	0	0	26	217	88
>= 5	0	0	0	0	0	0	0	0	0	0	0	1	24	0

Figure B.10: Significant wave height and mean wave period frequency diagram for point 10.

CURRICULUM VITAE

Name Surname: Navid JADIDOLESLAM

Place and Date of Birth: Tabriz - 1989

E-Mail: Jadidoleslam@itu.edu.tr

B.Sc.: University of Tabriz (Iran)

M.Sc.: Istanbul Technical University (Turkey)